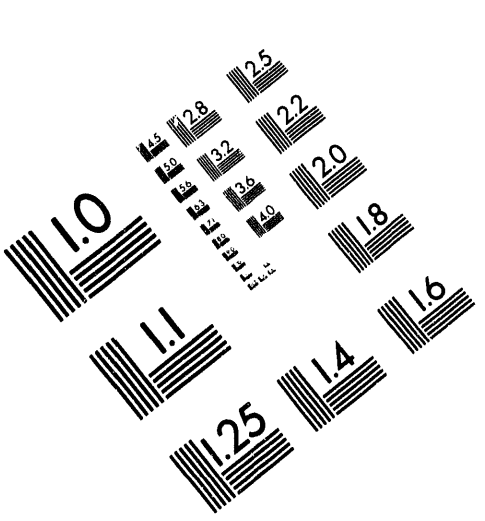

Association for Information and Image Management
1100 Wayne Avenue, Suite 1100
Silver Spring, Maryland 20910
301/587-8202

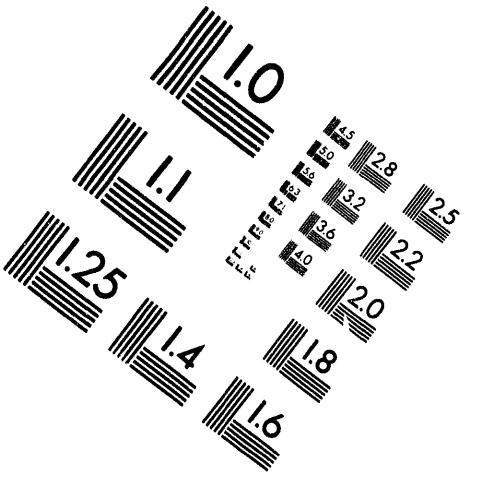

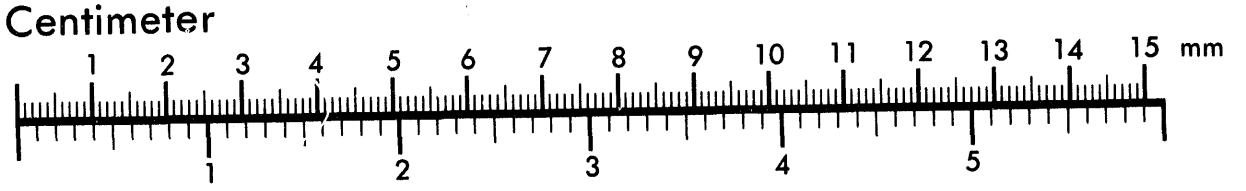

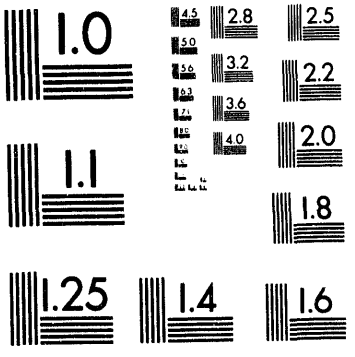

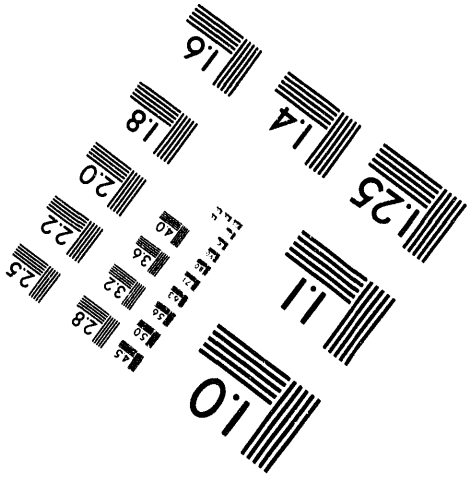

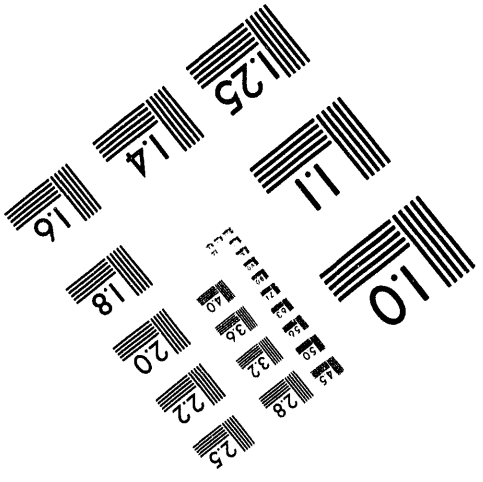

1 of 2

NRTSC
NUCLEAR REACTOR TECHNOLOGY AND SCIENTIFIC COMPUTATIONS

WSRC-TR-92-534
Task No.: 92-104-1

KEYWORDS:
ONSET OF FLOW INSTABILITY
ONSET OF SIGNIFICANT VOID
DEMAND CURVES
LOSS OF COOLANT ACCIDENT
ANNULUS

RETENTION:
PERMANENT

NUCLEATE BOILING PRESSURE DROP IN AN ANNULUS, BOOK 2 (U)

James A. Block, Christopher Crowley, Francis X. Dolan, Richard G. Sam, and Brant H. Stoedefalke

ISSUED: NOVEMBER, 1992

D. Allen Coutts
Authorized Derivative Classifier/
Reviewing Official

SRL SAVANNAH RIVER TECHNOLOGY CENTER, AIKEN, SC 29808
Westinghouse Savannah River Corporation
Prepared for the U.S. Department of Energy under
Contract DE-AC09-89SR18035

Creare

TECHNICAL NOTE

NUCLEATE BOILING PRESSURE DROP IN AN ANNULUS

VOLUME I

TN-499 OCTOBER 1990

Final Report

NUCLEATE BOILING PRESSURE DROP IN AN ANNULUS

Volume 1

SUMMARY AND INTERPRETATION OF RESULTS

Prepared by
James A. Block
Christopher J. Crowley
Francis X. Dolan
Richard G. Sam
Brant H. Stoedefalke

Prepared for
U.S. Department of Energy
and
Savannah River Laboratory
Subcontract AX-721102

CREARE INC.
HANOVER, NH 03755

TN-499
OCTOBER, 1990

Creare

EXECUTIVE SUMMARY

Purpose. The application of the work described in this report is the production reactors at the Savannah River Site, and the context is nuclear reactor safety. The Loss of Coolant Accident (LOCA) scenario considered involves a double-ended break of a primary coolant pipe in the reactor. During a LOCA, the flow through portions of the reactor may reverse direction or be greatly reduced, depending upon the location of the break. The reduced flow rate of coolant (D_2O) through the fuel assembly channels of the reactor -- downflow in this situation -- can lead to boiling and to the potential for flow instabilities which may cause some of the fuel assembly channels to overheat and melt. That situation is to be avoided.

Figure 1 illustrates the overall pressure drop versus flow characteristic for a heated flow channel at a given power input. This is referred to as a "demand curve" because it represents the flow and pressure drop requirements which must be supplied by the pump and the rest of the system. The pump has a "supply curve", not shown in Figure 1, which generally has a negative slope. The intersection of the two curves is the operating point. At high liquid flow rate, the flow is single-phase or in subcooled nucleate boiling. In this region, the pressure gradient is dominated by friction, the pressure drop decreases with a decreasing liquid flow rate, and the slope of the pressure versus flow characteristic is positive. The flow is stable because a slight perturbation of flow drives the system back to its stable operating condition.

When the downflow rate is reduced significantly, the pressure drop may increase with a decreasing liquid flow rate, because the component of the pressure drop due to the production of vapor by boiling in the channel becomes important. The characteristic of a negative slope in this region can lead to an instability. The criterion for instability is if the negative slope of the demand curve is greater than the negative slope of the supply curve. The instability can manifest itself as a significant reduction in flow rate. This can lead to overheating of the channel.

Since it is common for the supply curve to have a very small negative slope, the instability will generally occur very close to the minima in the demand curve. The location of the minima is therefore very important to the prediction of the operation of the fuel assemblies in the reactors since it represents the condition for the Onset of Flow Instability (OFI). OFI occurs at higher velocity for higher input power. Data from this project can therefore serve as the basis, in conjunction with predictions of the velocity during a LOCA and with suitable factors of safety, for assessing the power level at which the fuel assembly and the reactor can be operated to prevent overheating in the event of a LOCA.

Objectives. The overall objective of the safety research program sponsored by SRL, of which this project is a part, is to provide key information about boiling in prototypical annuli to allow accurate predictions of the thermal and hydraulic behavior in the reactor assembly. The primary objective of this project is to provide data for the onset of a flow instability under various conditions:

- In a prototypical geometry with prototypical material (aluminum),
- With and without centering ribs on the inner annulus wall in order to assess that effect, and
- With uniform and circumferentially peaked (power tilt) heat flux distribution.

Creare

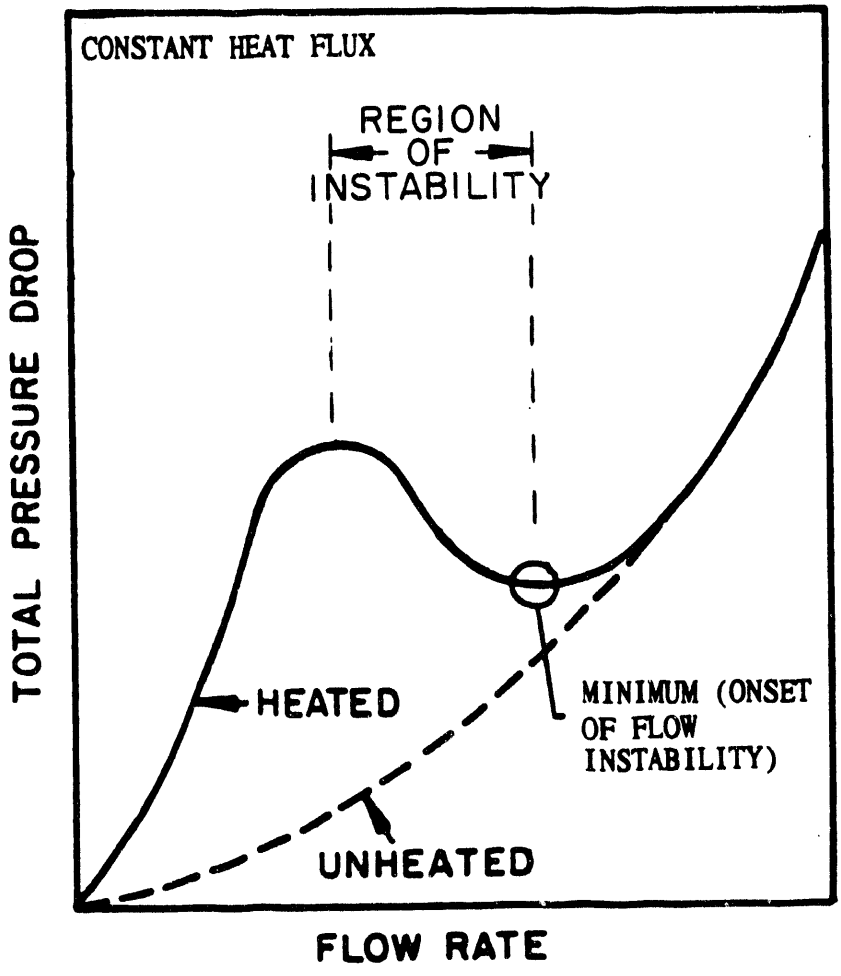

Figure 1. CHARACTERISTIC PRESSURE DROP VERSUS FLOW RATE CURVE FOR BOILING CHANNEL FLOW

Greare

The experimental demand curve in each of these cases is the key result.

A secondary objective of the project is to verify or develop correlations for:

- Single-phase heat transfer and pressure drop,
- Onset of Nucleate Boiling (ONB), and
- Heat transfer, pressure drop, and energy partition in subcooled nucleate boiling

Technical Approach. The experimental approach is to provide a test annulus which simulates geometry, materials, and flow conditions in a Mark-22 fuel assembly (Coolant Channel 3) to the extent possible. The annulus has a full-scale geometry, and in fact uses SRL dummy hardware for the inner annulus wall in the ribbed geometry. The material is aluminum. The annulus is uniformly heated in the axial direction, but the circumferential heat flux can be varied to provide "power tilt" or asymmetric heating of the inner and outer annulus walls. (Although the reactor fuel assemblies will have nonuniform axial heating profiles, it is believed that the integral power input is the most important factor.) The test facility uses H_2O rather than D_2O, but it includes the effects of dissolved helium gas present in the reactor.

The key analysis approaches are:

- To compare the minima in the measured demand curves with analytical criteria, in particular the Saha-Zuber (1974) model, and
- To compare the pressure and temperature as a function of length in the annulus with an integral model for flow boiling in a heated channel.

Work Completed. Nineteen test series and a total of 178 tests were performed. Testing addressed the effects of:

- Heat Flux
- Pressure
- Helium gas
- Power Tilt
- Ribs
- Asymmetric Heat Flux

The ranges of pressure, fluid temperature, flow rate, dissolved helium gas concentration, and heat flux (symmetric, asymmetric, and power tilt) are typical of conditions during a large break LOCA. Within a given test series, all boundary conditions except for inlet velocity were held approximately constant -- only the inlet flow rate was varied in order to be able to map out demand curves like the illustration in Figure 1.

Analysis activities included:

- Comparisons of the minima in the demand curve from each series with various models using software called OSV (Crowley, 1990) developed for this project, and

- Comparisons of pressure and temperature profiles in the annulus from selected tests with predictions of the computer program ANNULUS developed at Creare (Barry, Crowley and Wallis, 1989).

Due to funding constraints on the project, detailed comparisons with alternative models for each boiling regime could not be performed.

Key Conclusions. The standard OFI comparison relates the OFI point to the predictions of the model by Saha and Zuber (1974) for the Onset of Significant Voiding (OSV). The predictions of the model can be represented in dimensionless form by a modified Stanton number (a dimensionless heat transfer coefficient) and the Peclet number (a dimensionless flow rate parameter). For a given heat flux, the model predicts the subcooling at the outlet of the flow channel for which vapor bubbles generated by boiling heat transfer depart from the cavities of the heated surface and enter the bulk fluid flow. The two-phase pressure drop increases dramatically when this occurs, leading to the increase in pressure drop and the negative slope in the demand curve at velocities below that at which the minimum pressure drop occurs.

Figure 2 shows the results from the Creare experiments. With respect to the major objectives of the project, the results indicate that:

- A Stanton number of about 0.003, or about 50% lower than the Saha-Zuber model bounds all of the experimental data, including tests with ribs and power tilt.

- The minima for the ribbed geometry generally lie at lower Stanton number (larger subcooling) than the minima for the ribless geometry.

- The minima for the power tilt tests do not differ significantly from the minima for the uniform heat flux tests in the ribbed geometry. This may be because power tilt has little effect, or because the high power channel did not correspond with the channel which is normally the least stable. We believe that the most limiting power tilt tests were not performed.

The results from the Creare experiments in the ribbed geometry indicate that the conditions for OFI may generally lie at higher average velocity (higher average subcooling) than data without ribs. Creare data from the geometry without ribs are in agreement with other data obtained or compiled by SRL in geometries without ribs (see Figure 3).

It is believed that because of the geometrical variations in the annulus diameter and the rib tip clearance, and the distortions caused by heating of the annulus, each flow subchannel has a somewhat different geometry than the other subchannels. Thus, one subchannel might apparently become unstable before the others, when the flow conditions are based upon the average flow conditions in the four subchannels. In these experiments, the subchannel at the 312° location generally became unstable first in the ribbed geometry.

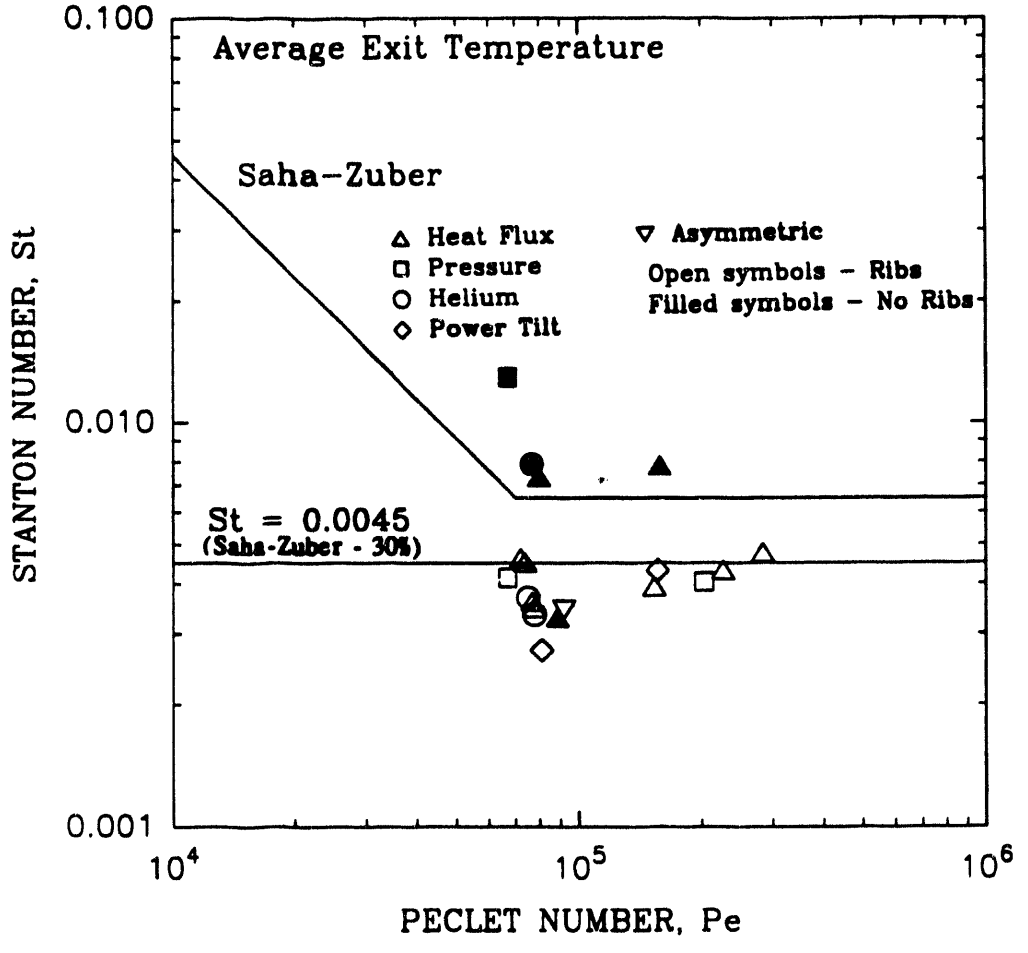

Figure 2. SUMMARY OF OFI RESULTS FROM CREARE EXPERIMENTS

Greare

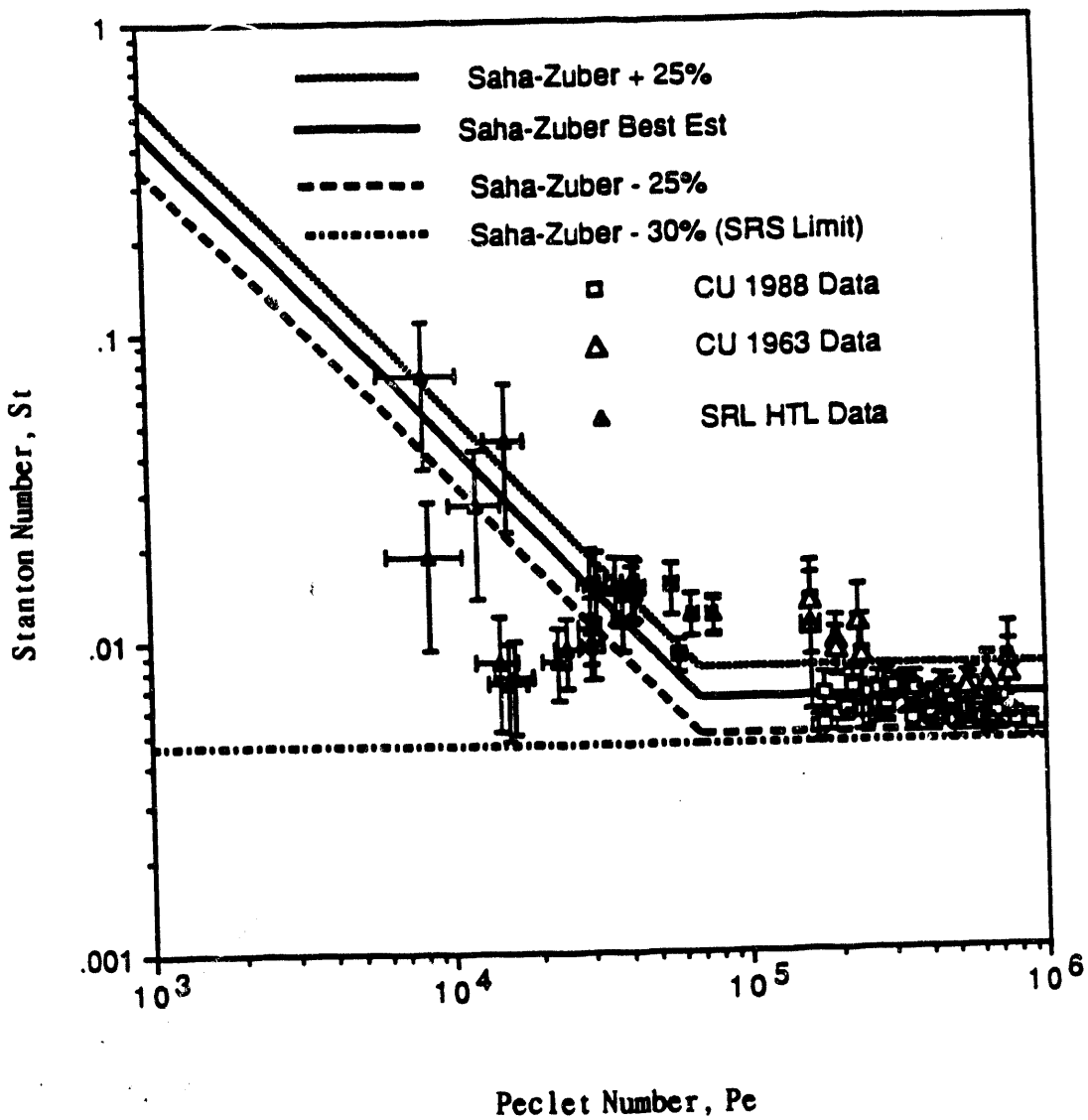

Figure 3. SUMMARY OF OFI RESULTS FROM OTHER SRL PROGRAM EXPERIMENTS (CHEN ET AL., NOVEMBER, 1989)

Greare

TABLE OF CONTENTS
Volume 1

Creare

TABLE OF CONTENTS
Volume 2

Creare

NOMENCLATURE

A_f	cross-sectional flow area in annulus
c_{pf}	heat capacity of liquid
dz	distance between measurement locations in annulus
D_h	hydraulic diameter of annulus
D_i	inner diameter of annulus
D_o	outer diameter of annulus
f_{tp}	two-phase friction factor in subcooled boiling
f_{wl}	single-phase liquid friction factor
g	acceleration of gravity
G	mass flux ($\rho_f V_f$)
h	heat transfer coefficient
h_{fc}	heat transfer coefficient in forced convection flow
h_{fg}	latent heat of vaporization
h_{tp}	two-phase heat transfer coefficient in boiling
J	conversion factor of Btu to ft-lb_f
k_f	thermal conductivity of liquid
L	length of annulus
Nu	Nusselt number
p	pressure
Pe	Peclet number ($Re_f Pr_f$)
Pr_f	Prandtl number of liquid ($c_{pf}\mu_f/k_f$)
Re_f	Reynolds number of liquid ($\rho_f D_h V_f/\mu_f$)
St	Stanton number ($Nu/Re_f Pr_f$)
T_f	fluid temperature
T_{fo}	fluid temperature at annulus inlet
T_{sat}	saturation temperature
T_w	wall temperature
v_f	specific volume of liquid phase
v_g	specific volume of vapor phase
v_{fg}	difference of specific volumes ($v_g - v_f$)
x	flow quality (ratio of mass flow rate of vapor to total mass flow rate)
Y_b	bubble size in nucleate boiling
z	distance along heated length

Creare

NOMENCLATURE (CONCLUDED)

Greek

ϕ	wall heat flux
ϕ_{fc}	portion of wall heat flux in forced convection heat transfer
ϕ_{onb}	wall heat flux at ONB point
ϕ_{osv}	wall heat flux at OSV point
ϕ_{sc}	portion of wall heat flux in subcooled boiling
μ_f	liquid phase viscosity
μ_g	gas phase viscosity
ρ_f	liquid phase density
ρ_g	gas phase density
τ_w	wall shear stress
σ	liquid-vapor of annulus
θ	inclination of annulus (θ = -90°, sinθ = -1)

Subscripts

c	calculated
fdb	fully developed boiling
m	measured
onb	onset of nucleate boiling

Creare

LIST OF FIGURES

Creare

LIST OF FIGURES (CONCLUDED)

Creare

LIST OF TABLES

Creare

1. GUIDE TO THIS REPORT

This report has been prepared in two volumes. This Volume 1 summarizes our interpretation our experiments and analysis of nucleate boiling in an annulus during downflow. The companion report, Volume 2, is a data report which comprehensively presents the experimental data so that independent review and analysis of the data can be performed.

Table 1.1 summarizes the key features of the facility. The specific purpose of Section 2 of this document is to describe the facility, particularly each of the test section geometries used on the project. Geometries both with and without centering ribs are described. With the reconstruction of the test facility which was required following various failures of the heaters, two slightly different test geometries were used with each of the ribbed and ribless geometries. Section 2 documents the small differences in these test section geometries. It also provides the locations of the instruments as installed in the facility and the keys to their location on the data records in Volume 2. Further details about the facility can be found in the Test Plan documents (Sam, et al., 1988, Barry, 1989, and Crowley and Dolan, 1989) and Design Drawings in the project records.

Section 3 discusses the technical results on the project for:

- Baseline Tests (including Repeatability),
- Effect of Heat Flux,
- Effect of Pressure,
- Effect of Helium Gas,
- Asymmetric Heat Flux,
- Effect of Ribs, and
- Effect of Power Tilt.

Table 1.2 lists the conditions for the completed experiments. Nineteen test series, a total of 178 tests, have been performed with a heated annulus. The demand curves from various test series are overlaid in order to illustrate the effects listed above. Temperature and pressure profiles in the annulus from selected tests are also presented.

The demand curve and profile data are compared with the predictions of the ANNULUS computer program developed by Creare. That program predicts the detailed behavior of a heated flow channel from single-phase through saturated boiling heat transfer regimes. Figure 1.1 illustrates the boiling regimes and transitions with sketches of the associated pressure and temperature profiles for downflow in a heated channel. The boiling regimes and transitions of interest here include:

- Single-phase forced convection regime,
- Transition at Onset of Nucleate Boiling (ONB),
- Partially developed subcooled nucleate boiling regime,
- Transition for Onset of Significant Voiding (OSV), and
- Fully developed subcooled nucleate boiling regime.

Table 1.1 CHARACTERISTICS OF STEADY-STATE FLOW BOILING EXPERIMENTS

- PROTOTYPICAL GEOMETRY WITH RIBS (MARK-22 FUEL ASSEMBLY)
- PROTOTYPICAL PRESSURE AND FLOW RATES
- PROTOTYPICAL WALL MATERIALS
- SYMMETRIC OR ASYMMETRIC HEATING OF ANNULUS WALLS (HEAT FLUX UP TO 500,000 BTU/HR-FT^2* IN EACH WALL)
- NON-UNIFORM CIRCUMFERENTIAL HEAT FLUX (POWER TILT)
- UNIFORM HEATING WITH LENGTH
- DOWNFLOW IN ANNULUS
- H_2O SIMULATES D_2O
- EFFECTS OF DISSOLVED HELIUM GAS INCLUDED

* 375,000 Btu/hr-ft^2 achieved in experiments

Table 1.2 MATRIX OF FLOW BOILING EXPERIMENTS IN A PROTOTYPICAL ANNULUS

Test Series Number	Date	Effect	Geometry	Heat Flux (Btu/hr-ft^2)	Inlet Pressure (psia)	Helium Saturation Pressure (psig)	Coolant Inlet Temperature (°F)	Number of Tests
1	5/03/90	Baseline	Ribbed(3)	100,000	40	5	86	11
1A	8/01/90	Baseline	Ribbed(4)	100,000	40	5	86	8
5	8/16/90	Baseline	Ribbed(4)	100,000	40	5	86	7
13	8/17/90	Baseline	Ribbed(4)	100,000	40	5	86	6
4	8/01/90	Heat Flux	Ribbed(4)	200,000	40	5	86	10
6	8/17/90	Heat Flux	Ribbed(4)	300,000	40	5	86	8
9	8/17/90	Heat Flux	Ribbed(4)	375,000	40	5	86	8
2	5/07/90	Pressure	Ribbed(3)	100,000	60	5	86	9
7	8/17/90	Pressure	Ribbed(4)	300,000	60	5	86	9
3	5/08/90	Helium	Ribbed(3)	100,000	40	1	86	8
3A	8/17/90	Helium	Ribbed(4)	100,000	40	15	86	6
15	8/15/90	Power Tilt	Ribbed(4)	100,000±20%	40	5	86	12
16	8/15/90	Power Tilt	Ribbed(4)	200,000±20%	40	5	86	10
10	8/1/90	Asymmetric	Ribbed(4)	200,000/0	40	5	86	7
1	11/14/89	Ribs	No Rib(1)	100,000	40	5	86	13
1A	02/01/90	Ribs	No Rib(2)	100,000	40	5	86	11
4	02/08/90	Ribs	No Rib(2)	200,000	40	5	86	11
2	02/05/90	Ribs	No Rib(2)	100,000	60	5	86	15
3	02/06/90	Ribs	No Rib(2)	100,000	40	1	86	9
								178

Greare

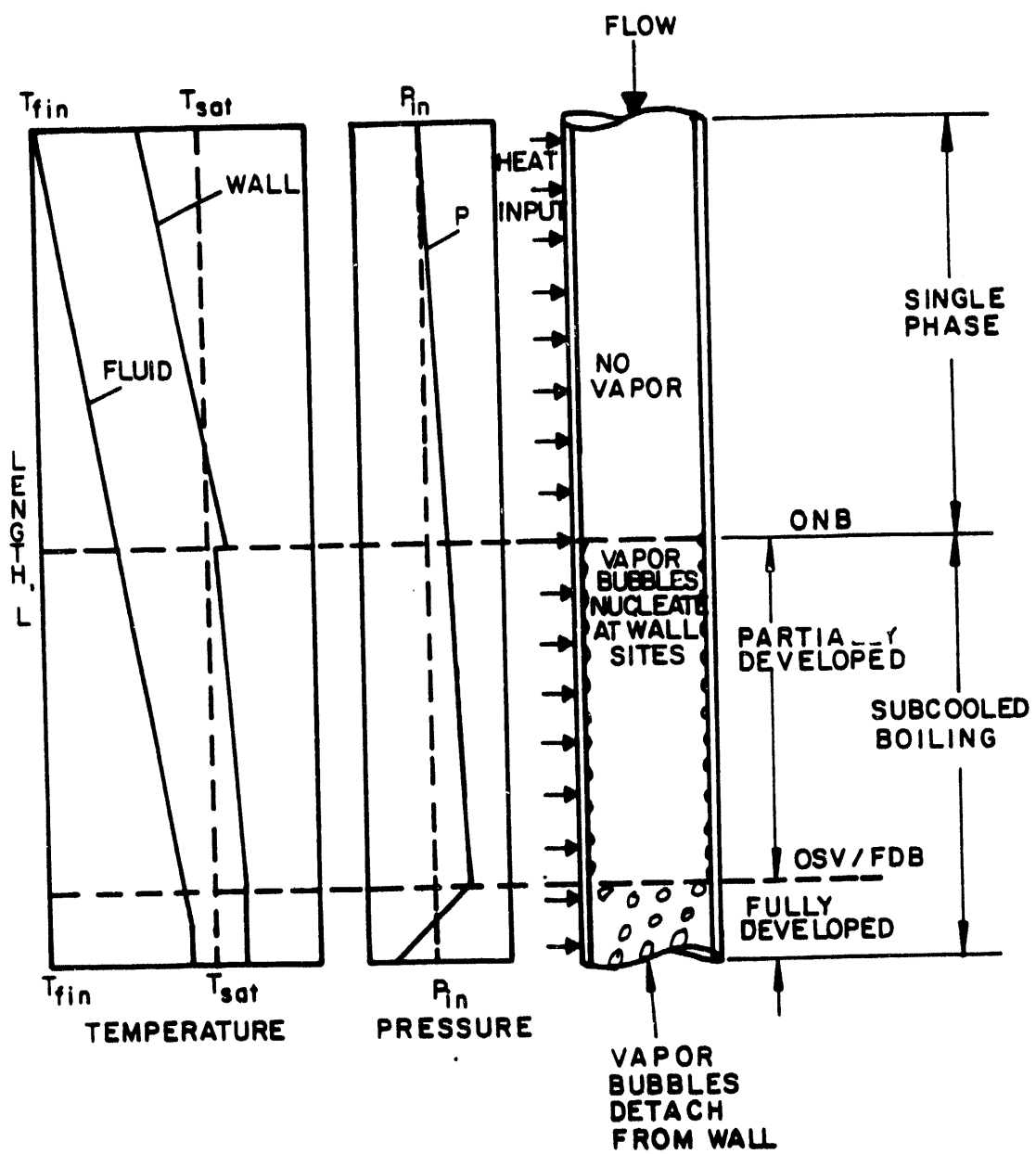

Figure 1.1 ILLUSTRATION OF BOILING FLOW PHENOMENA IN DOWNFLOW

The ANNULUS program uses selected models for heat transfer, energy balances, and momentum in each regime. The analysis comparisons are used to identify systematic trends in modelling the heat transfer and pressure drop. Appendix A summarizes the models used in the ANNULUS program for the comparisons presented in this report.

Section 4 summarizes the conclusions based upon the Creare experiments. It describes those effects which were found to be important experimentally. It also summarizes the areas in which the analytical models were found to work well and where alternative models are needed based upon the limited analytical modelling performed on the project.

2 TEST FACILITY

The test facility used for all of the non-ribbed and ribbed annulus tests is closed-loop, designed for steady-state testing with independent control of the annulus inlet pressure and temperature, flow rate, dissolved helium saturation pressure, and annulus wall heat flux. Test measurements include annulus wall and fluid temperatures, annulus pressure and pressure drop, flow rate and annulus wall heat input. These measurements are monitored and recorded by a computer-based data acquisition system. A second computer controls the power input to the annulus and monitors other test section temperatures and numerous safety interlocks in order to rapidly shut down the power. The facility is installed at Stern Laboratories in Hamilton, Ontario where there is a high quality DC power supply, adequate cooling water and other essential test support facilities and personnel. The following subsections provide additional descriptions of the Flow Loop (Section 2.1), Test Facility Operation and Control (Section 2.2), the Annulus Test Sections (Section 2.3) and the Test Measurements (Section 2.4).

2.1 Flow Loop

The flow loop is shown schematically in Figure 2.1. The main components of the loop (besides the annulus test sections which are described in Section 2.3) are listed in Table 2.1. Water is pumped from the Reservoir vessel through an orifice flow meter to the top of the annulus. After it is discharged from the bottom of the annulus into the Separator, the water is pumped through the heat exchangers and back to the Reservoir. Some of the cooled water is also circulated back to the Separator in order to maintain the temperature below saturation at the annulus exit pressure. The flow loop can also be operated in the reverse direction, i.e. with single-phase upflow in the annulus in order to purge air out of the loop when it is initially filled with water and for in-place thermocouple calibration tests. A helium gas "blanket" is maintained in the vapor space above the liquid in both the Reservoir and Separator vessels. Helium is also used for pressurizing the gas space in the Separator in order to maintain the desired pressure at the annulus inlet.

Power to the electrical heaters in the inner and outer annulus walls is supplied by a six-zone, 3.75 MW power supply. The current supply is generated with 12 pulse rectification which results in only a small amount of AC "ripple" at relatively high frequency (720 Hz) which does not affect the measurements. Each of the power supply zones (3 are 0.25 MW each and 3 are 1.0 MW each) are controlled independently, and the total power input to the test section heaters is controlled by the laboratory computer.

To ensure water quality, all of the flow loop components, piping and vessels are fabricated from either stainless steel (300 series) or aluminum alloys. No copper alloys are used in contact with the water in the closed-loop. Prior to testing the flow loop was cleaned with a detergent-type degreaser/emulsifier and then was thoroughly rinsed and flushed with de-ionized water. During test operation a small pump maintains a flow of water from the Reservoir through a set of 10 micron and 1 micron cartridge filters in order to remove particulate matter that may have loosened after the final rinse. This water is returned to the closed-loop at the inlet to the main circulating pump. The pH, conductivity and dissolved oxygen in the loop flow water are monitored.

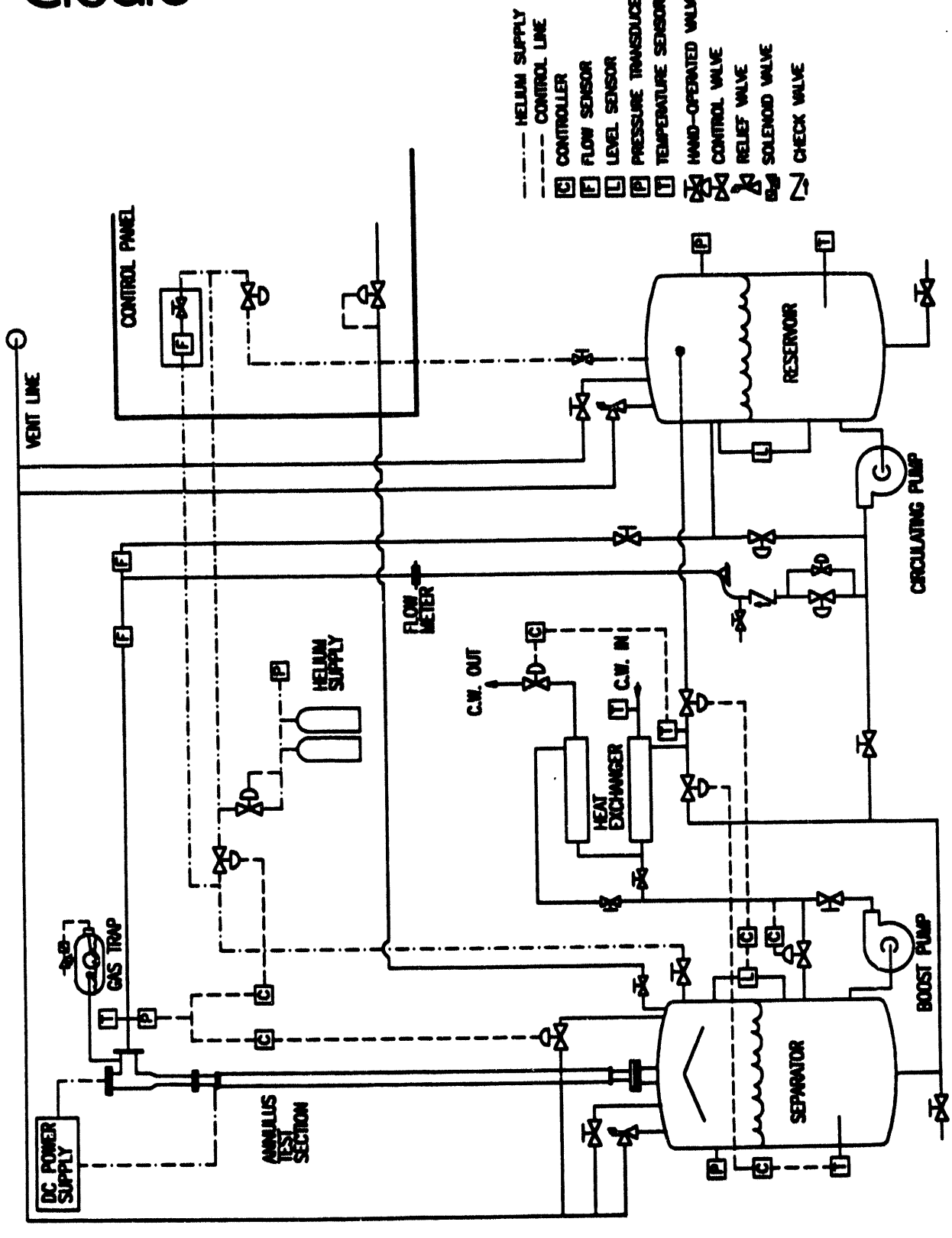

Figure 2.1 FLOW FACILITY FOR NUCLEATE BOILING PRESSURE DROP IN ANNULUS

Table 2.1 TEST FACILITY COMPONENT SPECIFICATIONS

ITEM	SIZE	SPECIFICATIONS	MATERIALS	VENDOR	MODEL NUMBER
Separator Vessel	5 ft. dia. x 8 ft. high Approx. 1000 gal.	100 psig W.P. ASME Sec.VIII Div.I	S30400	Massachusetts Eng.	Special
Reservoir Vessel	5 ft. x 8 ft. high Approx. 1000 gal.	100 psig W.P. ASME Sec.VIII Div.I	S30400	Massachusetts Eng.	Special
Heat Exchanger	(2) 1 ft. dia. x 12 ft. long 688 ft^2 Heat Transfer Surface	10.86 x 10^6 Btu/hr.	S30400	R. P. Adams	(2) AR14412-1NS
Circulating Pump	1 1/2 x 3-8, 30 HP	150 gpm @ 220 ft.	S31600	Gould Pumps	3196 ST
Boost Pump	1 1/2 x 3-8, 30 HP	150 gpm @ 220 ft.	S31600	Gould Pumps	3196 ST
Flow Control Valves	1 1/2 in.	Cv_{max} = 100	S31600	Jamesbury	21-3600-TT-0 B 30 S ACTUATOR
Check Valve	3 in.	ANSI 150 lbf	S31600	MUESSCO	3.0-72-H-H-H-G-H
Reservoir Press. Control	3/8 in.	50 scfm Supply 5 scfm Vent	Aluminum	Bellofram	231-960-091-010
Vessel Relief Valves	2 in.	@ 60 psig set 4887 lbm/hr. Steam 4960 scfm He 271 gpm Water	S31600	Kunkle	911JG31
Separator Level Control	Sensor Controller Valve 1 1/2 in.	25 - 150 in. W.C. Digital Cv_{max} = 86.8	S31600 - S31600	Fisher Controls	1151DP DPR 900 1 1/2-V100-1052 3620J
Boost Pump Pressure Control	Controller Valve 2 in.	Pneumatic/Mechanical Cv_{max} = 163	- S31600	Fisher Controls	4150 K 2-V150-1052
Annulus Inlet Temperature Control	Sensor Controller Valve 2 in.	RTD Digital Cv_{max} = 163	- - Steel	Fisher Controls	TE 1240 DPR 900 2-V150-1052-3620J
Annulus Inlet Pressure Supply Control	Sensor Controller Valve 2 in.	17-100 PSIG Digital $C_{v\ max}$ = 44.2	- - S31600	Fisher Controls	1151 GP DPR 900 2-1250RGL-3582G
Annulus Inlet Pressure Vent Control	Sensor Controller Valve 2 in.	17-100 psig Digital $C_{v\ max}$ = 369	- - S31600	Fisher Controls	1151 GP DPR 900 1-V150-1051-3620J
Separator Temperature Control	Sensor Controller Valve 1 1/2 in.	RTD Digital Cv_{max} = 86.8	- - S31600	Fisher Controls	TE1240 DPR900 1 1/2-V100-1052-3620J

Creare

2.2 Test Facility Operation and Control

During the tests, the thermal/hydraulic boundary conditions at the annulus are individually and independently controlled in order to establish the desired test conditions and to maintain steady-state operation during the data acquisition interval. The test facility is designed to produce typical ranges for the boundary conditions anticipated in an annulus of a fuel assembly during a hypothetical LOCA. The control and setting of the main test parameters are briefly described in the following paragraphs.

The *inlet temperature* of the water entering the annulus is maintained by a temperature controller which regulates the amount of cooling water supplied to the heat exchangers. A manually operated bypass diverts the loop flow around part of the heat exchanger for tests at low power input. The nominal value of inlet temperature for all of the tests is 86°F with a tolerance of ± 2°F. For a single test, the variation of inlet temperature around the setpoint is smaller than this, usually of the order of ± 0.5°F around the average value for the test.

Annulus *inlet pressure* is controlled by adjusting the pressure in the Separator Vessel. In the normal test sequence, as flow rate is reduced to a new value and annulus pressure drop correspondingly decreases, helium gas is automatically added to the vapor space in the Separator in response to the reduction in annulus inlet pressure. This then raises the inlet pressure to the desired setpoint value of either 40 psia or 60 psia, depending on the condition selected for that test. The tolerance on inlet pressure is ± 1 psia, although variations during the steady-state tests are of the order of ± 0.5 psia.

Water entering the annulus test section contains an amount of dissolved helium gas which is determined by the conditions established in the Reservoir. The *helium saturation pressure* in these tests is either 1 psig, 5 psig or 15 psig (minus the water vapor pressure of about 0.6 psia at 86 °F) which is maintained by a flow of gas through a pressure regulator into the Reservoir. In order to increase the effectiveness of dissolution of gas into the water, both the loop flow returned from the heat exchangers and a bypass flow from the main circulating pump are sprayed into the vapor space in the Reservoir, which increases the surface area of contact between the liquid and gas and hence the rate of mass transfer. The gas pressure in the Reservoir and Separator is maintained above atmospheric pressure at all times in order to avoid possible inflow of air which would reduce the helium partial pressure and lower the concentration of helium dissolved in the water.

Annulus *wall heat flux* is held constant on both the inner and outer walls for a series of tests. In the setup for a particular type of test, specific heaters (there are 24 in the outer wall and 12 in the inner wall) are connected to specific power supply zones according to a prescribed plan to produce one of three desired heat flux distributions - uniform, power tilt or asymmetric. Each power supply zone has individual voltage and current measurements which are input to the power supply control computer. The computer then adjusts the power provided from each zone in a fixed relationship to the total power to provide the correct heat flux distribution. Total power input is also controlled to maintain the desired average value of wall heat flux. For a specific test or series of tests at the lowest value of wall heat flux (100 kBtu/hr-ft^2), the power input can be set to produce an average heat flux on each of the outer and inner walls which is within about 1% of the nominal value. Regulation and control are even better than this at higher power levels.

Creare

Setup and operation of the test facility is straightforward and steady test conditions can be maintained indefinitely with only small deviations, which are well within acceptable tolerance limits, during the steady-state data recording period.

2.3 Annulus Test Sections

Two types of annulus geometries were tested in this program - non-ribbed and ribbed. Due to problems encountered with the heaters it was necessary to rebuild each annulus so that there were actually two separate hardware assemblies or "builds" for each type of geometry.

Type of Annulus	Geometry Build Number	In Use Until
Non-Ribbed	1	11/15/89
Non-Ribbed	2	02/09/90
Ribbed	3	05/10/90
Ribbed	4	08/17/90

This section describes the general arrangement of the annulus test sections and provides details for the 4 different assemblies employed in the testing program.

The basic flow geometry being modeled is coolant channel 3 of the Mark-22 fuel assembly shown in cross-section in Figure 2.2. The flow channel of interest is bounded by the inner and outer fuel tubes and is further divided into "subchannels" by the ribs on the inner wall. Inner and outer wall diameters and the rib dimensions define the geometry of the annulus for these tests. The approximate length of the fuel assembly is 13 feet.

Figure 2.3 shows the construction of the ribbed (upper drawing) and the non-ribbed (lower drawing) test sections. Basic construction details for the two arrangements are essentially identical, except for the use of pins in the non-ribbed assembly in order to centrally position the inner wall in the annulus.

The *outer wall* of the test sections is formed by the inner surface of an extruded aluminum (alloy 6063) tube which has a nominal inside diameter of 2.892 inches and 1 inch thick walls. The extruded tube has internal cavities in the wall which contain the 24 resistive element heaters used for heat input to the outer annulus wall. These heaters are approximately 0.37 inches in diameter and are 13 feet long. (The actual dimensions of the heaters as well as other inspection data for the test sections are documented in the Design Record File. As-inspected measurements of important geometric parameters for all 4 of the test assemblies are provided later in this section.) The outer wall extrusion has 5 "webs" located between groups of heaters which provide access through the wall for the annulus temperature and pressure instrumentation. The webs are at 0°, 48°, 136°, 224° and 312° relative to the direction of the inlet pipe located at the top of the test section.

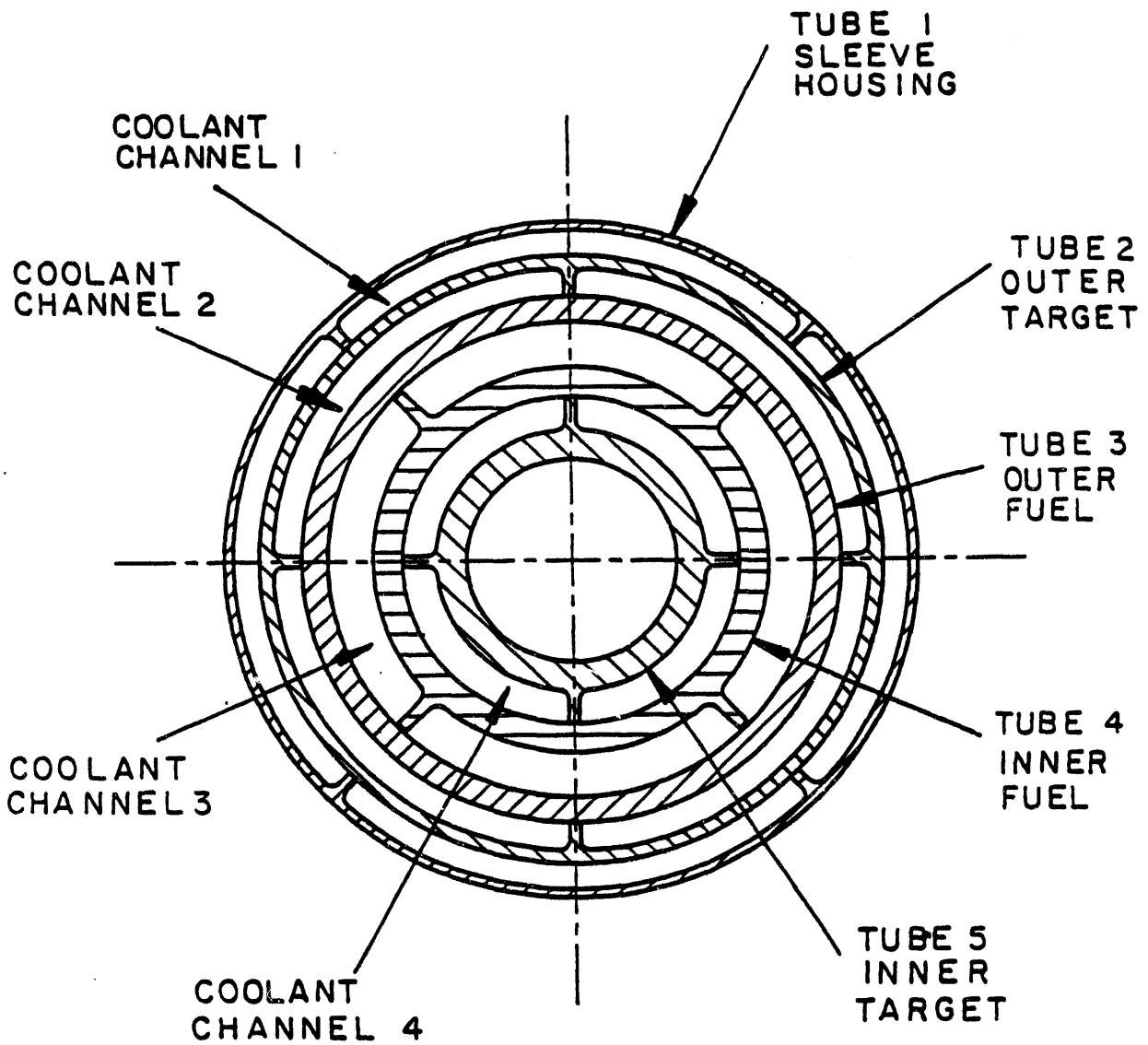

INNER FUEL RIB CIRCLE 2.862"
CLAD OD 2.353"
CORE OD 2.293"
CORE ID 2.055"
CLAD ID 1.995"

OUTER FUEL CLAD OD 3.200"
CORE OD 3.140"
CORE ID 2.952"
CLAD ID 2.892"

Figure 2.2 CROSS SECTION OF MARK-22 FUEL ASSEMBLY

Creare

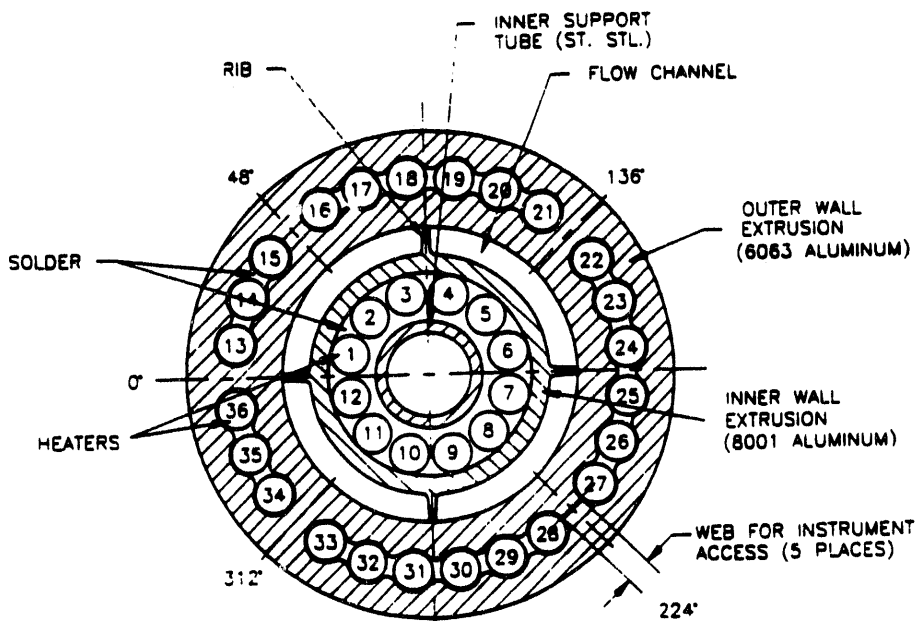

(a) Ribbed Annulus

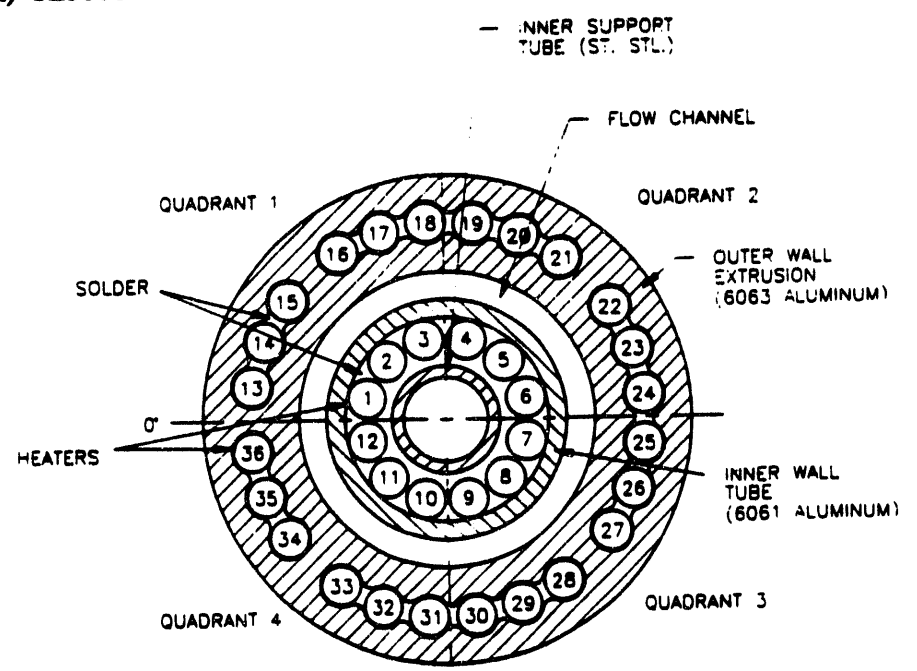

(b) Non-Ribbed Annulus

Figure 2.3 CROSS SECTION OF ANNULUS ASSEMBLIES IN THE EXPERIMENT

Ribbed inner wall tubes were extruded by Savannah River Laboratory using the same fabrication processes and surface cladding material (aluminum alloy 8001) as used for the fuel assemblies. The ribbed inner wall tube used for Geometry Build 3 is fabricated entirely from the alloy 8001, while the ribbed tube used for Build 4 has a core of aluminum alloy 5052 and is clad on both surfaces with alloy 8001. The *non-ribbed inner wall* is made from an aluminum tube (alloy 6061) which has been machined by sanding to the required outer wall diameter (for Geometry Builds 1 and 2). Sanding also produced a uniform surface finish. Twelve resistive heaters provide heat input to the inner wall of the annulus. These heaters are evenly spaced around the tube and are positioned against the inside surface of the aluminum tube by metal guides which are attached to the central support tube.

The narrow spaces surrounding the heaters in the outer wall cavities and inside the inner wall tube are filled with eutectic alloy tin-lead solder (63% tin/37% lead). The solder provides a conductive path between the heaters and the aluminum test section walls in order to ensure uniform and sufficient heat removal from the heaters and a known annulus wall heat flux.

The following subsections describe the main geometric features of the non-ribbed and ribbed annuli and provide dimensional data for the as-built test sections.

2.3.1 Non-Ribbed Test Section

Two versions of the non-ribbed annulus were constructed in this program (Geometry Builds 1 and 2). The major difference in the hardware between Builds 1 and 2 is the type of centering pin used to position the non-ribbed wall centrally within the annulus. Figure 2.4 shows the 0.094 inch diameter pins used for Build 1 and the "buttons" used for Build 2. Four centering pins or buttons are positioned evenly around the inner wall tube at 5 elevations as shown on the sketch of the test section in Figure 2.4. The heights of the pins and buttons above the tube surface are filed to produce a very small diametric clearance between the pins and the outer wall of the annulus.

Table 2.2a lists the as-built dimensions for the non-ribbed annuli, both Build 1 and Build 2. The information in this table is compiled from inspection reports which are located in the project Design Record File. The table gives a **Nominal Value** as well as a **Range** for each of the parameters. The Nominal Value, in the case of the measured parameters (inner and outer wall diameters and lengths), is simply the arithmetic average of the inspection measurements. For the calculated parameters (flow area, hydraulic diameter and surface area), the Nominal Value is calculated from these averages. The Range of the measurements given in the table is twice the standard deviation (2σ) of the data that comprise the averages; the Range of the calculated parameters is the calculated uncertainty based on twice the standard deviations of the average values.

2.3.2 Ribbed Test Section

Two versions of the ribbed wall test section were also constructed (Geometry Builds 3 and 4). The ribbed wall test sections were constructed to be as close to identical as possible; however, Build 4 used a different ribbed inner wall tube than was used in Build 3. As described earlier, Build 3 used an SRL-supplied "dummy" inner fuel tube which had been extruded from a solid piece of alloy 8001, whereas the inner wall for Build 4 was a sandwich

Creare

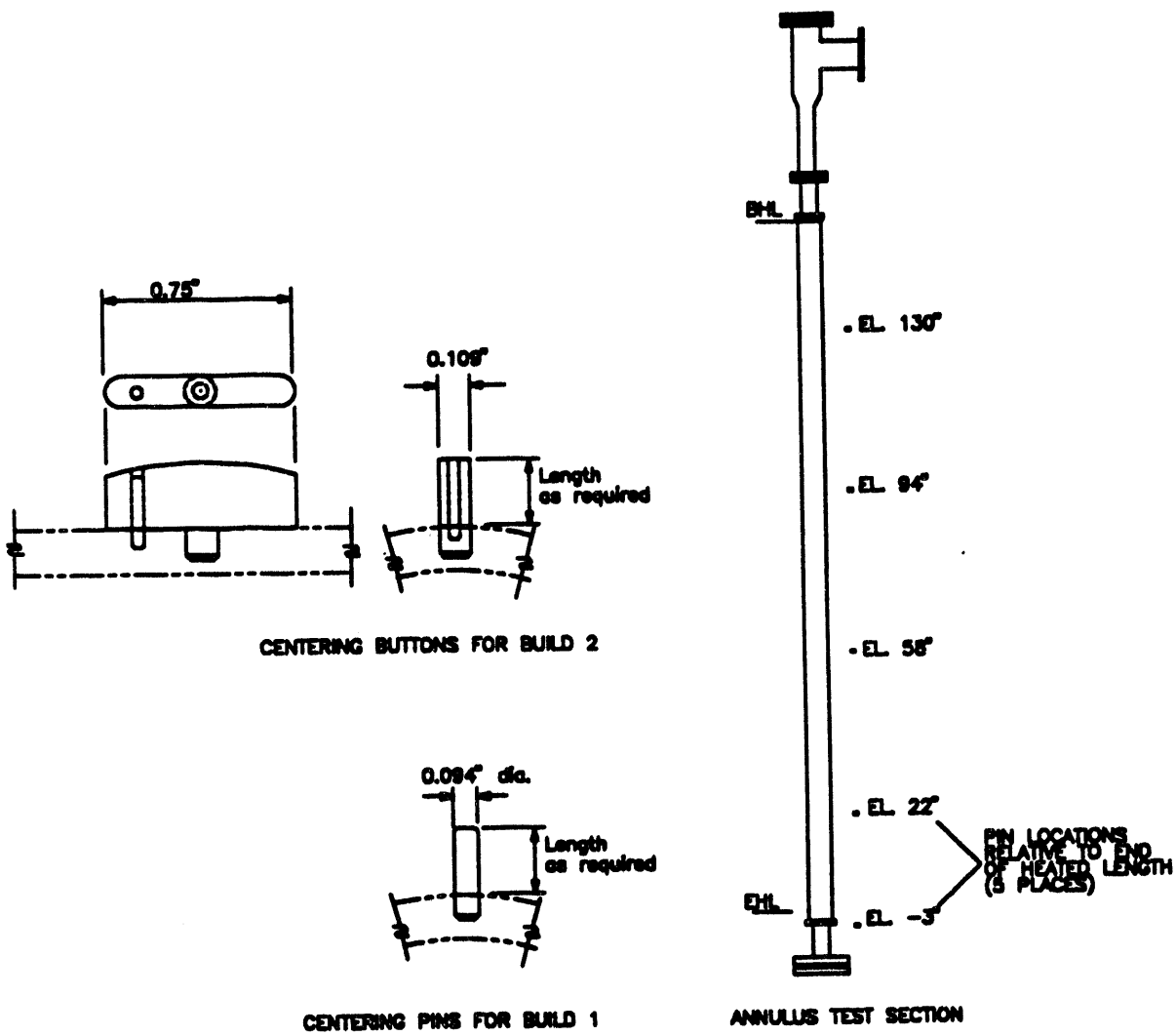

Figure 2.4 DETAILS OF PINS FOR CENTERING NONRIBBED INNER WALL

Greare

Table 2.2a GEOMETRY DATA FOR NON-RIBBED ANNULUS TEST SECTIONS		
Parameter	Nominal Value and Range	Nominal Value and Range
Geometry Build Number	1	2
Outer Wall Diameter, inches	2.894 ± 0.006	2.894 ± 0.006
Inner Wall Diameter, inches	2.368 ± 0.018	2.368 ± 0.018
Flow Area, ft^2	0.0151 ± 0.0005	0.0151 ± 0.0005
Hydraulic Diameter, ft	0.0438 ± 0.0003	0.0438 ± 0.0003
Outer Wall Heater Length, ft	12.815 ± 0.054	12.815 ± 0.054
Inner Wall Heater Length, ft	12.861 ± 0.058	12.861 ± 0.058
Outer Wall Surface Area, ft^2	9.709 ± 0.046	9.709 ± 0.046
Inner Wall Surface Area, ft^2	7.973 ± 0.070	7.973 ± 0.070
Pin/Button Clearance, inches	0.005 (min.)	0.007 (min.)

Table 2.2b GEOMETRY DATA FOR RIBBED ANNULUS TEST SECTIONS		
Parameter	Nominal Value and Range	Nominal Value and Range
Geometry Build Number	3	4
Outer Wall Diameter, inches	2.896 ± 0.006	2.896 ± 0.006
Inner Wall Diameter, inches	2.354 ± 0.0006	2.353 ± 0.0016
Flow Area, ft^2	0.0150 ± 0.0002	0.0150 ± 0.0002
Hydraulic Diameter, ft	0.0389 ± 0.001	0.0390 ± 0.001
Outer Wall Heater Length, ft	12.807 ± 0.064	12.807 ± 0.064
Inner Wall Heater Length, ft	12.855 ± 0.086	12.861 ± 0.058
Outer Wall Surface Area, ft^2	9.710 ± 0.053	9.710 ± 0.053
Inner Wall Surface Area, ft^2	7.922 ± 0.053	7.923 ± 0.036
Rib Clearance, inches (0°/180°)	0.045 (avg)	0.045 (avg)
Rib Clearance, inches (90°/270°)	0.027 (avg)	0.020 (avg)

construction with 8001 on the outer and inner surfaces of the tube with a core of alloy 5052 (clad and core thickness have not been specified to Creare). Also, the heaters in the inner wall are different for the two builds and as a result have slightly different average lengths.

Table 2.2b lists the geometric data compiled from the inspection reports for Builds 3 and 4 and calculated as described above. The effect of the ribs on the flow area and hydraulic diameter is included in the calculated values for these parameters. The rib cross-section area (which reduces the available flow area in the annulus) and the wetted perimeter of the ribs (which increases the perimeter of the annulus thereby reducing the hydraulic diameter) are based on design values for the ribs on the fuel tubes. The surface area of the inner wall and, consequently, the calculated inner wall heat flux are based on the mean diameter of the inner wall tube without regard to the presence of the ribs.

2.4 Test Measurements

The test facility and the annulus test sections are instrumented for measuring pressure, pressure drop, temperature, flow rate and input power. In total, 132 instruments are connected through signal conditioners and amplifiers to a computer-based data acquisition system (DAS). These are the principal data which are used for analysis of the boiling heat transfer and pressure drop behavior of the annulus. In addition, there are approximately 50 other measurements, primarily temperatures, which are monitored by the laboratory power control computer for facility safety considerations. The details of the design of the instruments and the DAS are adequately described in the test plan report (Sam, et al., 1988), the related Appendix D (Crowley and Dolan, 1989) and the DAS operation manual (Stoedefalke, 1989). This section describes the overall arrangement and locations of the instruments and provides additional information which may be of assistance in the identification of the measurements and interpretation of the data.

2.4.1 Instrument Locations

Figure 2.5 and Table 2.3 (which is keyed to the symbols in Figure 2.5) give an overview of the instrumentation installed in the flow loop and in the test section annulus. The test facility instruments provide information to the operators for setting the test conditions. These measurements are also used to define the boundary conditions of the tests for data analysis. Instruments in the annulus measure the absolute pressure, pressure drop, and fluid and wall temperatures at numerous locations along the annulus length and around the circumference of the annulus.

Each instrument in the test facility which is connected to the DAS is assigned a unique 9-character identification describing the type of measurement as well as the location of the measurement in the test facility. Table 2.4 gives a general definition of this numbering system. The initial three letters of the code are self-explanatory. The 6 digits following the letters describe the specific locations of the measurements. For many of the measurements the digits are simply a sequential numbering of similar instruments. For example, IHT000001 to IHT000036 designate the current transducers and measurements corresponding to the 36 annulus wall heaters. Similarly, TRF000001 and TRF000002 designate the two reference junction thermocouples.

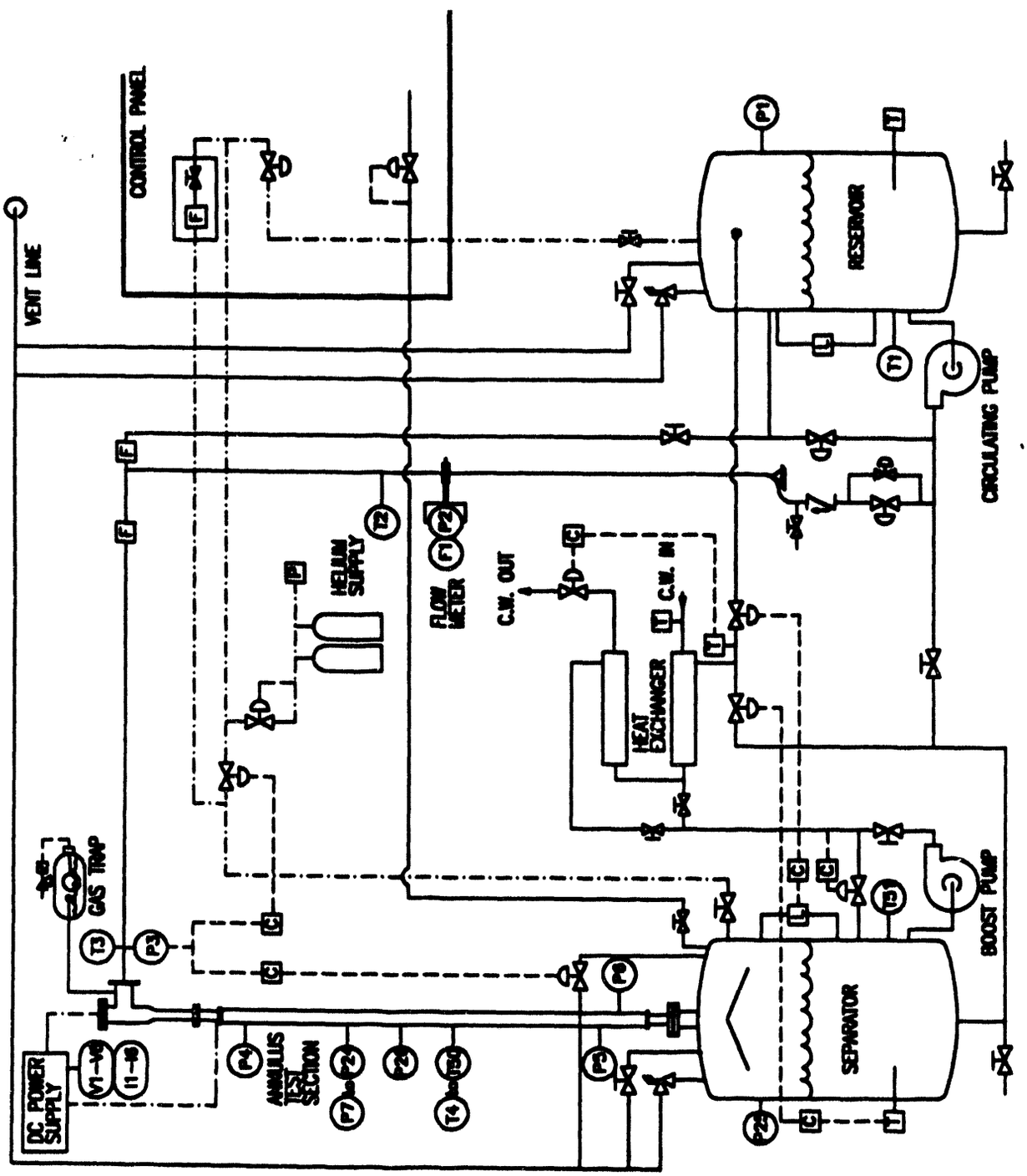

Figure 2.5 FACILITY INSTRUMENT LOCATIONS

Table 2.3 TEST FACILITY INSTRUMENT SPECIFICATIONS
(Identification keyed to Figure 2.5)

FACILITY LOCATION	MEASUREMENT	IDENTIFICATION	INSTRUMENT TYPE	MEASUREMENT RANGE
PROCESS	RESERVOIR PRESSURE	P1	GAUGE PRESSURE TRANSDUCER	0 - 100 psig
	RESERVOIR TEMPERATURE	T1	THERMOCOUPLE	32 - 310 °F
	WATER FLOW RATE	F1	ASME FLANGE TAP ORIFICE METER	20 - 200 gpm
		P2	DIFFERENTIAL PRESSURE TRANSDUCER	27 in. H_2O 150 in. H_2O
		T2	THERMOCOUPLE	32 - 310 °F
	ANNULUS INLET PRESSURE	P3	GAUGE PRESSURE TRANSDUCER	0 - 100 psig
	ANNULUS INLET WATER TEMPERATURE	T3	THERMOCOUPLE	32 - 310 °F
	SEPARATOR PRESSURE	P25	GAUGE PRESSURE TRANSDUCER	0 - 100 psig
	SEPARATOR TEMPERATURE	T51	THERMOCOUPLE	32 - 310 °F
	HEATER POWER SUPPLY VOLTAGE	V1-V6 (6 ZONES)	VOLTAGE TRANSDUCER	400 VDC
	POWER SUPPLY CURRENT	I1-I6 (6 ZONES)	CURRENT TRANSDUCER	1000 A 4000 A
	HEATER CURRENT	NOT SHOWN (36 TOTAL)	CURRENT TRANSDUCER	400 A rms
ANNULUS	ANNULUS PRESSURE	P4 - P6 (3 TOTAL)	ABSOLUTE PRESSURE TRANSDUCER	15 - 75 psia
	ANNULUS PRESSURE DROP	P7 - P24 (18 TOTAL)	DIFFERENTIAL PRESSURE TRANSDUCER	-36 to +214 in. H_2O
	ANNULUS OVERALL DIFFERENTIAL PRESSURE	P26	DIFFERENTIAL PRESSURE TRANSDUCER	-151 to +599 in. H_2O
	ANNULUS WALL AND RIB TEMPERATURES	T4 - T32 (29 TOTAL)	THERMOCOUPLE	32 - 350 °F
	ANNULUS WATER TEMPERATURE	T33 - T50 (18 TOTAL)	THERMOCOUPLE	32 - 310 °F

Creare

Table 2.4 ALPHA-NUMERIC IDENTIFICATION OF TEST INSTRUMENTATION			
Type of Measurement	Location	Number of Measurements	Identification Number
Temperature	Reference Junction	2	TRF000001, TRF000002
	Reservoir	1	TRV000001
	Separator	1	TSR000001
	Flow Meter	1	TFM000001
	Annulus Inlet	1	TIN000001
	Annulus Fluid	18	TAF*
	Annulus Outer Wall	18	TAO*
	Annulus Inner Wall	4	TAI*
	Wall at Rib Tip	6	TRT*
	Rib Root	1	TRR*
	Inner Seal Water	2	TSI000001, TSI000002
	Outer Seal Water	2	TSO000001, TSO000002
Pressure	Reservoir	1	PRV000001
	Separator	1	PSR000001
	Flow Meter ΔP	2	PFM000001, PFM000002
	Annulus Inlet	1	PIN000001
	Annulus ΔP	19	PAN*
	Annulus Absolute	3	PAB*
Current	Heater Element	36	IHT000001 to IHT000036
	Power Supply Zone	6	IPW000001 to IPW000006
Voltage	Power Supply Zone	6	VPW000001 to VPW000006

*Note: Identification Numbers marked with asterisk (*) are further defined in Table 2.5

Table 2.5 lists all of the measurements in the annulus. The table is supplemented by Figure 2.6, which shows the annulus measurement locations approximately to scale on a sketch of the annulus outer wall, and Table 2.6, which lists the exact location of each annulus instrument.

2.4.2 Data Acquisition and Reduction

All of the instruments connected to the DAS computer are recorded at the rate of 10 times per second. The computer displays a 5 second "rolling average" of the measurements as well as all reduced parameters (e.g., velocity, heat flux, etc) on a video monitor. The readings are also stored by the computer in a data block which contains the most current 5 minutes of data and which is updated as each measurement is recorded. The data acquisition process is halted manually by the test operator after at least 5 minutes of steady-state operation at the desired test conditions. The raw data file from a test consists of 3000 readings for each instrument, or a total of about 400,000 readings in the entire data block. This block of data is further reduced to produce summary tabulations of the measurements and the calculated parameters for the first 5 seconds of the test (.SM1 file) and for the last 5 seconds (.SM2 file), as well as the differences between these files (.DIF file).

Copies of the summary files from the non-ribbed and the ribbed annulus tests are provided in the companion data report, Volume 2. The summary data files are also available on compatible media (3.5" or 5.25" floppy disks) as standard ASCII text files. Creare has previously provided information (letter, Crowley to Miller, 1990) which describes the file formats and an approach that would enable reading the files into other computer systems.

Some of the instruments, primarily annulus wall and fluid temperature probes, failed for a variety of reasons during the course of the testing program. These failures do not compromise the overall quality of the tests because it is required that the essential parameters be recorded in order for a test to be acceptable. Since it is not always possible to repair or replace failed instruments during a test, some of the tests may have fewer valid instruments than the total number of instruments described above. The failed instruments have been identified and lists of them are provided with the summary data in Volume 2.

2.4.3 Measurement Uncertainty

The summary data files also contain estimates of the uncertainty (at 20:1 odds) for the measured and calculated parameters. These estimates consider the possible errors from the instruments, signal conditioners and the analog-to-digital converter, plus the range of geometry variations described earlier. Table 2.7 lists the values of uncertainty determined for the measurements in this program. The uncertainties are given as a constant value plus a variable term which depends on the magnitude of the measurement. These would be combined to form a single value in a complete uncertainty analysis.

The error terms in general are independent of one another and are assumed to be random (bias or fixed errors are dealt with separately). Moreover, each test is essentially a single-sample experiment in which a single (averaged) value is obtained for each measurement. Thus, the uncertainty is calculated following the classical approach described by Kline and McClintock (1953) in which the uncertainty in the result is the

Creare

Table 2.5 INSTRUMENT IDENTIFICATION NUMBERS FOR ANNULUS MEASUREMENTS			
FLUID TEMPERATURE	ANNULUS OUTER WALL TEMPERATURE	ANNULUS INNER WALL TEMPERATURE	ANNULUS PRESSURE DROP
TAF120048	TA0120048	TAI130048	PAN120048
TAF130048	TA0130048	TAI130136	PAN130048
TAF020136	TA0020136	TAI130224	PAN020136
TAF050136	TA0050136	TAI130312	PAN050136
TAF070136	TA0070136		PAN070136
TAF080136	TA0080136		PAN080136
TAF090136	TA0090136		PAN090136
TAF100136	TA0100136		PAN100136
TAF105136	TA0105136		PAN105136
TAF110136	TA0110136		PAN110136
TAF115136	TA0115136		PAN115136
TAF120136	TA0120136		PAN120136
TAF125136	TA0125136		PAN125136
TAF130136	TA0130136		PAN130136
TAF120224	TA0120224		PAN120224
TAF130224	TA0130224		PAN130224
TAF120312	TA0120312		PAN120312
TAF130312	TA0120312		PAN130312
			PAN000136

ANNULUS RIB TIP TEMPERATURE	ANNULUS RIB ROOT TEMPERATURE	ABSOLUTE PRESSURE
TRT020000	TRR130000	PAB000316
TRT070000		PAB100136
TRT100000		PAB125136
TRT120000		
TRT125000		
TRT130000		

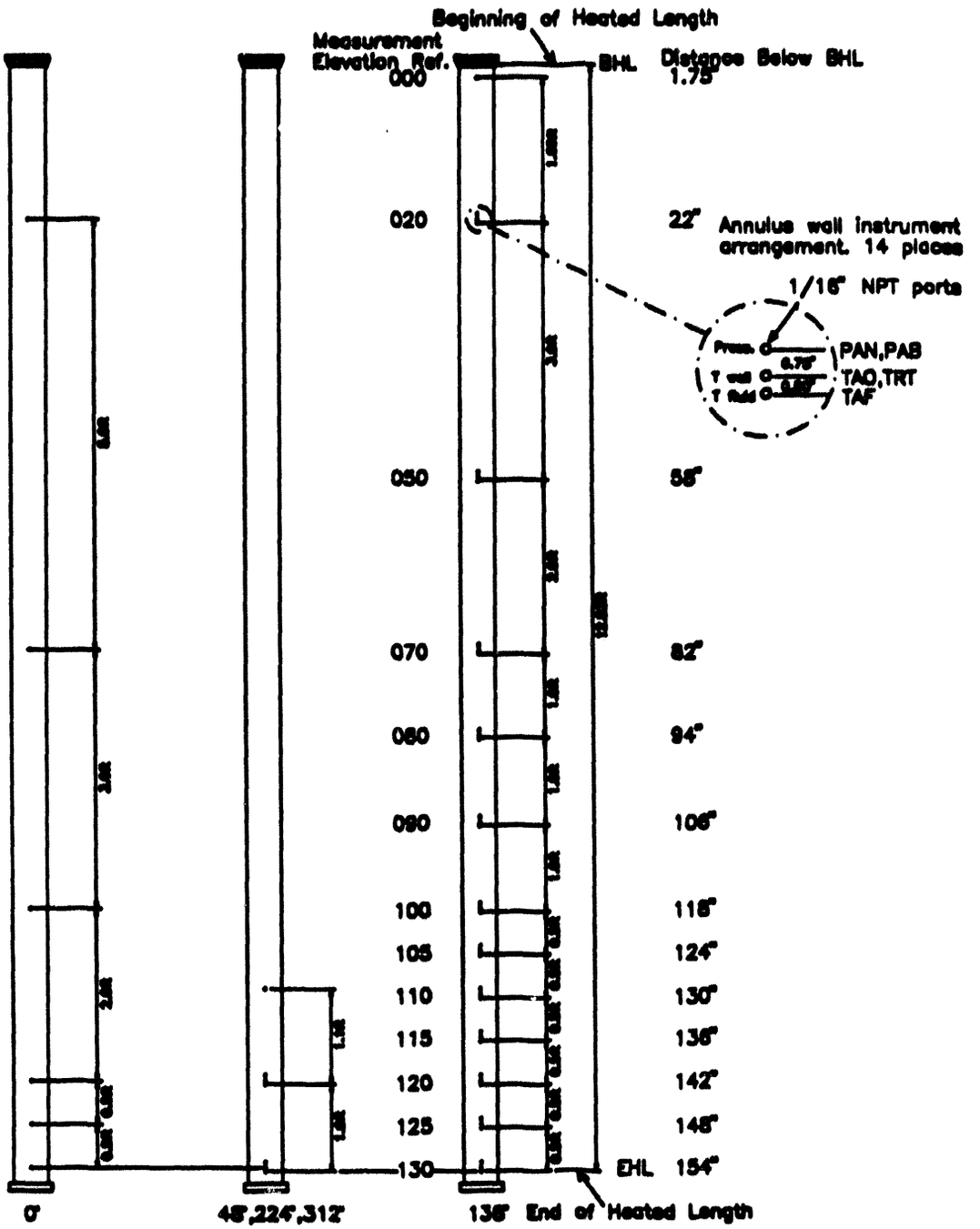

Figure 2.6 TEST SECTION INSTRUMENT LOCATIONS

Greare

Table 2.6 DETAILED LOCATIONS OF ANNULUS INSTRUMENTS

LOCATION IDENTIFIER YYY (FROM BEGINNING OF HEATED LENGTH)	ACTUAL DISTANCE FROM BEGINNING OF HEATED LENGTH (IN)				
	PAN YYY ZZZ		PAB YYY ZZZ	TAO YYY ZZZ TAI YYY ZZZ TRT YYY ZZZ TRR YYY ZZZ	TAF YYY ZZZ
	UPPER TAP	LOWER TAP			
000	1.75	152.75	1.75	-	-
020	1.75	20.75	-	21.50	22.00
050	20.75	56.75	-	57.50	58.00
070	56.75	80.75	-	81.50	82.00
080	80.75	92.75	-	93.50	94.00
090	92.75	104.75	-	105.50	106.00
100	104.75	116.75	116.75	117.50	118.00
105	116.75	122.75	-	123.50	124.00
110	122.75	128.75	-	129.50	130.00
115	128.75	134.75	-	135.50	136.00
120	134.75	140.75	-	141.50	142.00
125	140.75	146.75	146.75	147.50	148.00
130	146.75	152.75	-	153.50	154.00

IDENTIFIER: XXX YYY ZZZ

- ZZZ — Circumferential Location (048°, 136°, 224°, 312°)
- YYY — Distance from BHL, ft x 10
- XXX — Measurement type

Creare

Table 2.7 ESTIMATED MEASUREMENT UNCERTAINTIES (at 2σ level)		
Measured Parameter	Instrument and DAS Errors	
	Constant [1] (Units)	Variable [1] (% of Reading)
Temperature	1.9 °F	0.16
Annulus Pressure Drop	4.9 in. H_2O	0.25
Annulus Pressure Drop (local)	0.9 to 1.7 in. H_2O	0.25
Annulus Pressure	0.58 psia	0.25
Process Pressure	0.75 psia	0.25
Flow Meter Pressure Drop (1)	0.50 in. H_2O	0.25
Flow Meter Pressure Drop (2)	0.18 in. H_2O	0.25
Power Supply Voltage	0.82 VDC	0.60
Power Supply Current (Zones 1 to 3)	8.1 A	0.78
Power Supply Current (Zones 4 to 6)	2.0 A	0.78
Heater Element Current	4.1 A	1.0

[1] Constant and Variable terms to be combined as absolute values by RSS method

root-sum-of-squares of the weighted uncertainty in the individual factors which comprise the result. Each term in the calculation is evaluated at twice the standard deviation (2σ) of the average value used to calculate the result.

Creare

3. DISCUSSION OF TEST RESULTS

This section describes the experimental results. Comparisons of

- Demand curves,
- The onset of the flow instability, and
- Steady state pressure and temperature profiles.

are used to support the discussion where appropriate. Section 4.2 compares the minima in the demand curves with the Saha-Zuber model for OSV and discusses those results in detail.

3.1 Baseline

This subsection describes typical results from the experiments in the ribbed geometry at the baseline test conditions. Refer to Table 1.2 for the test conditions.

Baseline Demand Curves. Figure 3.1 shows the demand curve data for the baseline test conditions in the ribbed geometry. The basic character of the curve is consistent with data from the simple annular geometry at SRL and the tubular geometry at Columbia University. In the ribbed geometry of the Creare experiments, four baseline series were run between early May and the end of August 1990, including Series 1 in Build 3 and Series 1A, 5 and 13 Build 4 (see Table 1.2). Good repeatability is demonstrated. (Small variations occur at high velocity due to geometry changes in the facility -- see Section 2.) The minimum pressure drop occurs at a velocity between 3.20 and 3.44 ft/s in the four series of tests. The variation in velocity (0.2 ft/s) is approximately equal to the measurement uncertainty and hence the accuracy with which the velocity can be set in the tests. As described below, steady-state pressure drop data could not be obtained at lower velocities.

The pressure drop predicted by the ANNULUS computer program is shown by the solid line in Figure 3.1. The minimum pressure drop and corresponding velocity are predicted reasonably well. At this low velocity, the minimum pressure drop is dominated by the hydrostatic component, so the measured and predicted values represent primarily a head of 13 feet of water. The minimum pressure drop is predicted at only slightly lower velocity than observed in the data. This is consistent with the conditions at OFI lying at lower Stanton number, i.e. at higher velocity and higher subcooling, than calculated (Figure 1).

The pressure drop predicted by the ANNULUS computer program is 5% to 15% higher than the measured values at high flow velocity. This result is consistent with single-phase pressure drop data in the annulus with no heat flux, as shown in Figure 3.2. In the program, a hydraulic diameter of $D_h = 0.039$ ft has been estimated by strict application of the formula that the hydraulic diameter is four times the cross-sectional area divided by the wetted perimeter of the channel, where the wetted perimeter includes the surface of the ribs. If the ribs were not present, the hydraulic diameter for the annulus would be $D_h = 0.044$ ft. Calculated pressure drops with these two values of the hydraulic diameter bound the data, as illustrated by the pressure drop data for the unheated annulus in Figure 3.2.

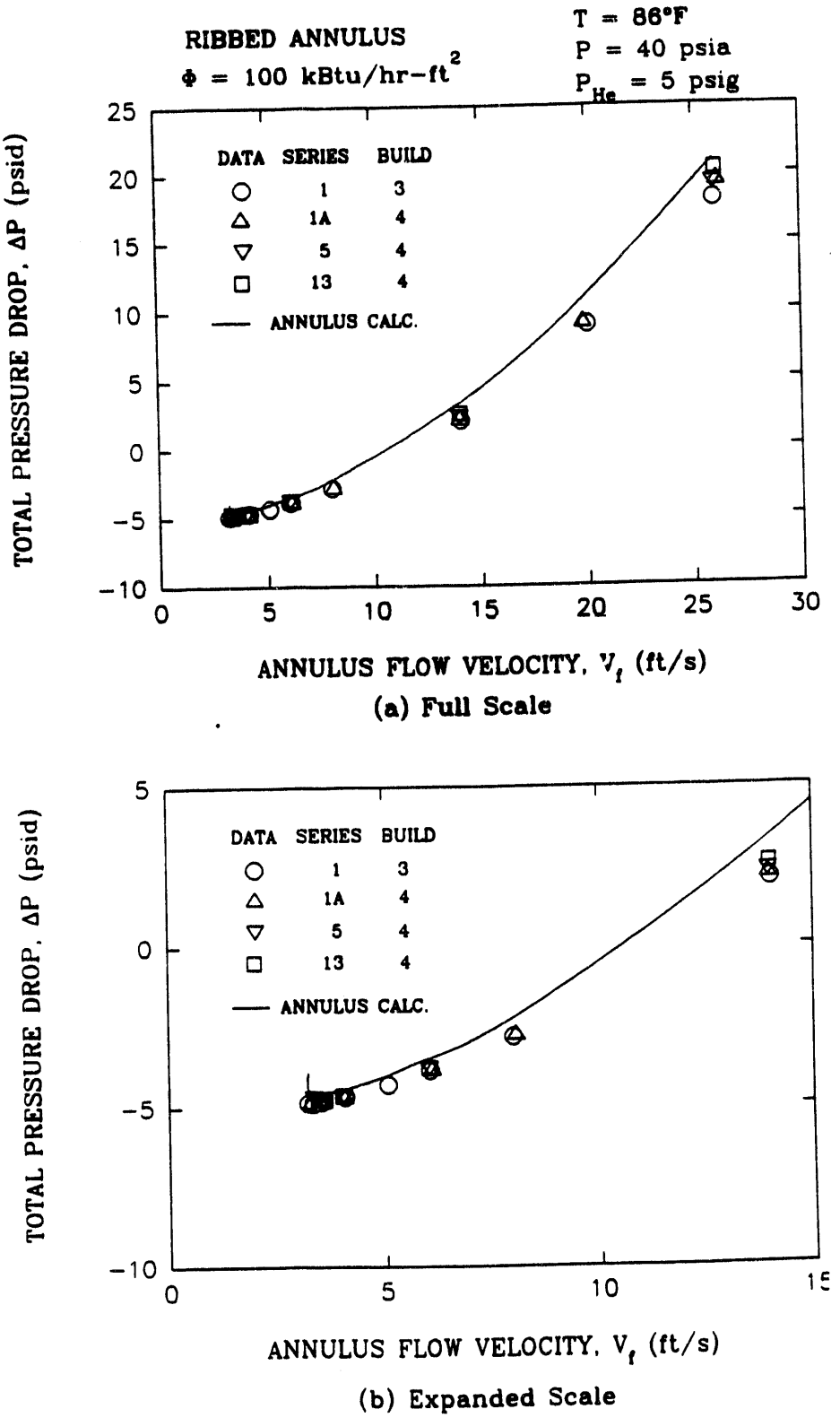

Figure 3.1 DEMAND CURVE FOR BASELINE TESTS IN THE RIBBED GEOMETRY

Creare

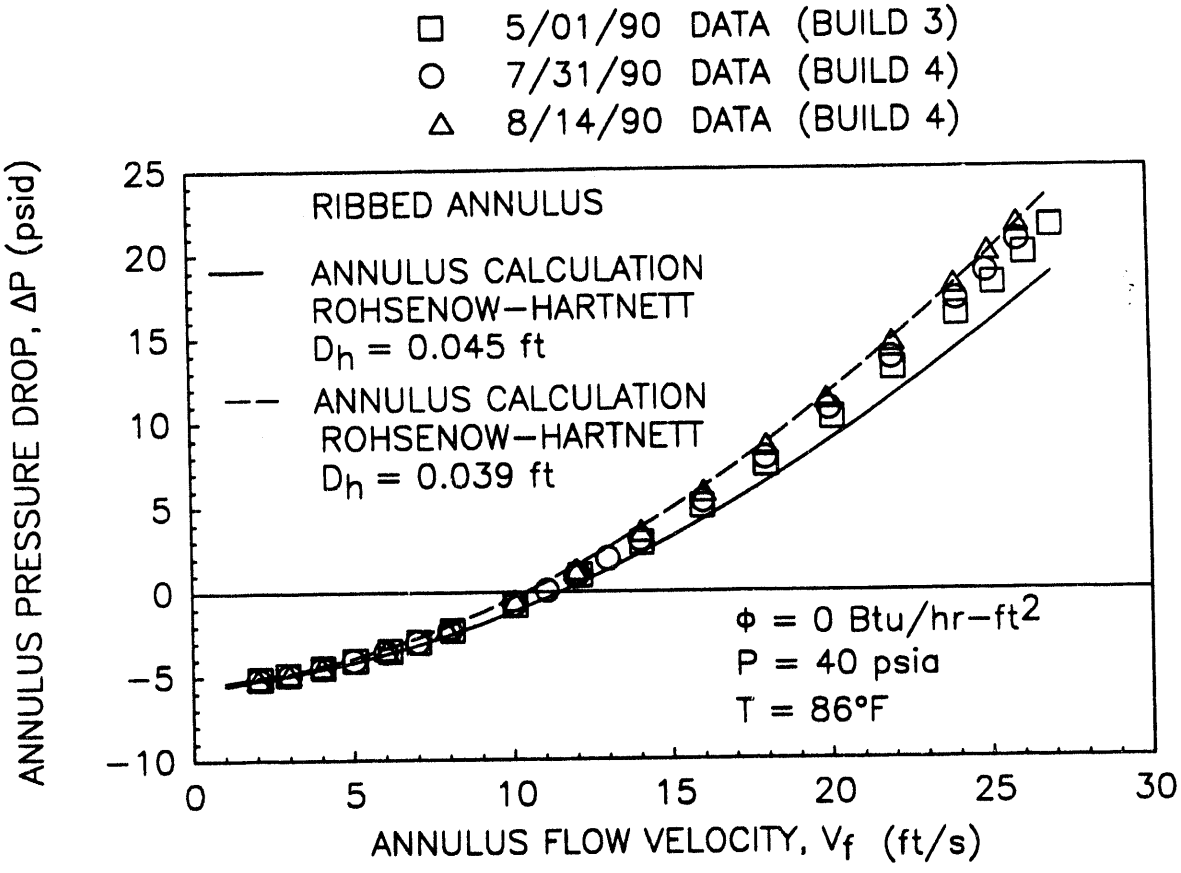

Figure 3.2 SINGLE-PHASE PRESSURE DROP IN THE RIBBED GEOMETRY

Creare

Onset of Flow Instability. In the ribbed geometry, it was not possible to obtain steady-state data at velocities below the minimum pressure drop. The pressure drop and wall temperature increase dramatically at velocities below this value. Figure 3.3 illustrates the unstable behavior in Test May07_10 from Series 2 in the ribbed geometry. (Because conditions were not steady in this test, the results are not incorporated in subsequent data evaluations.) The figure includes (a) the overall pressure drop in the annulus, (b) the outer wall temperature at 12.5 feet below the beginning of the heated length (BHL) in the annulus, and (c) the pressure drop at the orifice meter. With the flow and pressure boundary conditions nominally steady, the wall temperature and pressure drop in the annulus suddenly begin to increase. The wall temperature continues to increase after the pressure drop reaches a maximum value, and until the flow rate is increased by the operator to protect the facility.

Figures 3.4a and 3.4b show the outer wall and fluid temperature transients for four elevations in the instrumented flow channel at the 136° position for the same test and time period. The instability in temperature is initiated at the bottom and progresses toward the top of the annulus. The wall temperature near the bottom of the annulus continues to increase (Figure 3.4a), and fluid temperatures remain near saturation (Figure 3.4b) until the flow rate is increased by the operator. Recovery following the increase in flow rate is shown by the rapid decrease in the wall and fluid temperatures.

Circumferential variations in temperature are also observed. For the same test and time period, Figure 3.5a shows the wall temperatures in three subchannels near the annulus exit at 12 feet from the BHL. Figure 3.5b shows the corresponding fluid temperatures. Data are from the subchannels at 48°, 224°, and 312° positions. At the time of the instability, the wall temperature in the subchannel at 224° increases while the wall temperatures in the other two subchannels decrease (Figure 3.5a). Since the wall temperature at 12.5 feet from the BHL increased in the channel at 136° (Figure 3.4a), we conclude that the subchannels at 136° and 224° became unstable first, resulting in some of the flow being diverted to the other two channels. The fluid temperatures (Figure 3.5b) support this conclusion. The fluid temperature in the subchannel at 224° jumps to the saturation temperature. The temperatures in the other two subchannels oscillate between the saturation temperature and lower values, suggesting increased but possibly unsteady flow.

Pressure and Temperature Profiles. In Figures 3.6 through 3.9 detailed pressure and temperature profiles are shown for Series 1 in the ribbed geometry for:

- Non-boiling situation at high velocity (Figures 3.6 and 3.7),
- Near the onset of nucleate boiling at the exit (Figure 3.8), and
- At the minimum stable pressure drop (Figure 3.9)

To first order, the predictive models in the ANNULUS computer program represent the data very well. If the wall heat transfer coefficient used in the code calculations was about 10% larger, the agreement would be excellent.

The calculated and measured pressure gradients are linear in each case. The calculated and measured pressure gradients agree well at low velocity (Figures 3.8 and 3.9), but the pressure gradient is overpredicted by 15% at high velocity (Figure 3.6). This result is consistent with the pressure drop data for the unheated annulus, compared with the friction factor model using $D_h = 0.039$ in Figure 3.2. Note that the measured pressure gradient given by the summation of the individual differential pressures (open circles) agrees with the measured absolute pressure drops (solid circles).

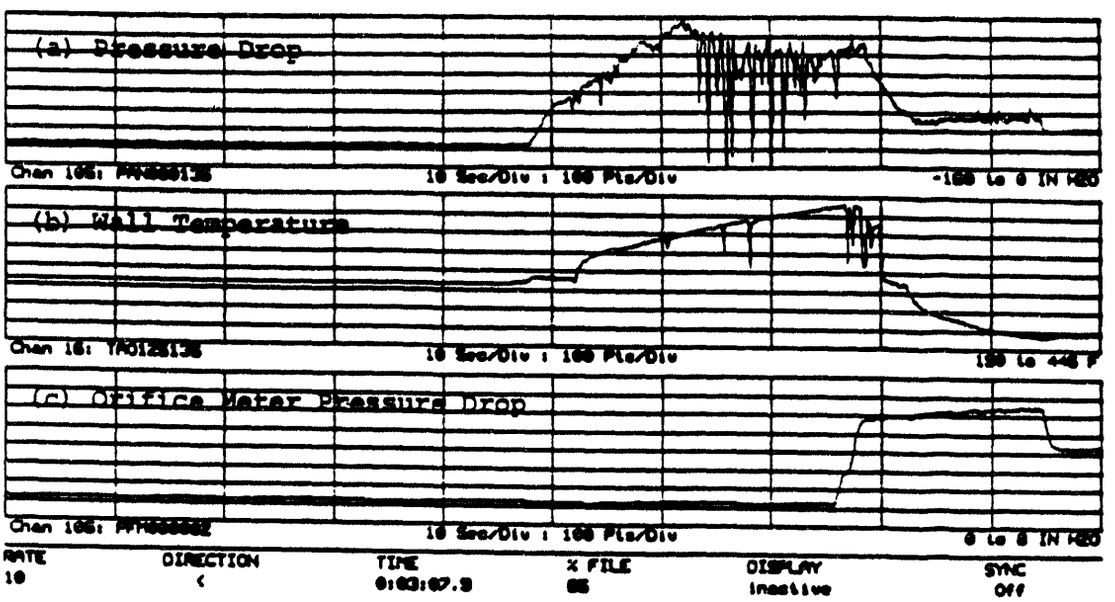

Figure 3.3 PRESSURE DROP AND WALL TEMPERATURE BEHAVIOR AT THE ONSET OF AN INSTABILITY

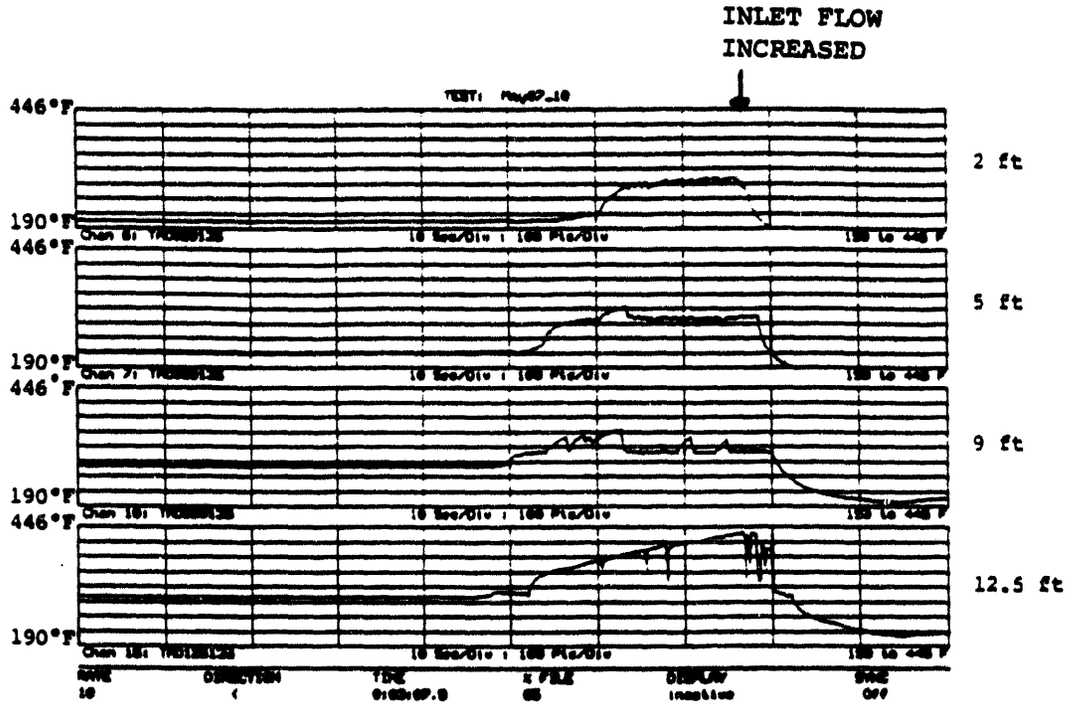

(a) Wall Temperatures

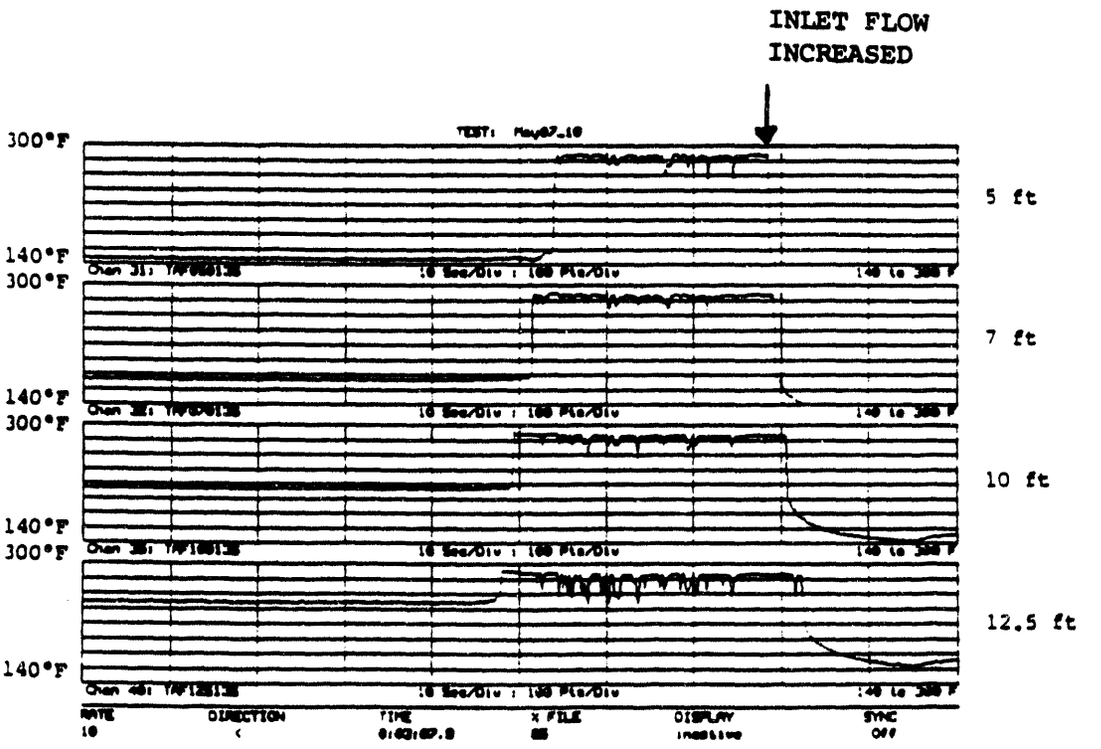

(b) Fluid Temperatures

Figure 3.4 TEMPERATURES ALONG ANNULUS AT THE ONSET OF AN INSTABILITY

Creare

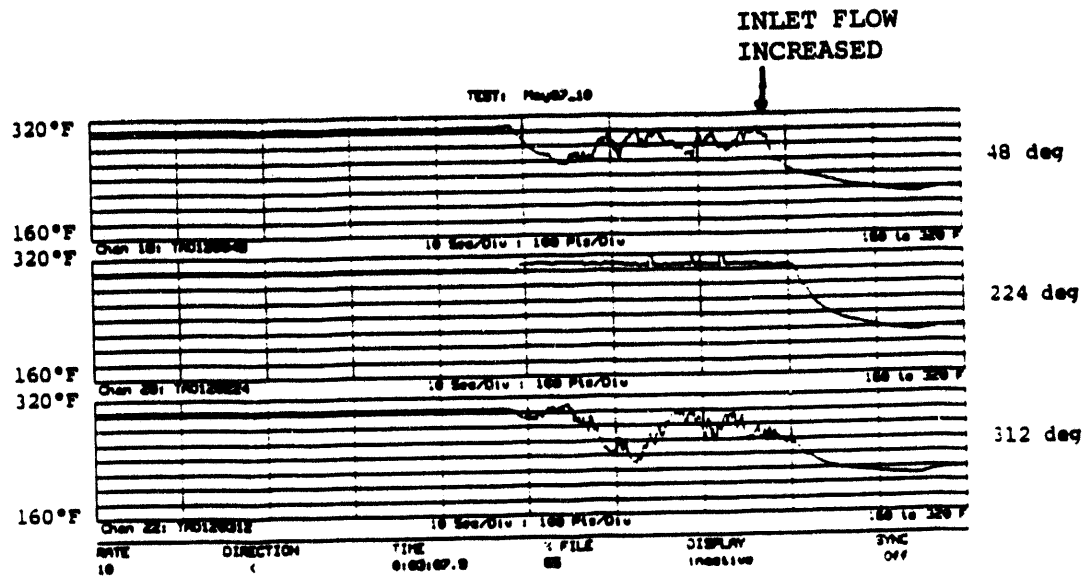

(a) Wall Temperatures

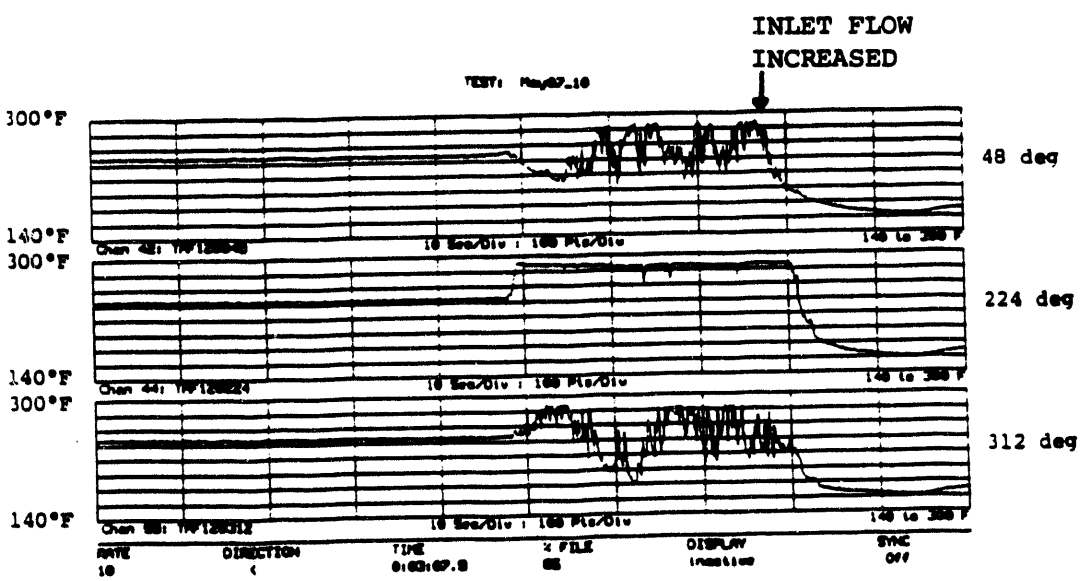

(b) Fluid Temperatures

Figure 3.5 EXIT TEMPERATURE AROUND THE CIRCUMFERENCE OF THE ANNULUS AT THE ONSET OF AN INSTABILITY

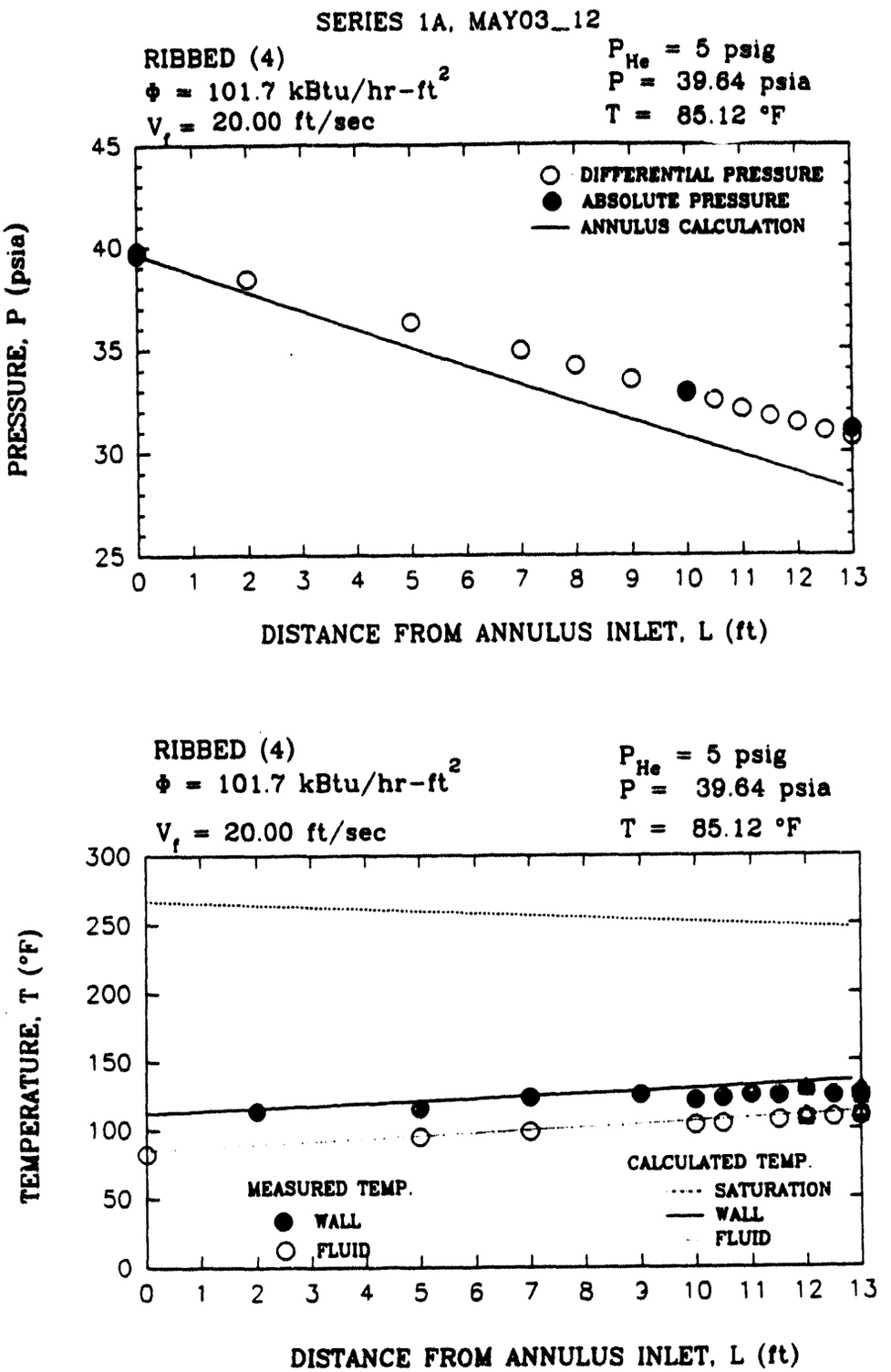

Figure 3.6 PROFILES FOR SINGLE-PHASE EXIT FLOW AT BASELINE CONDITIONS (V_f = 20 FT/S)

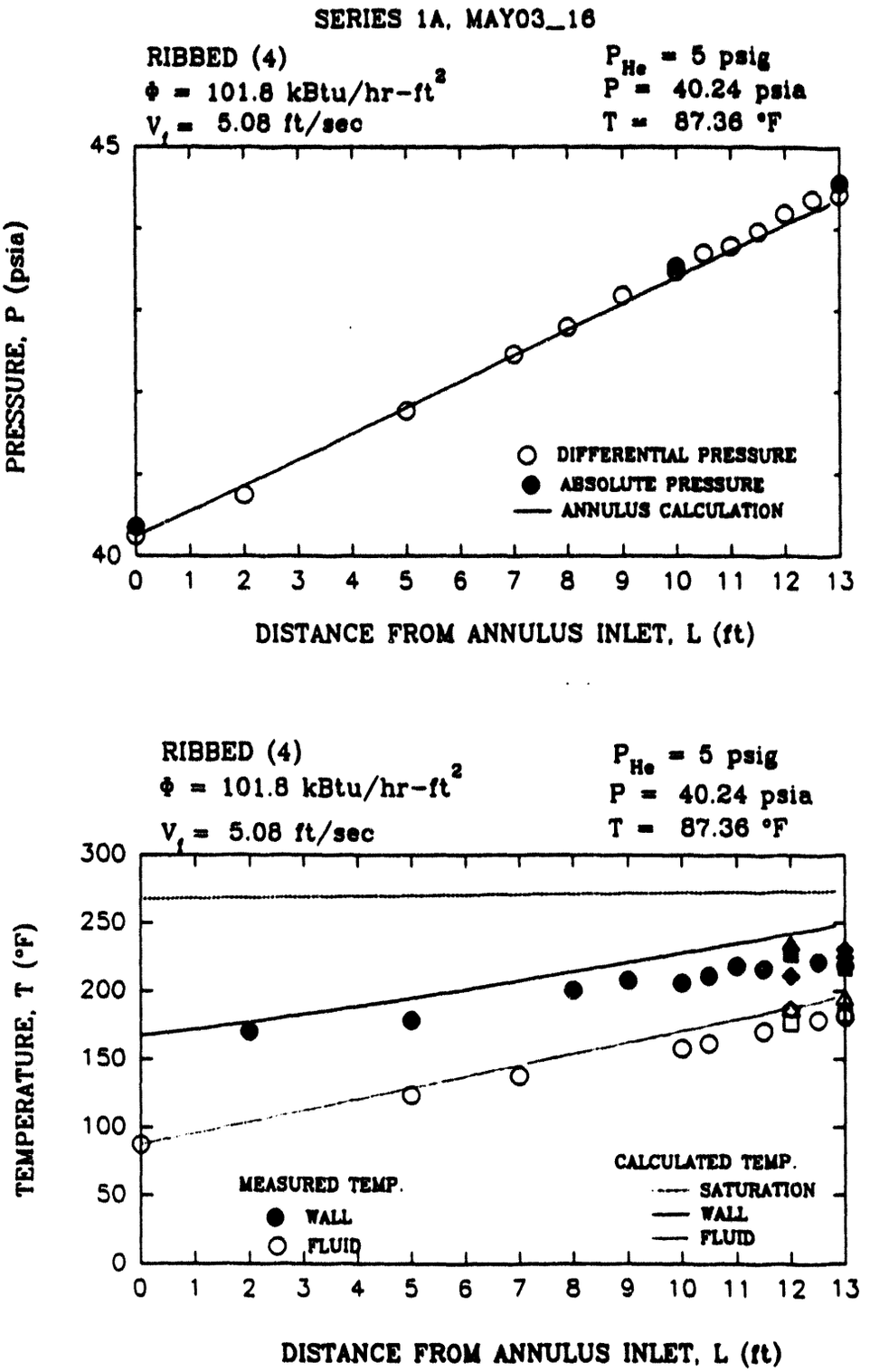

Figure 3.7 PROFILES FOR SINGLE-PHASE EXIT FLOW AT BASELINE CONDITIONS (V_f = 5 FT/S)

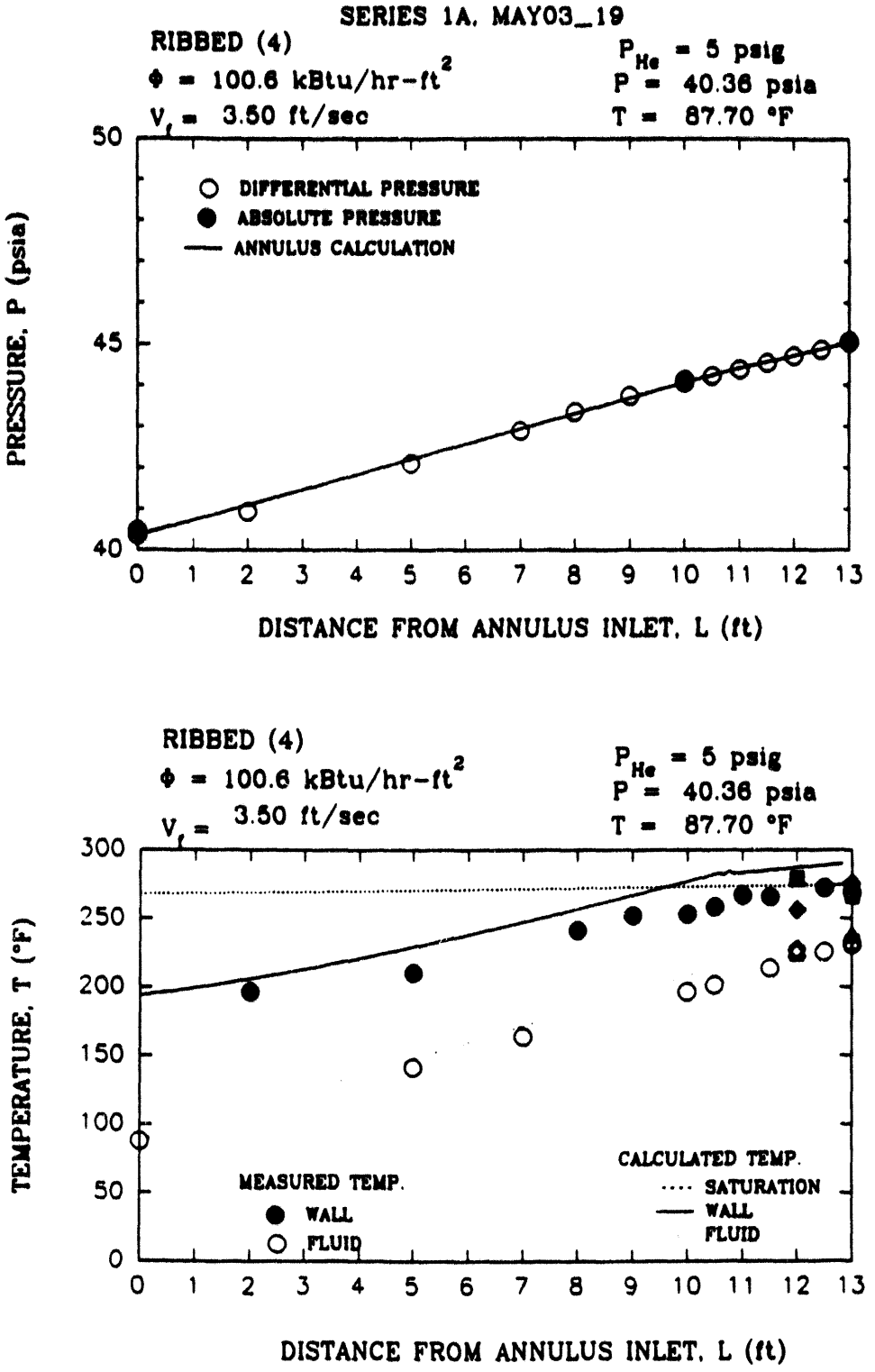

Figure 3.8 PROFILES FOR PARTIALLY DEVELOPED EXIT FLOW AT BASELINE CONDITIONS (V_f = 3.5 FT/S)

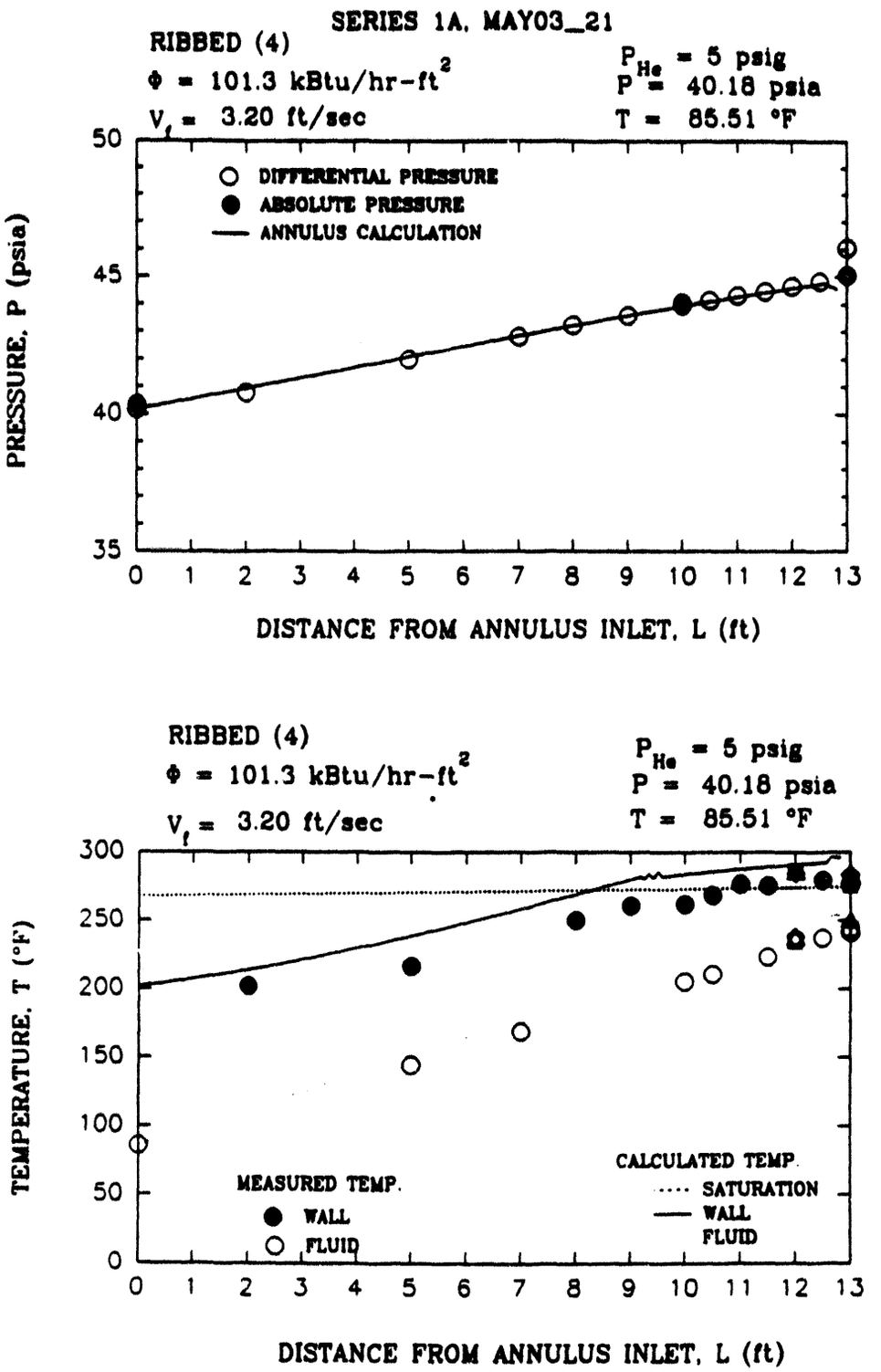

Figure 3.9 PROFILES FOR OFI EXIT FLOW AT BASELINE CONDITIONS (V_f = 3.2 FT/S)

Creare

The calculated and measured fluid temperatures also show a linear heatup. Calculated and measured values agree.

Wall temperature calculations illustrate a systematic trend observed in all of the data: the calculated wall-to-fluid temperature difference is about 10% larger than the measured value in the single-phase heat transfer region, i.e. before the wall temperature reaches saturation. At this heat flux, the overprediction is about 10% of the temperature difference. As a result, the wall temperature reaches saturation closer to the beginning of the heated length in the calculations than in the data (see Figures 3.7 and 3.8).

This series of figures also illustrates how the wall-to-fluid temperature difference increases as the inlet fluid velocity decreases. This is as expected since the heat transfer coefficient is lower at lower velocity. The analysis predicts this trend, though the calculations have a larger difference than the data, as mentioned above.

3.2 Effect of Heat Flux

The wall heat flux in the baseline experiments is 1×10^5 Btu/hr-ft^2. Heat fluxes up to 3.75×10^5 Btu/hr-ft^2 have been obtained in the ribbed geometry. Peak heat fluxes in the reactor fuel assemblies might be as high as 5×10^5 Btu/hr-ft^2, so heat fluxes up to three-fourths of the maximum were achieved.

Demand Curves. Figures 3.10 and 3.11 show the demand curves at various heat fluxes in the ribbed and nonribbed geometries, respectively. The minima in the demand curves occur at higher velocity and higher pressure drop for increased heat flux. For example, the minima occur at velocities of 3.27, 6.79, 10.03 and 12.60 ft/s for the heat fluxes of 1×10^5, 2×10^5, 3×10^5, and 3.75×10^5 Btu/hr-ft^2, respectively in the ribbed geometry (Figure 3.10, Series 1A, 4, 6 and 9). It can be shown by a simple equation that the velocity at the calculated OSV point should be approximately proportional to the heat flux, therefore it is not surprising that the velocities at the minima are also approximately proportional to the heat flux in both the data and the ANNULUS calculations.

For the higher heat fluxes, the calculated demand curves show a distinct change in slope as the minimum pressure drop is approached, though the slope is still positive. In the calculations, this deviation is associated with the Onset of Nucleate Boiling (ONB). The model for pressure gradient in the partially developed nucleate boiling regime calculates pressure gradients which are larger than in the single phase region, and apparently larger than in the data. The pressure and temperature profiles shown below illustrate the behavior in greater detail.

Pressure and Temperature Profiles. Figure 3.12 shows the pressure and temperature profiles for a single phase case at the highest heat flux tested (3.75×10^5 Btu/hr-ft^2). The only significant difference between the results at the highest and lowest heat fluxes is that the wall-to-fluid temperature difference in the single-phase regime is overpredicted by about a factor of two at the higher heat flux (Figure 3.12) rather than 10% as seen at the lower heat flux (Figure 3.6). The predicted temperature difference is between these limits (10% and 100% larger than measured) at the intermediate heat fluxes.

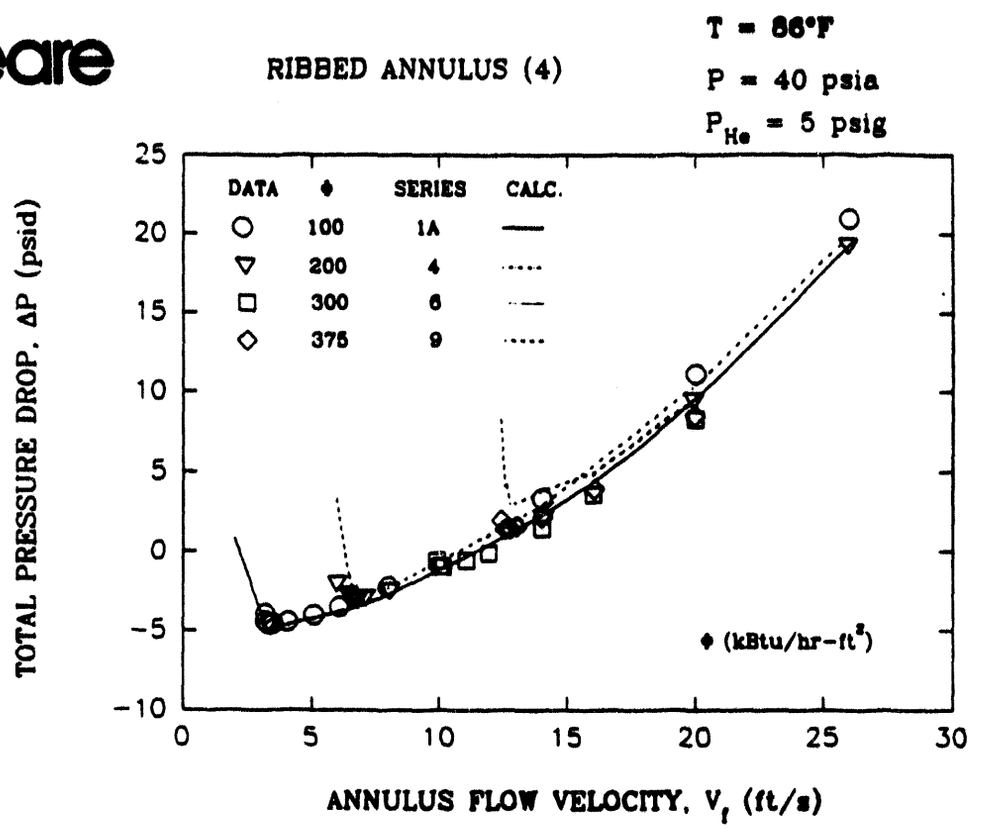

Figure 3.10 DEMAND CURVES FOR THE EFFECT OF HEAT FLUX IN THE RIBBED GEOMETRY

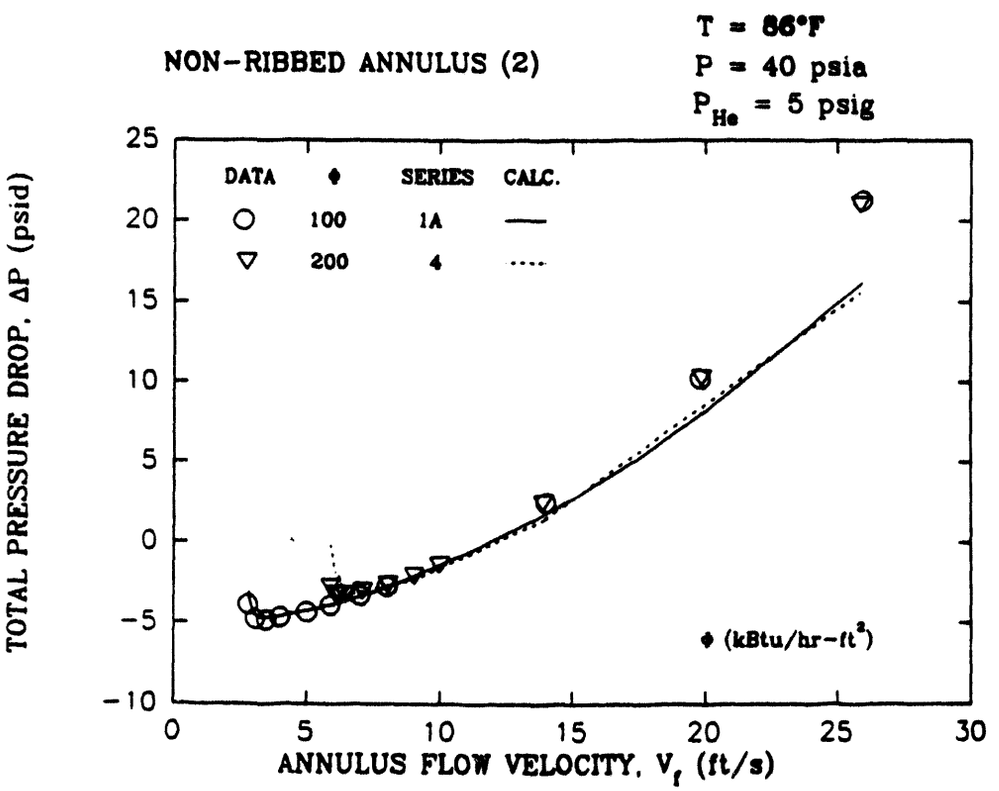

Figure 3.11 DEMAND CURVES FOR THE EFFECT OF HEAT FLUX IN THE NONRIBBED GEOMETRY

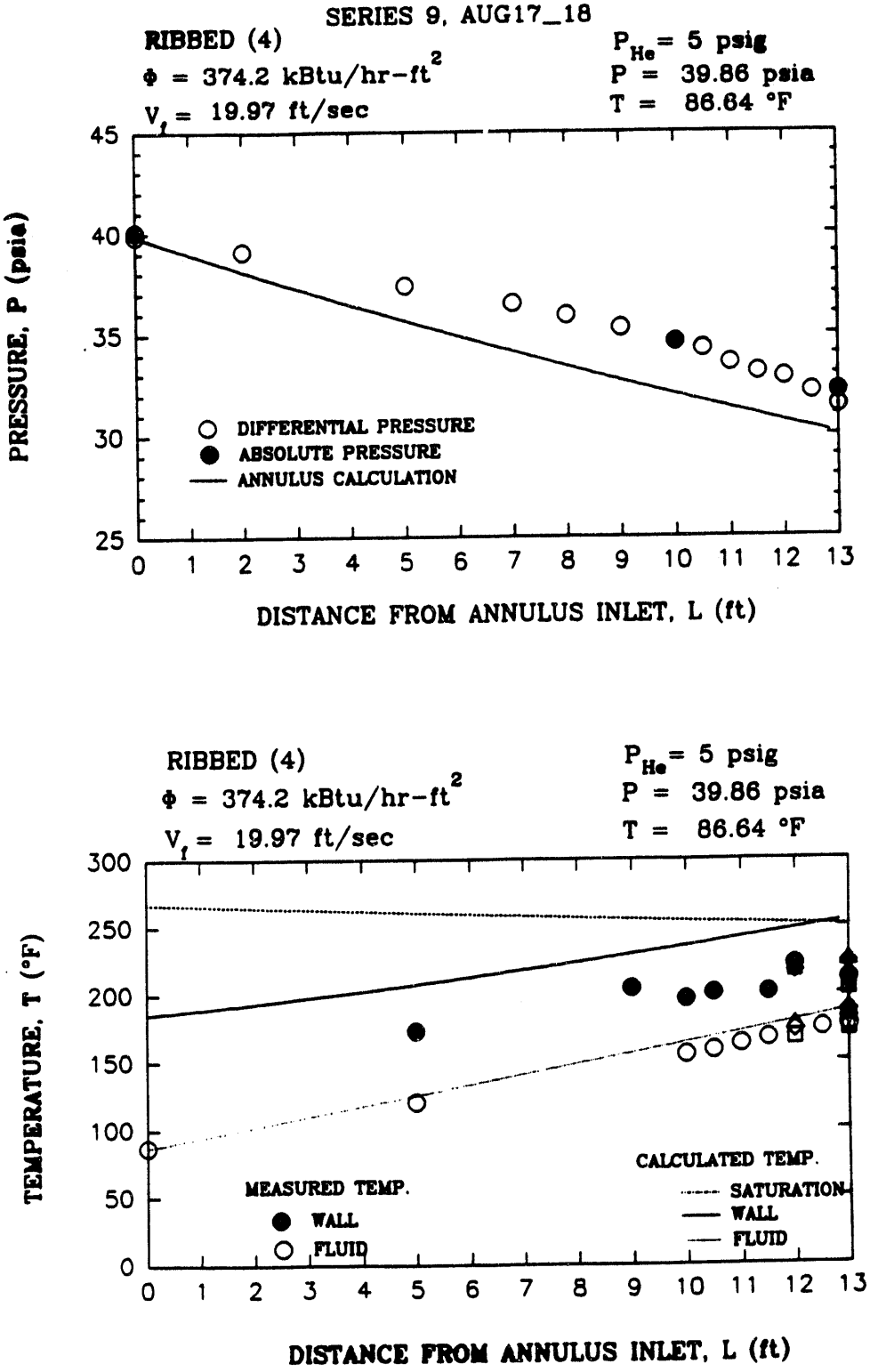

Figure 3.12 PROFILES FOR SINGLE-PHASE EXIT FLOW AT HIGH HEAT FLUX (V_f = 20 FT/S)

Figure 3.13 shows the data and calculations for a test near the minimum pressure drop at the highest heat flux tested. Although the velocities are different, this result can be compared with Figure 3.9, the test near the minimum pressure drop at the lowest heat flux tested. The wall and fluid temperature profiles are very similar in both cases; that is because both the heat flux and the velocity are higher in about the same proportion. The fact that the fluid subcooling at the exit of the annulus is about the same (about 20°F) near the minimum is consistent with relating the minimum to the Saha-Zuber model for the Onset of Significant Voiding. That model predicts OSV at a constant subcooling (in this velocity range).

At the higher heat flux in Figure 3.13, the measured pressure gradient changes noticeably to a steeper gradient at the point where the wall temperature reaches saturation (at 9 to 10 feet from BHL), i.e. near the location where the onset of nucleate boiling is expected. This behavior is not apparent at the lower heat flux (Figure 3.9). The calculations of the ANNULUS program include a model (Levy, 1967) for increased pressure gradient after ONB. The concept is that the wall is effectively rougher due to the presence of vapor bubbles which nucleate on the surface. Calculation of increased friction is consistent with the data, though the calculated pressure gradient is somewhat larger than observed in the data. Similar trends are observed at the intermediate heat fluxes.

3.3 Effect of Inlet Pressure

Demand curves illustrating the effect of inlet pressure in the ribbed geometry are shown for two different heat fluxes in Figures 3.14 (Series 1 and 2) and 3.15 (Series 6 and 7). Two inlet pressures of 40 and 60 psia have been tested in each case, representing the possible range of pressures during a LOCA in the reactor. Increasing the inlet pressure raises the saturation temperature. Therefore, in order for the fluid subcooling at the higher inlet pressure to reach the same value at OSV, a lower mass flux (velocity) is allowed at higher pressure for a given heat flux and inlet water temperature. That is, the minimum is expected to occur at a lower velocity, and this is evident in the data, particularly at the higher heat flux (Figure 3.15). At a heat flux of 1×10^5 Btu/hr-ft^2, the minima occur at velocities of 3.20 and 2.94 ft/s at the pressures of 40 and 60 psia, respectively. At a heat flux of 3×10^5 Btu/hr-ft^2, the minima occur at 10.03 and 8.84 ft/s, respectively.

At the low heat flux (Figure 3.14), the predictions of the ANNULUS program are in good agreement with the measured demand curve data. At high heat flux (Figure 3.15), the calculated velocities at the minima are slightly lower than observed in the data. In addition, the calculated pressure drop is somewhat larger than measured after ONB is calculated. This deviation is consistent with the discussion in Section 3.2 about the pressure gradient at high heat flux after ONB occurs.

Thus, the overall effect of pressure is entirely as expected.

3.4 Effect of Helium

In the reactor, helium blanket gas may be present at a saturation pressure of up to 5 psig. In the experiments, helium is used as the cover gas in the fluid supply reservoir. Pressures of 1, 5, and 15 psig have been tested. Figure 3.16 displays the demand curves obtained with the helium pressure varied in this range in Series 3, 1A, and 3A. The effect, if any, lies within the uncertainties in the measurements. No significant differences are observed in the pressure and temperature profiles.

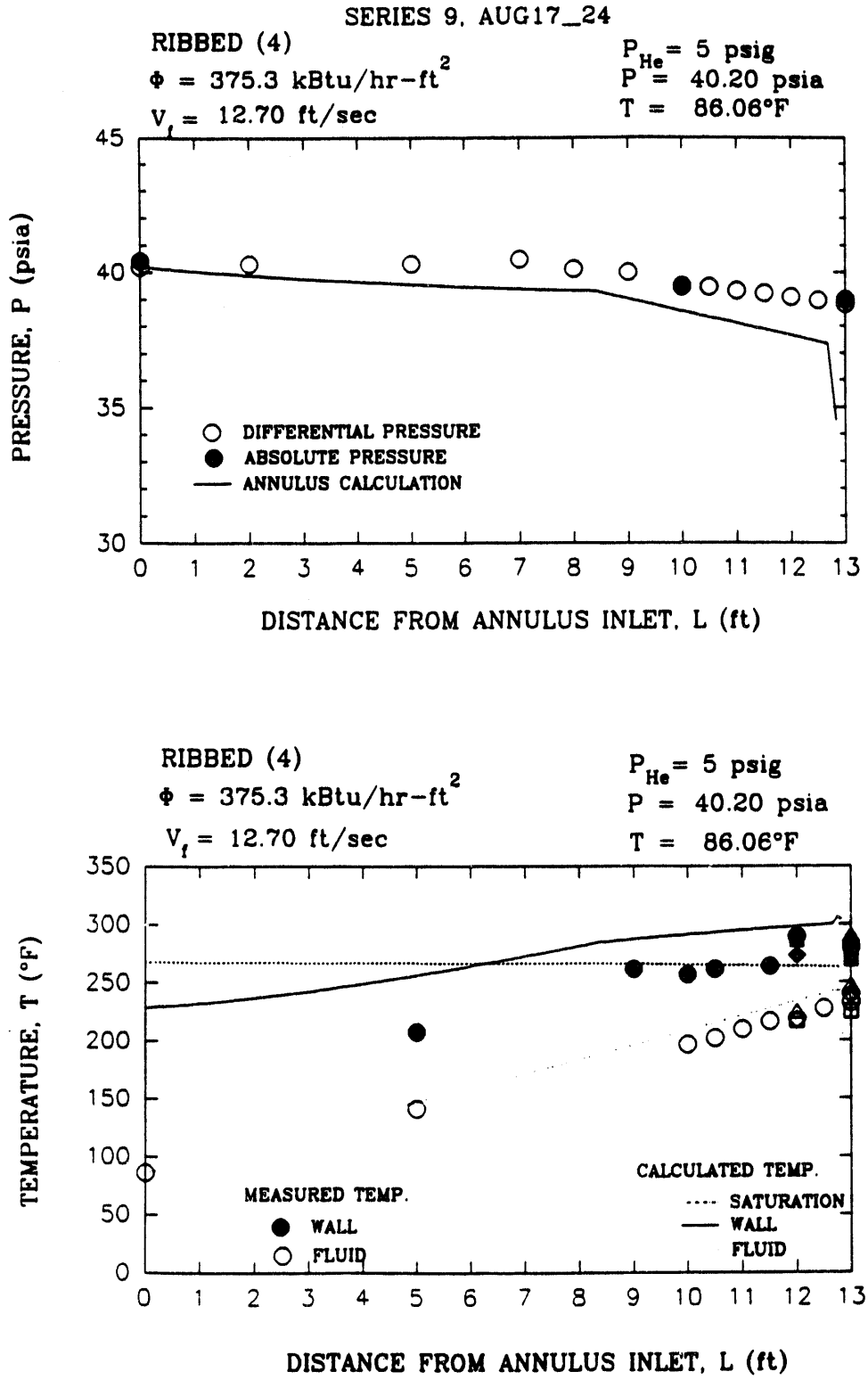

Figure 3.13 PROFILES FOR OFI EXIT FLOW AT HIGH HEAT FLUX (V_f = 12.7 FT/S)

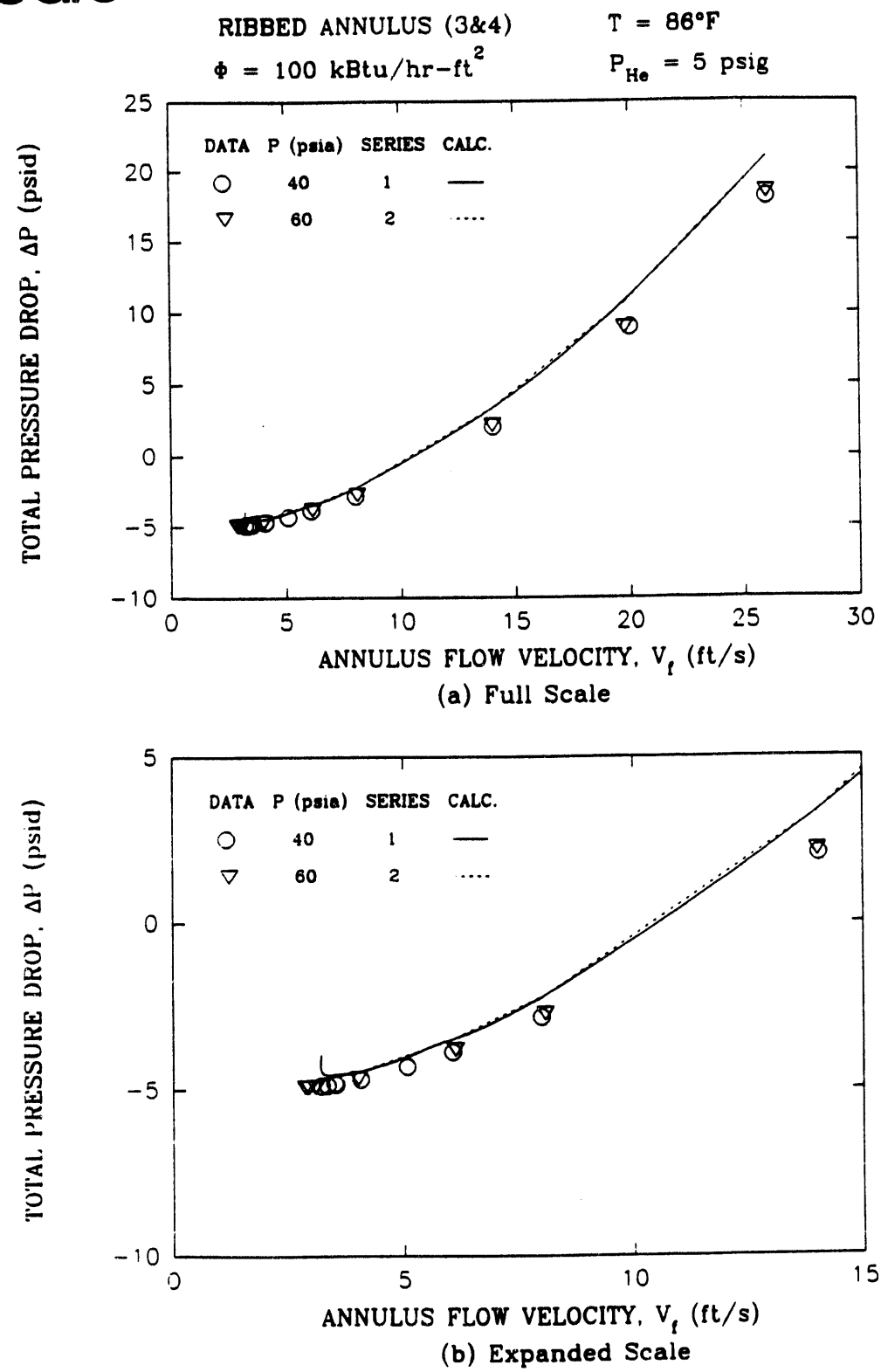

Figure 3.14 DEMAND CURVES FOR THE EFFECT OF INLET PRESSURE AT $\phi = 1 \times 10^5$ BTU/HR-FT² IN THE RIBBED GEOMETRY

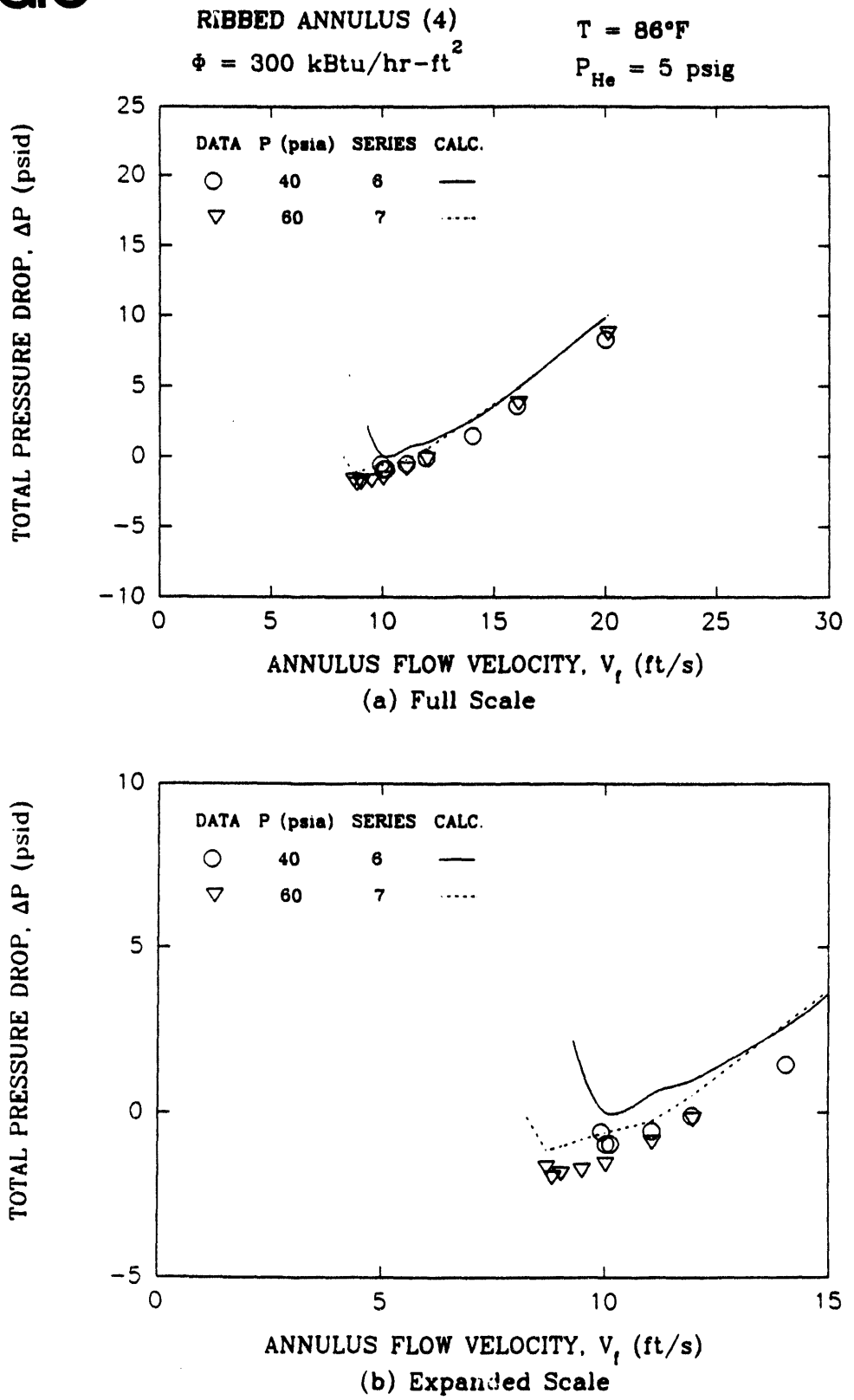

Figure 3.15 DEMAND CURVES FOR THE EFFECT OF INLET PRESSURE AT ϕ = 3 X 10^5 BTU/HR-FT² IN THE RIBBED GEOMETRY

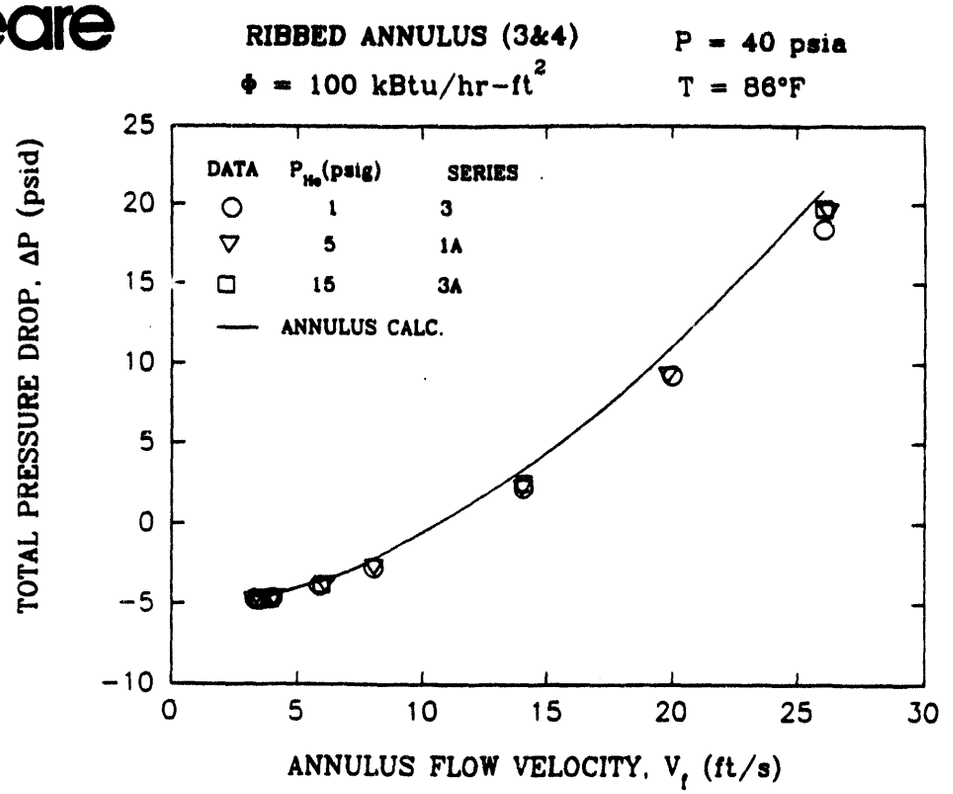

(a) Full Scale

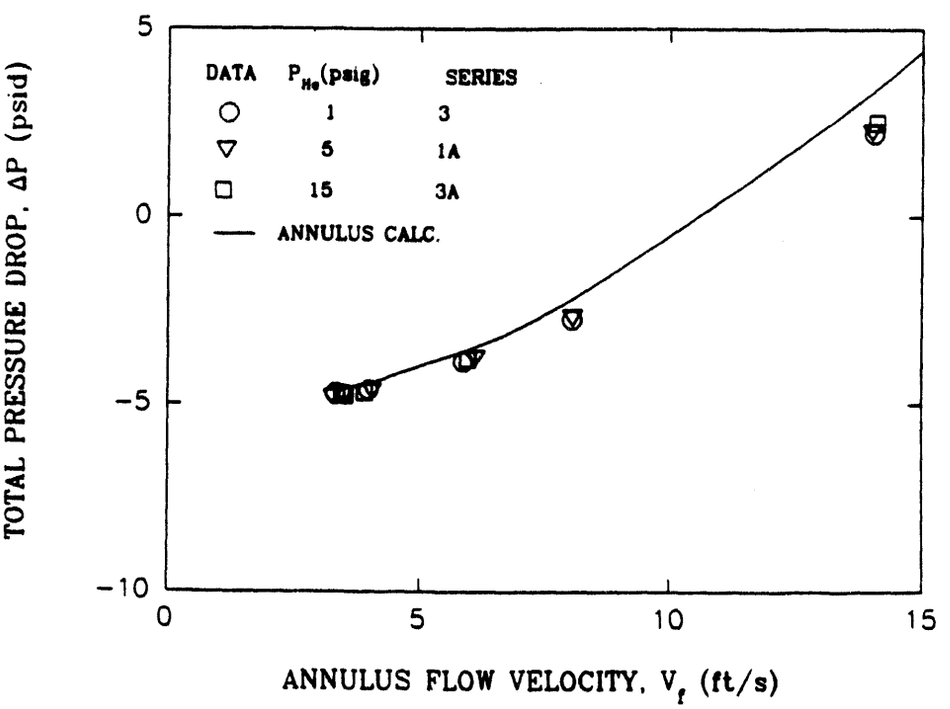

(b) Expanded Scale

Figure 3.16 DEMAND CURVES FOR THE EFFECT OF HELIUM PRESSURE IN THE RIBBED GEOMETRY

Creare

A separate analysis to estimate the maximum amount of dissolved helium expected to be liberated in the experiments as the fluid is heated in the annulus indicates that the amount is negligible (Crowley, letter to Z. Qureshi, 1988)). There should be no significant effect on ONB or the pressure drop in the annulus as a result of helium vapor, which is consistent with these data. Therefore, the ANNULUS program includes no effect of helium in its calculations.

3.5 Asymmetric Heating

Figure 3.17 compares the demand curves for two series of experiments with different distributions of the wall heat flux. The first is the baseline test condition at a heat flux of $1x10^5$ Btu/hr-ft^2 on both walls of the annulus (Series 1A). The second case is asymmetrically heated, with a heat flux of $2x10^5$ Btu/hr-ft^2 on the outer wall and no heat input to the inner wall (Series 10). The total power to the heaters is approximately 10% higher in the asymmetric case, which explains the difference in the velocity at the minimum pressure drop. The demand curves compare well at velocities above 5 ft/s. However, the minima occur at slightly different velocities: 3.27 ft/s in the uniformly heated annulus and 4.07 ft/s in the asymmetrically heated annulus. The small difference can be accounted for in the boundary condition for power input, because the ANNULUS calculations for these test series also show this same difference in the velocities at the minimum pressure drop. Since the difference is consistent with the ANNULUS calculations, no unusual effect is evident with asymmetric heating.

3.6 Effect of Ribs

Demand Curves. Figures 3.18 and 3.19 overlay demand curves with and without ribs on the inner annulus wall for similar boundary conditions. In Figure 3.18 at $\phi = 1x10^5$ Btu/hr-ft^2 (Series 1A in each geometry), the minimum pressure drop occurs at a velocity of 3.27 ft/s in the ribbed geometry and 3.07 ft/s in the nonribbed geometry. In Figure 3.19 at $\phi = 2x10^5$ Btu/hr-ft^2 (Series 4), the minimum occurs at a velocity of 6.79 ft/s in the ribbed geometry and 6.22 ft/s without ribs. This difference in the velocities at the higher heat flux is larger than the uncertainty in the velocity measurement, and therefore indicates a difference between the two geometries.

The data thus suggest a real difference between the two geometries, while the calculations do not. The ANNULUS calculations show a much smaller difference in the calculated minima for each demand curve, and that difference is accounted for by the hydraulic diameter with and without ribs. This is because ANNULUS assumes all subchannels are identical, while in reality they are not. The degree of channel-to-channel nonuniformity will dictate the degree of increase in the minimum stable velocity with ribs. The plots of Stanton number versus Peclet number in the Executive Summary (Figure 1.2) and Section 4.2 (Figure 4.1) graphically illustrate the difference between annuli with and without ribs.

Pressure and Temperature Profiles. Except as discussed below, no significant difference between experiments with and without ribs is found at velocities above the one where the minimum pressure drop occurs. Section 3.1 discusses the fact that in the ribbed geometry it is difficult to obtain steady-state data at velocities below the minima; a sharp transition to unstable heatup occurs. In the non-ribbed geometry that transition is somewhat "softer". Some data could be obtained beyond the minimum in the pressure drop. Figure 3.20 illustrates what happens under those conditions.

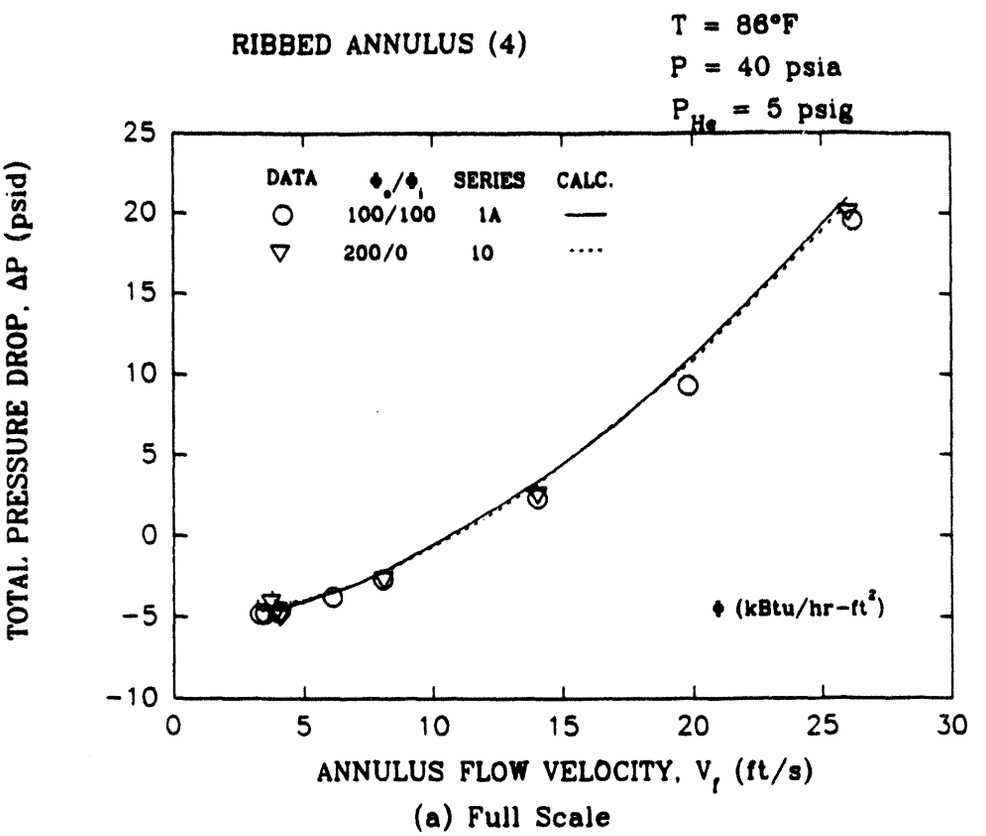

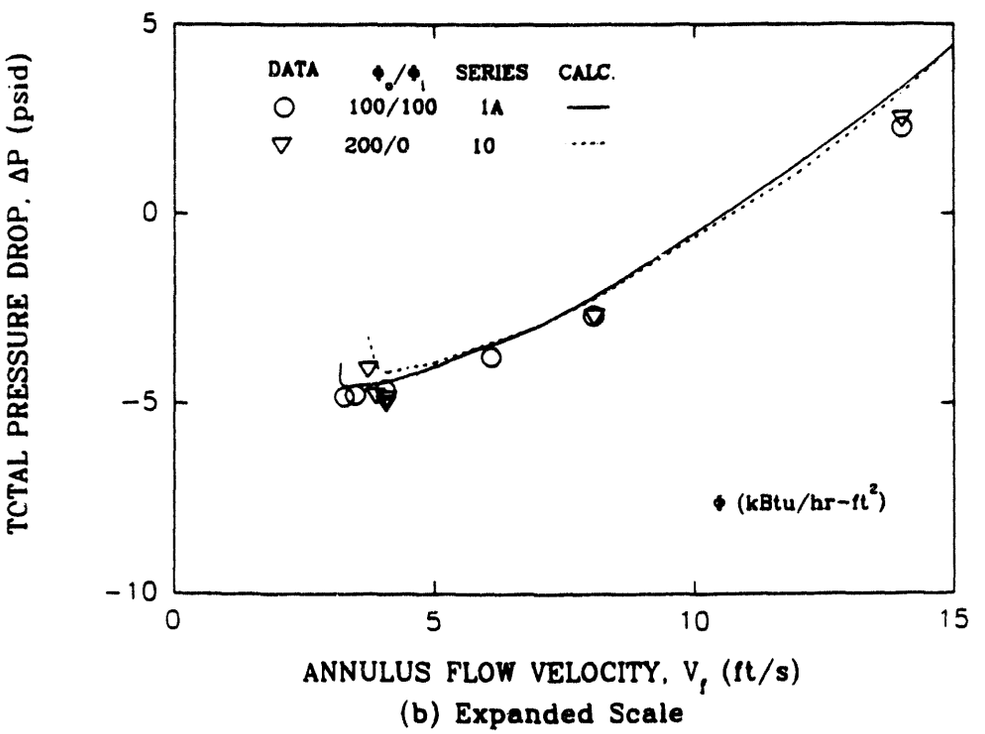

Figure 3.17 DEMAND CURVE FOR ASYMMETRIC HEATING

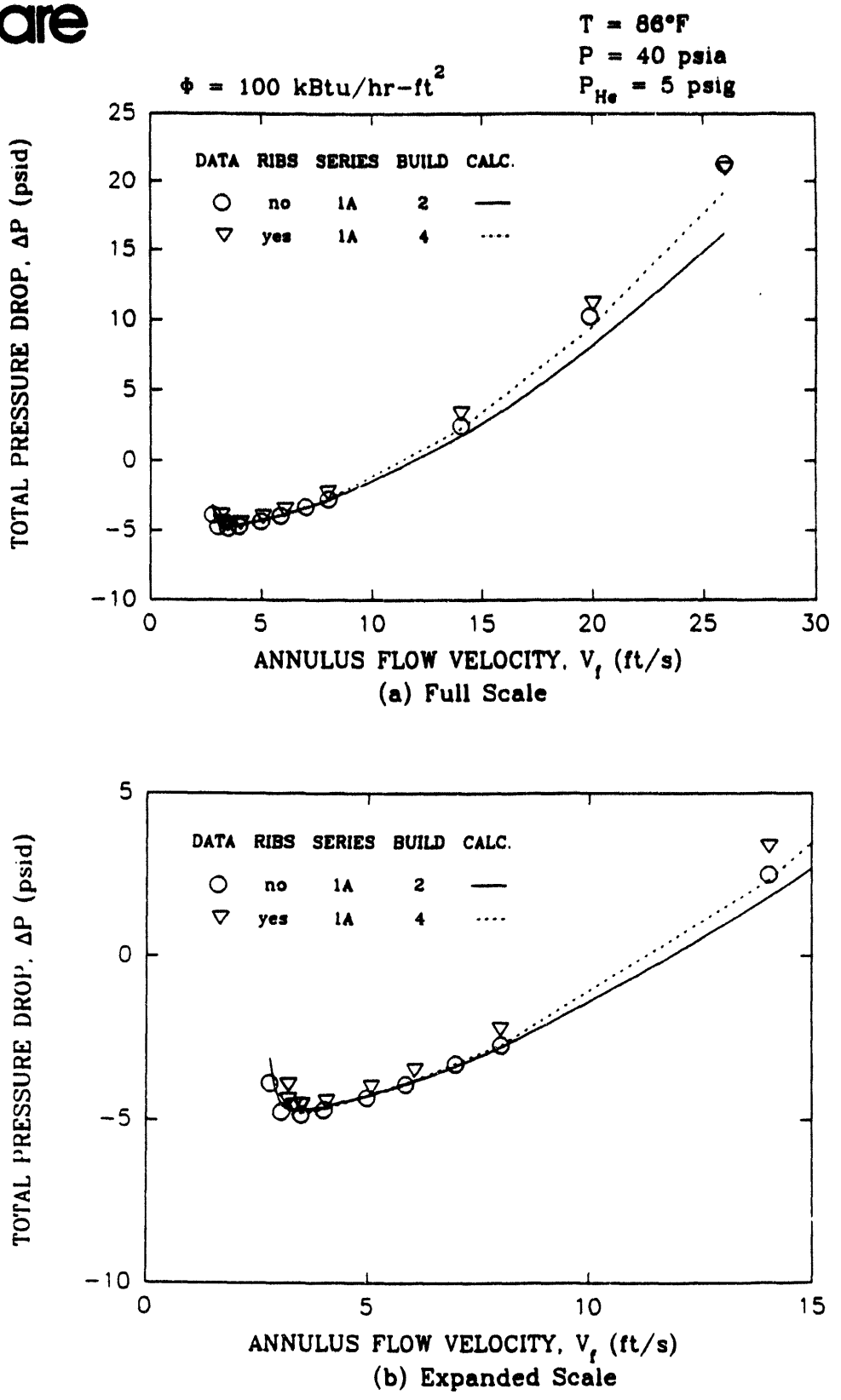

Figure 3.18 DEMAND CURVE FOR THE EFFECT OF RIBS AT ϕ = 1 x 10^5 BTU/HR-FT²

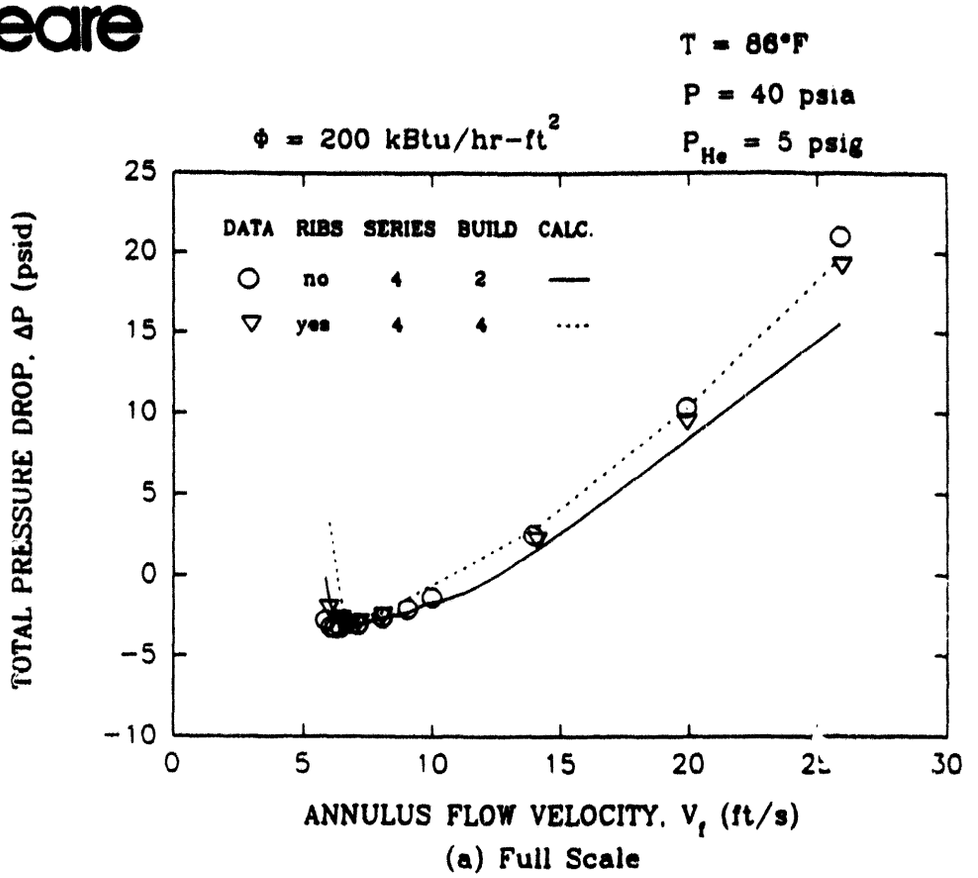

(a) Full Scale

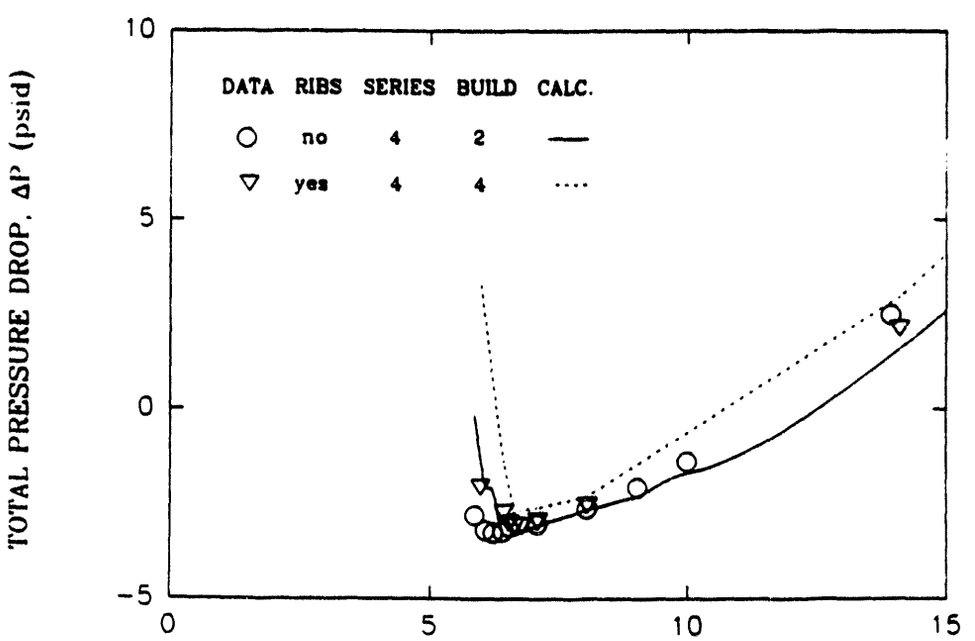

(b) Expanded Scale

Figure 3.19 DEMAND CURVE FOR THE EFFECT OF RIBS AT ϕ = 2 X 10^5 BTU/HR-FT^2

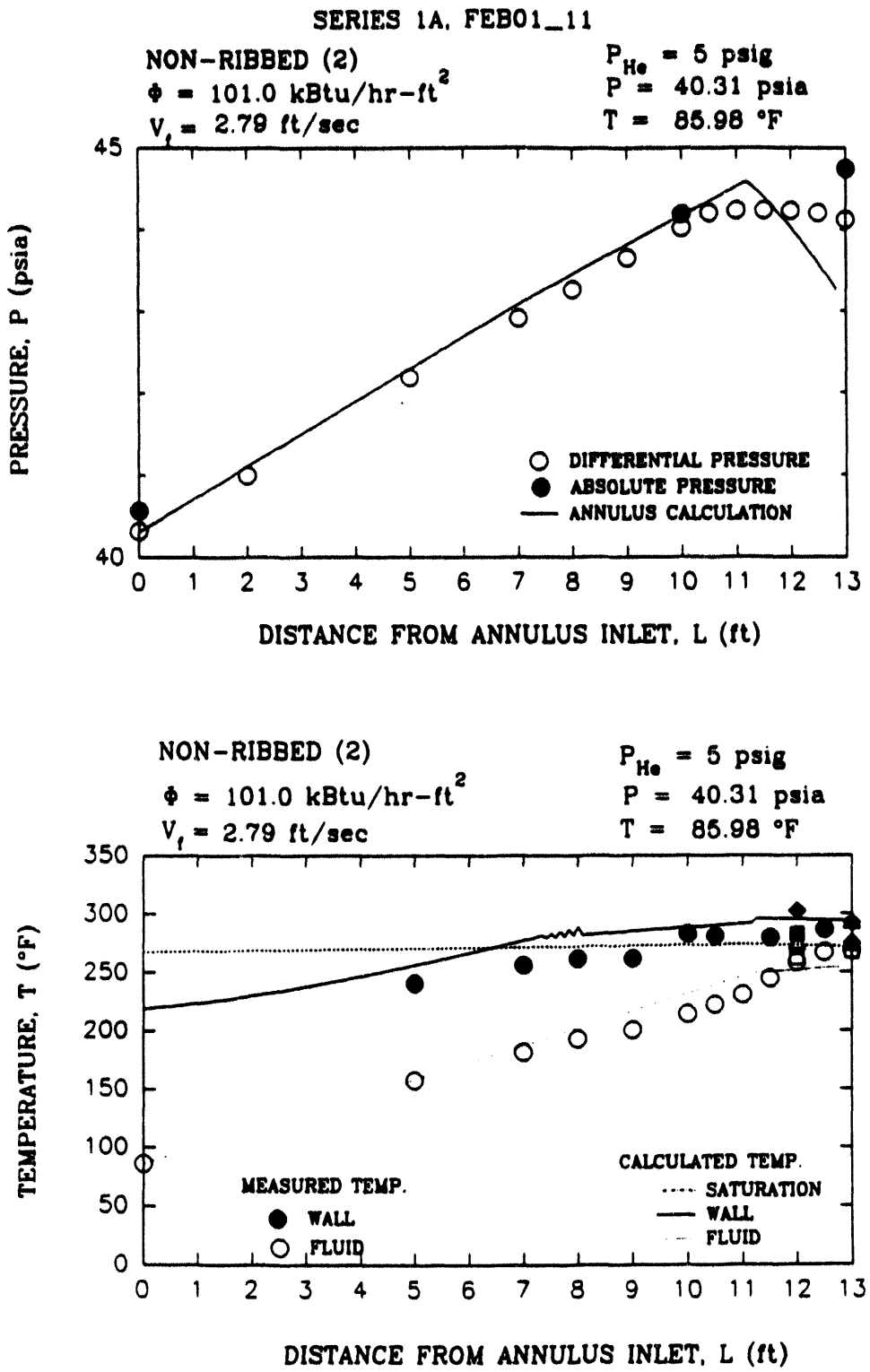

Figure 3.20 PROFILES BEYOND OFI EXIT FLOW FOR NONRIBBED GEOMETRY

Greare

The measured pressure in Figure 3.20 shows a definite change in slope between 11 and 12 feet from BHL. This change in slope is due to the increased pressure gradient with two-phase flow. ANNULUS correctly calculates the location of the change in pressure gradient (at the OSV point), but overpredicts the gradient. The demand curves also shows that the overall pressure drop calculated by ANNULUS is larger than the measured gradient at velocities below the minimum (see Figure 3.19 for example). This suggests that the model overpredicts the amount of energy which goes to vapor generation. The calculated rate of increase in the fluid temperatures between 11.5 and 13 feet is smaller than measured (Figure 3.20), and that is also consistent with partitioning too much energy to the vapor generation.

Subchannel Behavior. Figures 3.21a through 3.21d plot the fluid temperatures at the annulus exit (13 feet from BHL) for uniform heat fluxes from $1x10^5$ Btu/hr-ft^2 in Series 1A, 4, 6, and 9, respectively. Fluid temperatures in each subchannel (48°, 136°, 224°, and 312°) are plotted for each test in the series, that is, at each velocity tested. The fluid temperature data are plotted as a difference between the measured value in a given subchannel and the average of the values in all four subchannels.

What is striking about these comparisons is that the subchannel at 312° consistently shows temperatures hotter than the average, even for the uniform heat input. The deviation increases as the velocity approaches the value at the OFI point ($V_{n,in}$), where the temperature is 5°F to 10°F higher than average in this subchannel. Conversely, the subchannel at 136° consistently shows temperatures which are cooler than the average by about the same amount. We believe that the nonuniform distribution of temperatures is due to the geometry and is not an effect of nonuniformity in the power input. The same trend is seen in the corresponding measurements of the wall temperatures.

3.7 Power Tilt

The heat flux in a reactor fuel assembly may have a circumferential variation because of the spatial variation in the neutron flux and the orientation of the fuel assembly in the reactor. For that reason, experiments have been performed with a heat flux variation from 1.2 times the average at the midpoint of one subchannel to 0.85 times the average at 180° around the circumference to the midpoint of the opposite subchannel. Figure 3.22 shows the circumferential variation in heat flux, as a ratio of the local to the average heat flux (Barry, 1989). The profile in the experimental facility closely approximates the desired profile. This profile means that the instrumented subchannel at 136° (Figure 2.3) has an average heat flux about 15% larger than the circumferential average, the two adjacent subchannels (48° and 224°) have about the average heat flux, and the opposite subchannel (312°) has a heat flux about 15% below the average.

Figures 3.23 and 3.24 compare the demand curves for power tilt and uniform heat flux distributions. In the power tilt Series 15, the total power input and the average heat flux correspond to the baseline conditions in Series 1A. Power tilt test Series 16 corresponds to Series 4 with an average heat flux of $2x10^5$ Btu/hr-ft^2. The velocities at the minimum pressure for the measured data in Figure 3.23 are at 3.27 ft/s and 3.59 ft/s for the uniform and power tilt cases, respectively. The velocities at the minima for the higher heat flux in Figure 3.24 are 6.79 ft/s and 6.91 ft/s, respectively. The velocity at the minimum in the power tilt test Series 16 is only 2% larger than the velocity in Series 4 -- not as large a difference as might be expected if the subchannel with the highest heat flux controls the result. It is therefore difficult to assert that the power tilt had a significant effect on the results in these experiments. Further explanation is provided below.

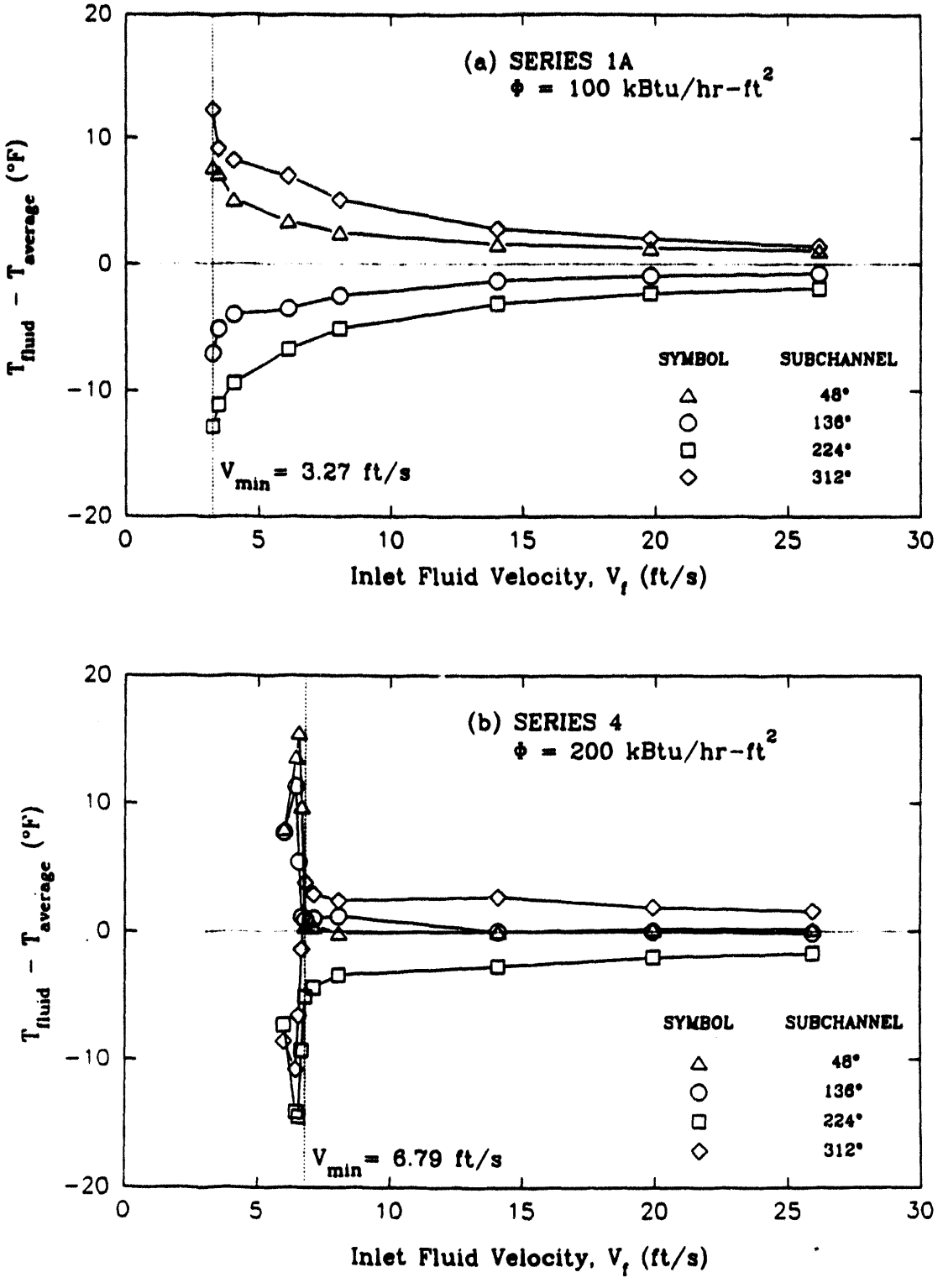

Figure 3.21 FLUID TEMPERATURES AT THE ANNULUS EXIT WITH UNIFORM HEAT FLUX IN THE RIBBED GEOMETRY

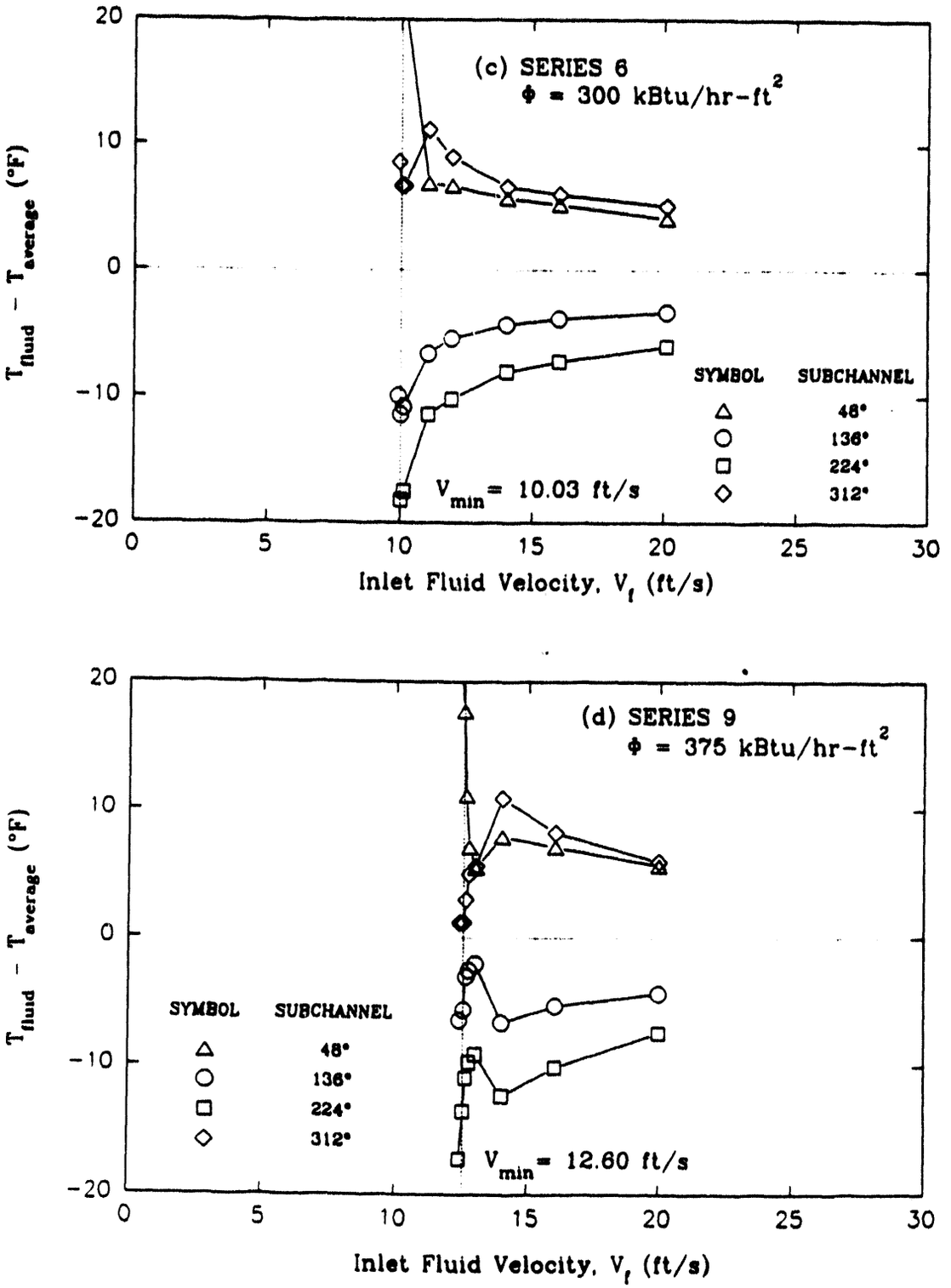

Figure 3.21 FLUID TEMPERATURES AT THE ANNULUS EXIT WITH UNIFORM HEAT FLUX IN THE RIBBED GEOMETRY (CONCLUDED)

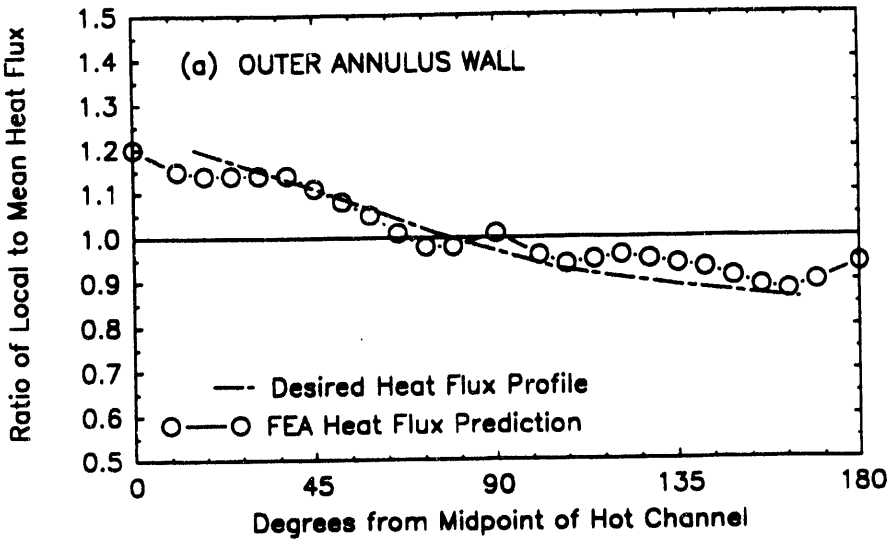

(a) OUTER WALL

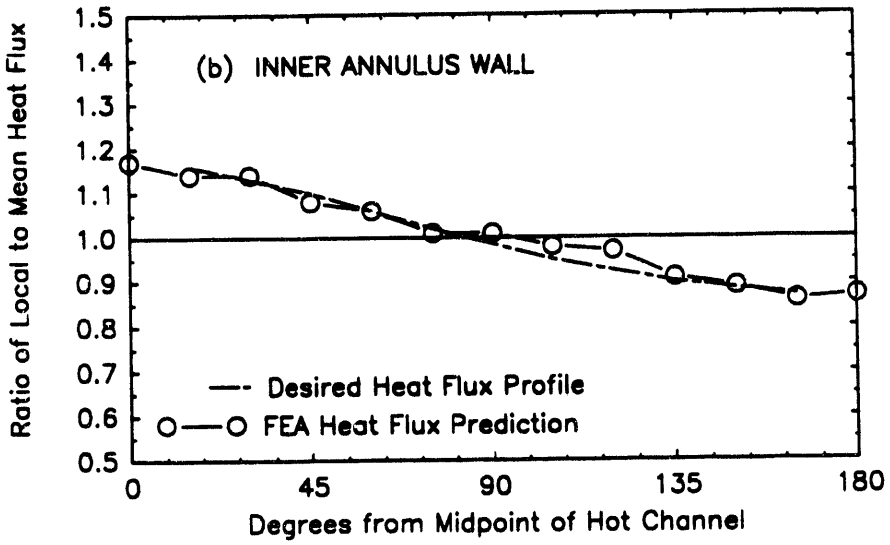

(b) INNER WALL

Figure 3.22 CIRCUMFERENTIAL VARIATION IN HEAT FLUX FOR POWER TILT

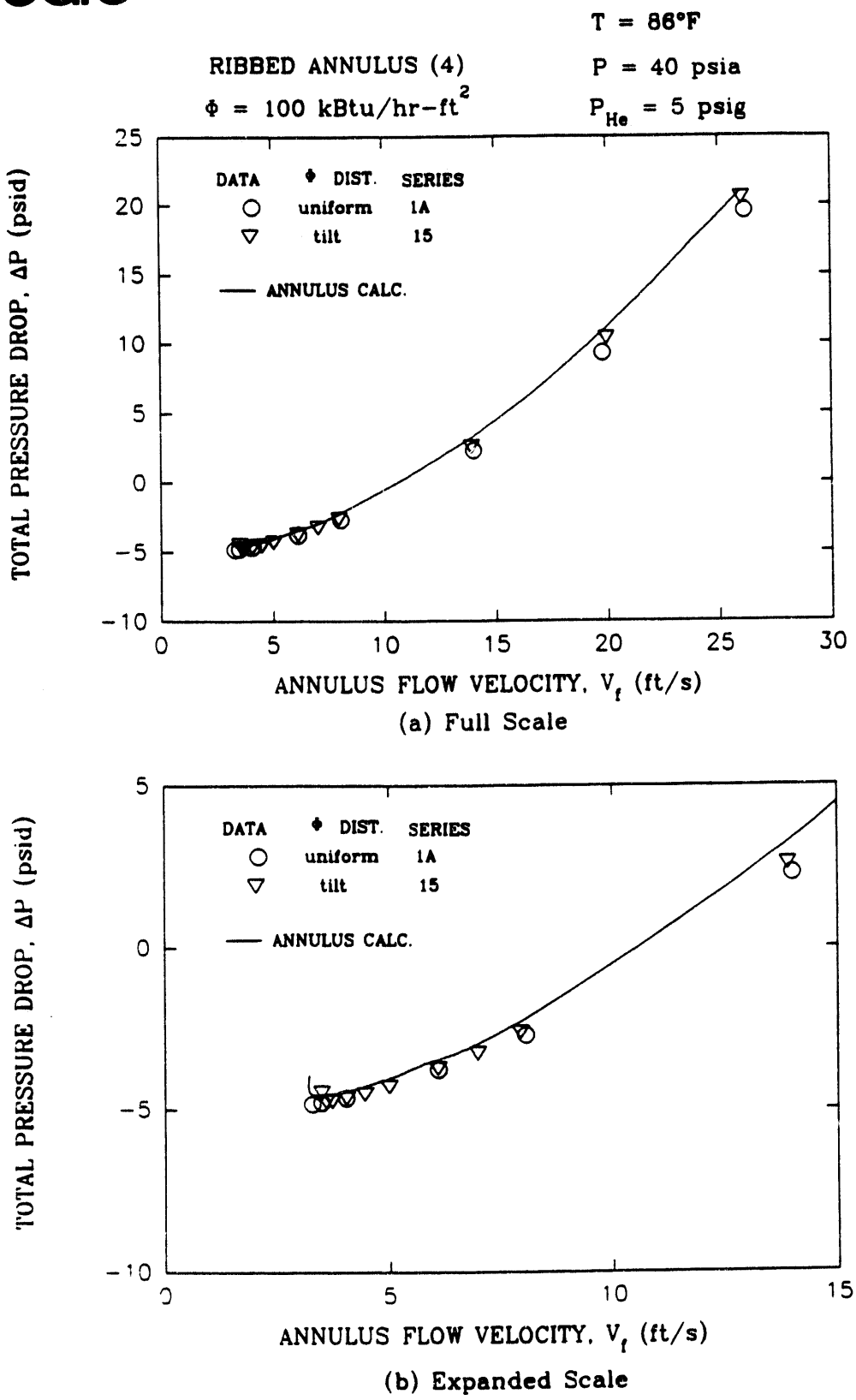

Figure 3.23 DEMAND CURVES FOR POWER TILT AT ϕ_{ave} = 1 X 10^5 BTU/HR-FT²

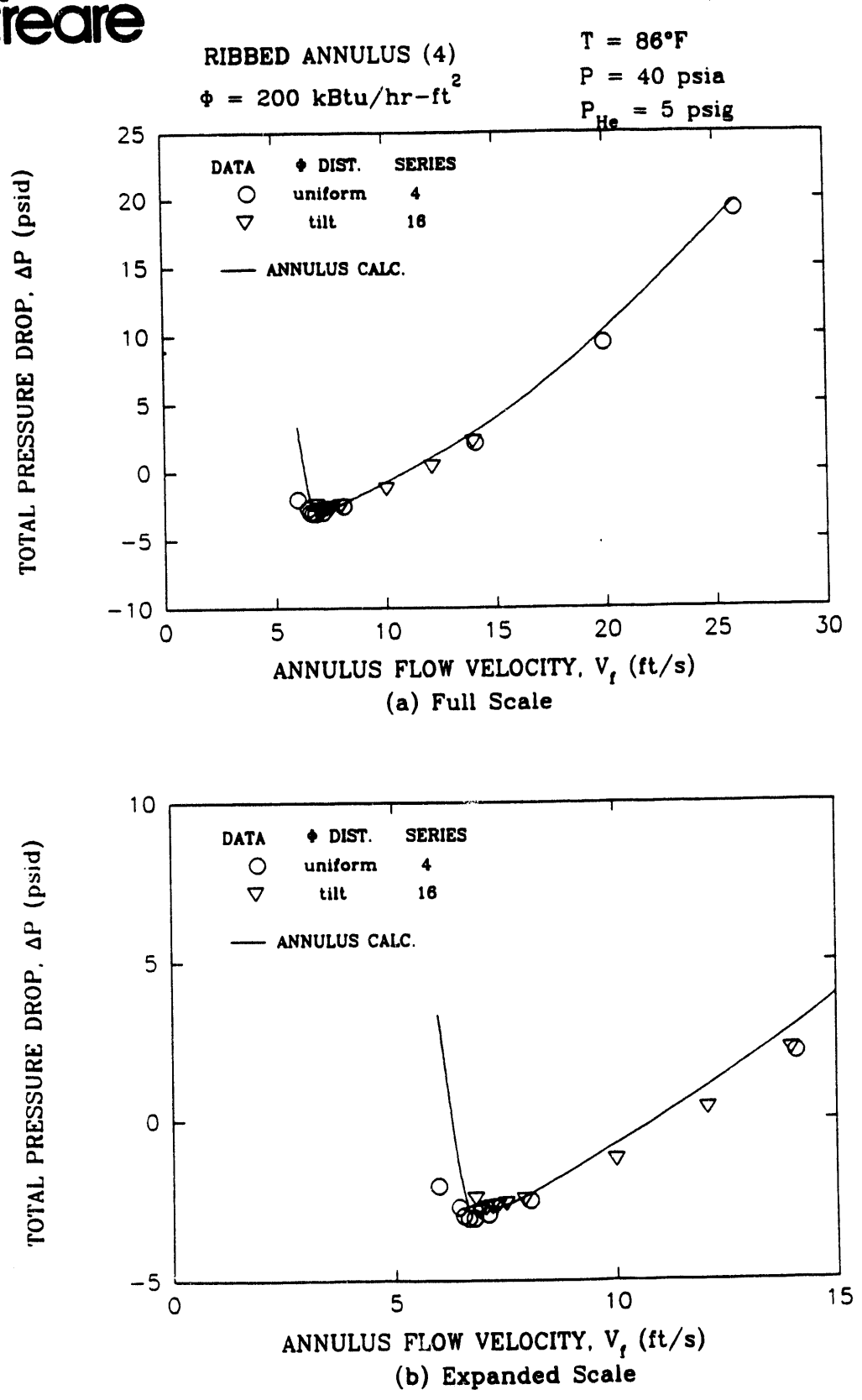

Figure 3.24 DEMAND CURVES FOR POWR TILT AT ϕ_{ave} = 2 X 10^5 BTU/HR-FT^2

Subchannel Behavior. Figure 3.25 shows the temperature profiles from Series 15 with power tilt. At these flow conditions, the exit flow is still single phase. A distribution in the temperatures around the circumference is evident in this power tilt test. With power tilt, the heating distribution is:

- Maximum heat flux at 136° location (circles)
- Average heat flux at 48° and 224° locations (triangles and squares)
- Minimum heat flux at 312° location (diamonds)

Maximum and minimum temperatures are found in the subchannels with the maximum and minimum heat fluxes, as expected. Temperatures in the 48° and 224° subchannels are intermediate to these values, also as expected. This configuration was selected prior to any testing with the objective of having the peak heat flux in the heavily instrumented subchannel.

For a uniformly heated annulus, Figures 3.21a through 3.21d show that wall and fluid temperatures around the circumference vary from the average temperature, especially as the minimum pressure drop is approached. Fluid temperatures in the subchannel at the 312° location are greater than in the other subchannels, even in the tests with uniform heating.

In the power tilt tests then, the peak heat flux was input to the 136° subchannel which ran cooler in the tests at uniform heat flux, and the minimum heat flux was input to the subchannel which consistently had higher temperatures in the tests at uniform heat flux. Figures 3.26a and 3.26b show that the subchannels at 136° and 312° exhibit the highest and lowest fluid temperatures as expected in the power tilt tests. However, the temperatures in the hottest subchannel (136°) in the power tilt tests are about the same as the temperatures in the hottest subchannel (312°) in the tests at uniform heat flux (Figures 3.21a and 3.21b). Even with the peak heat flux applied to the 136° subchannel in the power tilt tests, it did not run much hotter than the 312° subchannel in the uniform heat flux tests.

We believe that this illustrates why the results in the power tilt tests did not differ significantly from the results in the uniform heat flux tests. Although the controlling (hottest) subchannel is different, the temperatures are about the same in both cases.

These results in the uniform and power tilt experiments suggest that the subchannel with the peak heat flux should be systematically varied in order to more accurately assess the effect of power tilt. At least, the peak heat flux should be applied to the subchannel which is normally the hottest in the uniform heat flux tests.

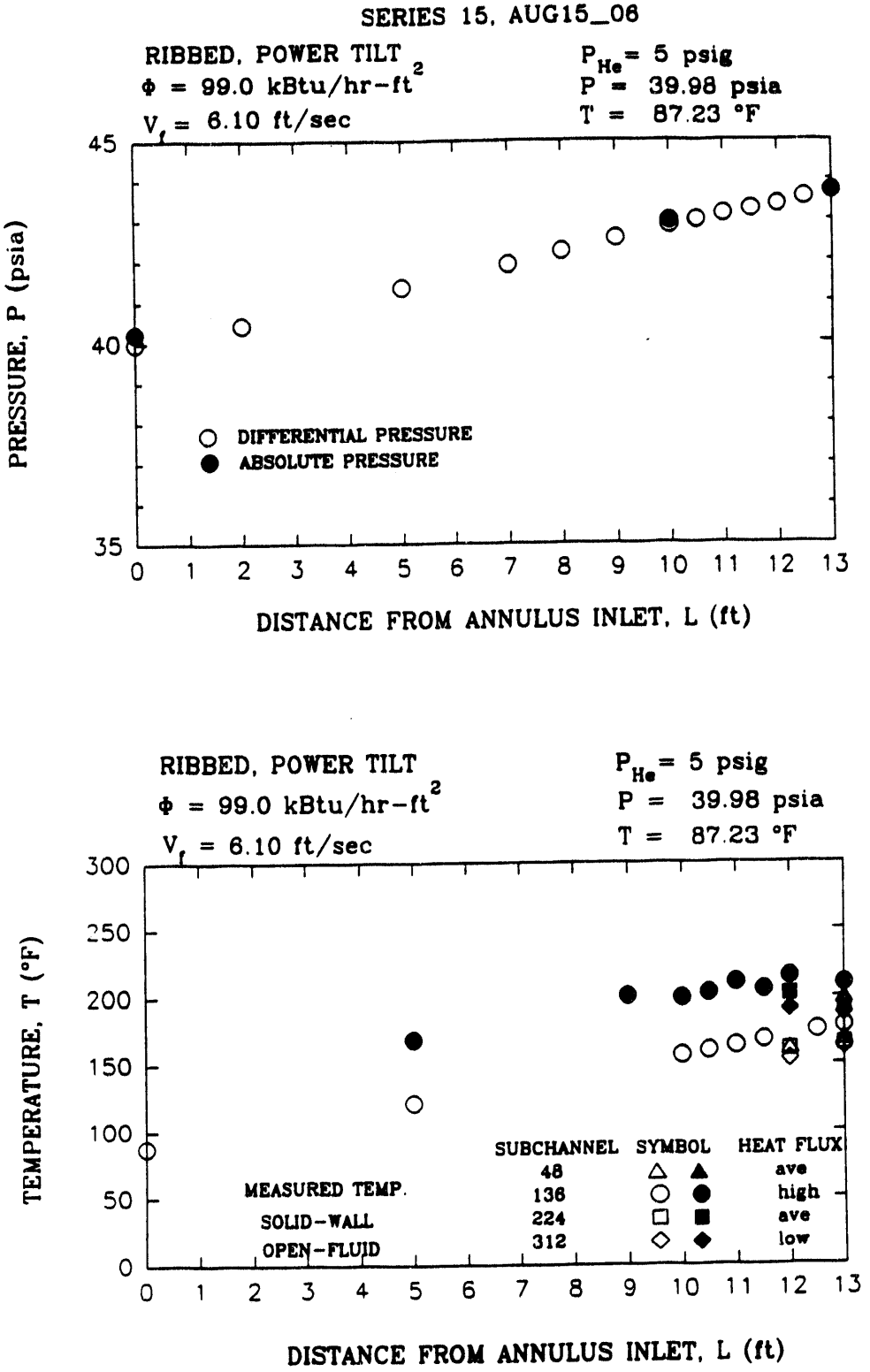

Figure 3.25 PROFILES FOR SINGLE PHASE EXIT FLOW FOR POWER TILT (ϕ_{ave} = 1 X 10^5 BTU/HR-FT^2)

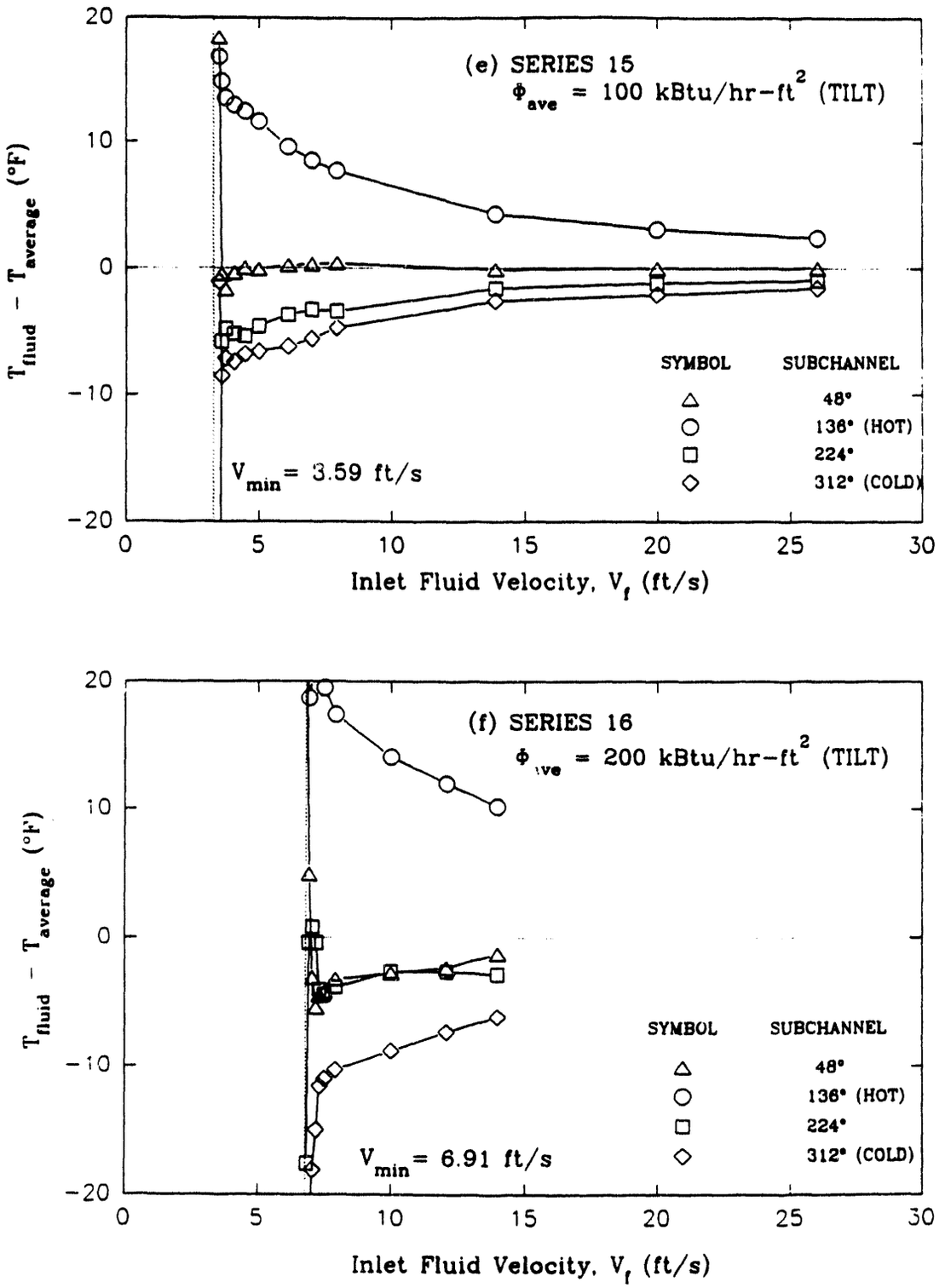

Figure 3.26 FLUID TEMPERATURES AT THE ANNULUS EXIT WITH POWER TILT IN THE RIBBED GEOMETRY

4. SUMMARY AND CONCLUSIONS

4.1 Summary of Parametric Effects

To summarize the detailed comparisons which are presented in Section 3:

- The effect of ribs in the test geometry seems to be the most important with respect to the key result -- the location of OFI. (See the extended discussion of OFI in Section 4.3 and the discussion in Section 3.6.)
- The effect of power tilt requires further study. The experiments show little effect of power tilt, but that appears to be a function of the particular configuration tested. (We believe we inadvertently located the peak power region in the most stable subchannel.)
- The effects of heat flux, inlet pressure, and asymmetric heating are consistent with expected trends based upon the analytical work.
- The effect of dissolved helium does not appear to be significant.

In addition, since the baseline test conditions were repeated four times during the course of the experiments in the ribbed geometry (from early May to mid-August 1990), and since the results are repeatable, there did not seem to be any significant effect of aging of the annulus wall surface on the results, within the time scale of this test program.

4.2 Summary of Analytical Model Comparisons

Volume 2 presents many detailed comparisons of temperature and pressure profiles with the predictions of the ANNULUS computer program. Appendix A describes the models used in the program. The conclusions from the analysis comparisons are summarized here for each heat transfer regime

- Single phase
- Partially developed nucleate boiling
- Fully developed nucleate boiling

and each transition between the regimes:

- Onset of Nucleate Boiling (ONB)
- Onset of Significant Voiding (OSV)

Analytical models for wall heat transfer, pressure drop, and fluid energy balances in the single phase and partially developed nucleate boiling regimes are important to predicting the conditions leading to the Onset of Flow Instability. Models for the fully developed nucleate boiling regime are of lesser interest because they are beyond the point of flow instability where it is intended to operate the reactor. Data in this regime may be of interest to transient code predictions for reactor safety, however.

Single Phase Region

- The predicted wall-to-fluid temperature difference is 10% to 100% larger than the measured difference, with closer agreement at lower heat fluxes. This means that the calculated heat transfer coefficient (Dittus-Boelter, 1930) should be larger in order to agree with the experimental data.

- Pressure gradient data from the unheated flow channel can be used to adjust the frictional component of the pressure gradient in the tests with heat input to obtain good agreement with data. The Rohsenow-Hartnett (1985) model is adequate.

- Measured fluid temperatures agree very well with simple energy balances.

Onset of Nucleate Boiling

- Wall superheat at the Onset of Nucleate Boiling (ONB) is impossible to assess from the experimental data. Because of the high thermal conductivity of the aluminum wall, axial heat conduction tends to smooth out discontinuities in wall temperature of the small size which the ONB condition represents.

Partially Developed Nucleate Boiling

- There is a small but detectable change in the pressure gradient at the location believed to correspond to ONB (close to where the measured wall temperature exceeds the saturation temperature). This is especially apparent at the higher heat fluxes tested. The analysis (Levy, 1967) appears to capture this trend, but overpredicts the pressure gradient.

- The uncertainty in the measured wall-to-fluid temperature difference in this region is large compared with the calculations. Just as for ONB, axial heat conduction due to the high thermal conductivity of the aluminum wall tends to smooth out temperature gradients over short distances. Thus, the uncertainties in the data make it difficult to assess particular heat transfer models, however the model used (Bowring, 1962) represents the data reasonably well.

- There is no apparent change in the rate of heatup of the fluid with length in this regime, as expected, indicating that no significant net vapor generation occurs.

Onset of Significant Voiding (OSV)

- The results in Figures 2 and 3 (Executive Summary) illustrate that the Saha-Zuber (1974) model is a good prediction of the OSV or OFI condition in the tests without ribs. In the tests with ribs, the OSV transition is predicted somewhat earlier (at twice the exit subcooling or 5% higher velocity) than without ribs. This is probably an indication that local fluid conditions in flow subchannels vary from the average, rather than an indication that the model does not apply.

Fully Developed Nucleate Boiling

- After OFI, the increase in pressure drop tends to be larger in the calculations than observed in the data, especially in tests without ribs. This suggests that the energy partitioned to vapor generation is actually weaker than calculated (Ivey-Morris, 1962).

- In order to calculate the partition of energy between fluid heating and vapor generation, void fraction data are needed. Fluid temperature measurements are too inaccurate to be used alone for this purpose, and are further complicated by circumferential variations in the measured values. Void fraction data have not been obtained in the experiments. Further work would be needed to improve the models for the energy partition, which would also improve the pressure drop comparisons.

- Wall superheat after OFI generally agrees with the calculated values (Thom, 1965).

4.3 Evaluation of OFI

A key objective in the Creare experiments is to assess the conditions at OFI for each test series. Figure 4.1 is a plot of Stanton number versus Peclet number which summarizes the data for the minima from each of the 19 test series and compares them with the OSV prediction of the Saha-Zuber model. Uncertainties in the values, based upon uncertainties in the measured data, are shown. Table 4.1 summarizes the values in the plot.

Basis. For each test series, we have selected the test in a given series which represents the minimum pressure drop on the demand curve of pressure drop versus velocity. The demand curves for each test series have been plotted in Volume 2, where the test having the minimum pressure drop is identified. We have used measured data and calculated fluid properties to evaluate the Stanton number and the Peclet number for the conditions at the annulus exit in the test selected as the minimum. Measured data have been used in the computer program called OSV (Crowley, 1990) in order to evaluate the dimensionless parameters.

The definition of the Stanton number is:

$$St = \frac{\phi}{(T_{sat} - T_f)c_{pf}G} \qquad (1)$$

where:

- ϕ is the diametral average value of the heat flux on the wall
- T_{sat} is the saturation temperature for the absolute pressure at the annulus exit
- T_f is the average of the fluid temperatures around the circumference at the annulus exit
- G is the mass flux ($\rho_f V_f$) based upon the inlet fluid density and velocity
- c_{pf} is the liquid heat capacity at T_{sat}

Table 4.1 TEST CONDITIONS AT MINIMUM PRESSURE DROP FOR EACH SERIES												
Annulus Geometry (build)	Series	Test	Diametral Ave. Heat Flux (k Btu/hr-ft^2)	Heat Flux Distribution	Velocity (ft/s)	Inlet Temp. (°F)	Outlet Ave. Temp. (°F)	Inlet Press. (psia)	Exit Press. (psia)	Helium Sat. Press. (psia)	Stanton Number x 10^3	Peclet Number x 10^{-4}
Non-ribbed (1)	1	Nov 14-13	100.6	uniform	3.07	87.3	256.2	40.2	45.9	19.6	7.31	7.98
Non-ribbed (2)	1A	Feb 01_09	100.7	uniform	3.49	87.7	236.8	40.4	45.4	19.5	3.30	8.85
	2	Feb 05_12	100.9	uniform	2.61	85.2	285.4	60.3	65.4	19.9	12.9	6.68
	3	Feb 06_08	99.6	uniform	3.02	85.1	256.5	40.0	45.3	15.5	7.86	7.66
	4	Feb 08_10	201.5	uniform	6.22	86.5	253.9	40.0	43.3	19.4	7.81	15.8
Ribbed (3)	1	May 03_21	101.3	uniform	3.20	85.5	244.9	40.2	45.3	19.8	4.62	7.21
	2	May 07_08	101.8	uniform	2.94	87.2	262.1	60.4	65.4	19.5	4.13	6.68
	3	May 08_08	101.4	uniform	3.33	87.3	238.6	40.1	45.2	15.5	3.69	7.50
Ribbed (4)	1A	Aug 01_08	100.9	uniform	3.27	87.2	244.9	40.1	45.3	19.6	4.51	7.38
	4	Aug 01_15	201.3	uniform	6.79	87.6	239.1	40.0	43.3	19.7	3.93	15.3
	10	Aug 01_24	110.6	asymmetric	4.07	87.1	240.8	40.0	45.5	19.7	3.45	9.19
	15	Aug 15_10	100.6	tilt	3.59	87.5	229.8	40.5	45.2	19.7	2.73	8.10
	16	Aug 15_26	200.2	tilt	6.91	86.8	242.8	40.2	43.4	19.7	4.31	15.6
	5	Aug 16_06	101.1	uniform	3.41	87.2	238.8	40.2	45.2	19.7	3.61	7.70
	6	Aug 17_06	299.2	uniform	10.03	85.4	239.2	40.1	41.5	19.6	4.32	22.6
	7	Aug 17_17	300.5	uniform	8.84	86.1	259.5	60.6	62.8	19.7	4.04	20.3
	9	Aug 17_23	374.3	uniform	12.60	86.0	238.7	40.1	39.2	19.6	4.77	28.4
	13	Aug 17_31	100.7	uniform	3.44	87.0	237.4	40.0	44.8	19.8	3.48	7.76
	3A	Aug 17_37	100.1	uniform	3.45	86.9	236.6	40.1	45.1	29.5	3.35	7.79

For the Peclet number

$$Pe = \frac{c_p G D_h}{k_f} \qquad (2)$$

D_h is the hydraulic diameter; 0.044 ft in the non-ribbed geometry and 0.039 ft in the ribbed geometry

k_f is the thermal conductivity of the liquid at T_{sat}

Results. The results indicate that:

- A Stanton number of about 0.003, or about 50% lower than the Saha-Zuber model bounds all of the experimental data, including tests with ribs and power tilt.
- The minima for the ribbed geometry generally lie at lower Stanton number (larger subcooling) than the minima for the ribless geometry.
- The minima for the power tilt tests do not differ significantly from the minima for the uniform heat flux tests in the ribbed geometry. (However, this result may be because we located the peak heat flux region in the most stable subchannel.)

Discussion of Results. It is believed that because of the geometrical tolerances in the annulus diameter and the ribs, and the distortions caused by heating of the annulus, one flow subchannel is created which has a somewhat different geometry than the other subchannels. For instance, if the inner assembly is positioned such that two adjacent ribs touch the outer annulus wall, the resulting subchannel between these ribs will have a smaller flow area (about 25% smaller) than the subchannel on the opposite side of the annulus. Assuming a share of the heat flux which is one-quarter of the total, but a share of the inlet flow which is less than one-quarter of the total in this subchannel, this subchannel might (apparently) become unstable before the others, when the flow conditions are based upon the average flow and heat flux in the four subchannels. In these experiments, the subchannel at the 312° location generally became unstable first in the tests with uniform heat flux.

The results from the power tilt tests indicate that the subchannel at the high power (136°) became unstable first, but the temperatures did not differ significantly from those in the unstable channel with uniform heat flux. That explains why the demand curves and OFI points in the power tilt experiments do not differ significantly from the tests at uniform heat flux.

Discussion of Uncertainties. The overall uncertainty in the Stanton number based on uncertainties in the instrument readings is about 10% to 20% as shown in Figure 4.1. This uncertainty takes into account the following measurement uncertainties: the 10% uncertainty in the measured fluid temperature (2°F out of a subcooling of 20°F), the 5% to 15% uncertainty in the inlet velocity (larger values at the lower end of the velocity range tested), and about 2% uncertainty in the heat flux. Uncertainty in the Stanton number is larger at low velocities (about 20%), compared with 10% at the higher velocities, due to the uncertainty in the velocity measurement.

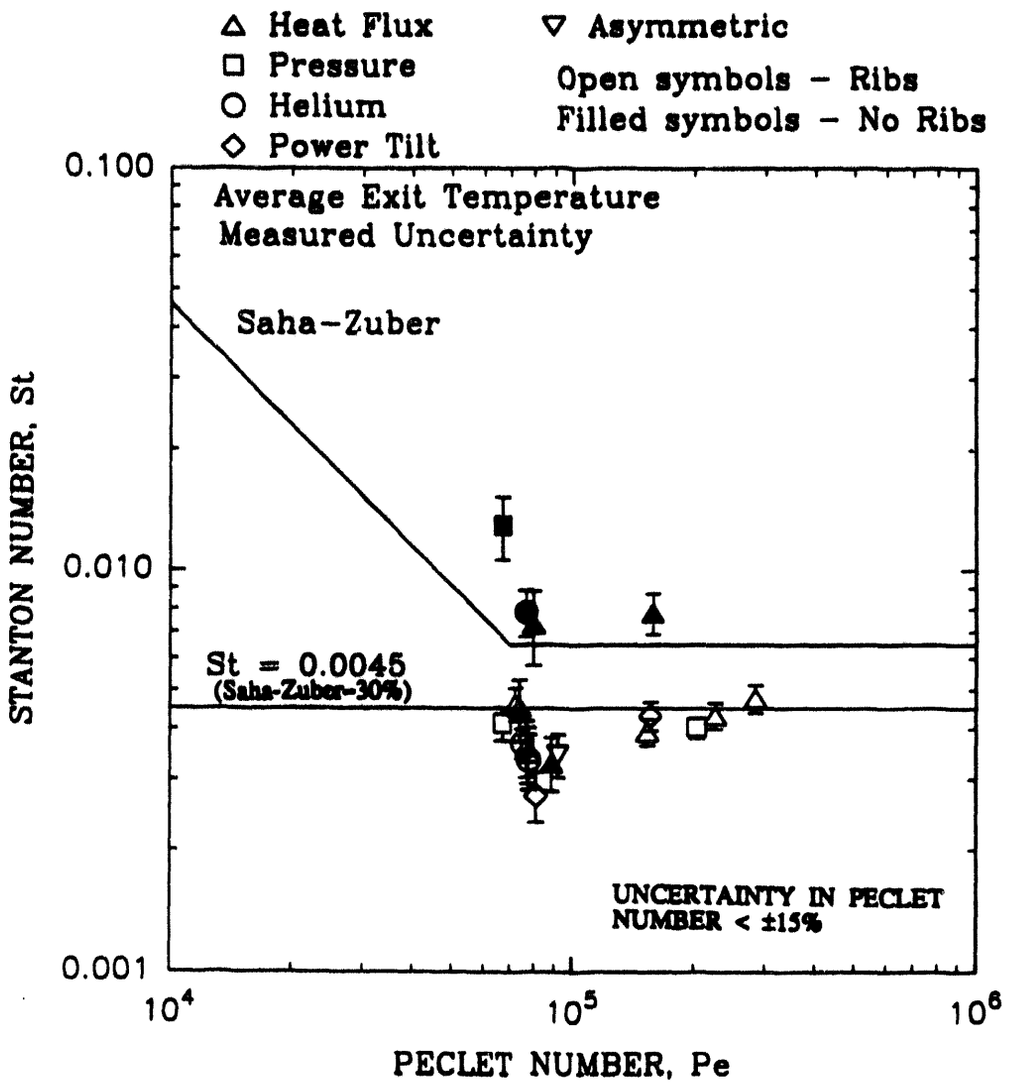

Figure 4.1 OFI RESULTS FROM CREARE EXPERIMENTS (UNCERTAINTIES BASED MEASUREMENT UNCERTAINTIES)

In the earlier tests, there was some problem in picking the velocity at the minimum pressure drop because the data points were spread at velocities which differed by more than the uncertainty in the measurement. Figure 4.2 shows the uncertainties in the Stanton number evaluated by using the difference in velocity between the minimum and the next lowest data point as the uncertainty in the velocity. In the later tests, there are experimental data points at velocities which are within the range of velocity uncertainty, so uncertainty in the velocity is about the same whether from uncertainties in measured data (Figure 4.1) or by trying to pick the minimum from actual data (Figure 4.2). Only in Series 1A in the non-ribbed geometry did the spacing of the data points contribute to a larger uncertainty. We suggest that this data point not be considered valid.

The circumferential variation in the measured fluid temperatures at the annulus exit varies more than the uncertainty in individual temperature measurements (2°F). Given that there is some uncertainty in the measured fluid temperatures, the Stanton-Peclet number plot can also be generated using a fluid temperature at the exit of the annulus as determined by an energy balance. The exit fluid temperatures calculated from an energy balance generally differ by about the same as the uncertainty in the temperature measurement, therefore the conclusions are not substantially modified using this approach to present the data.

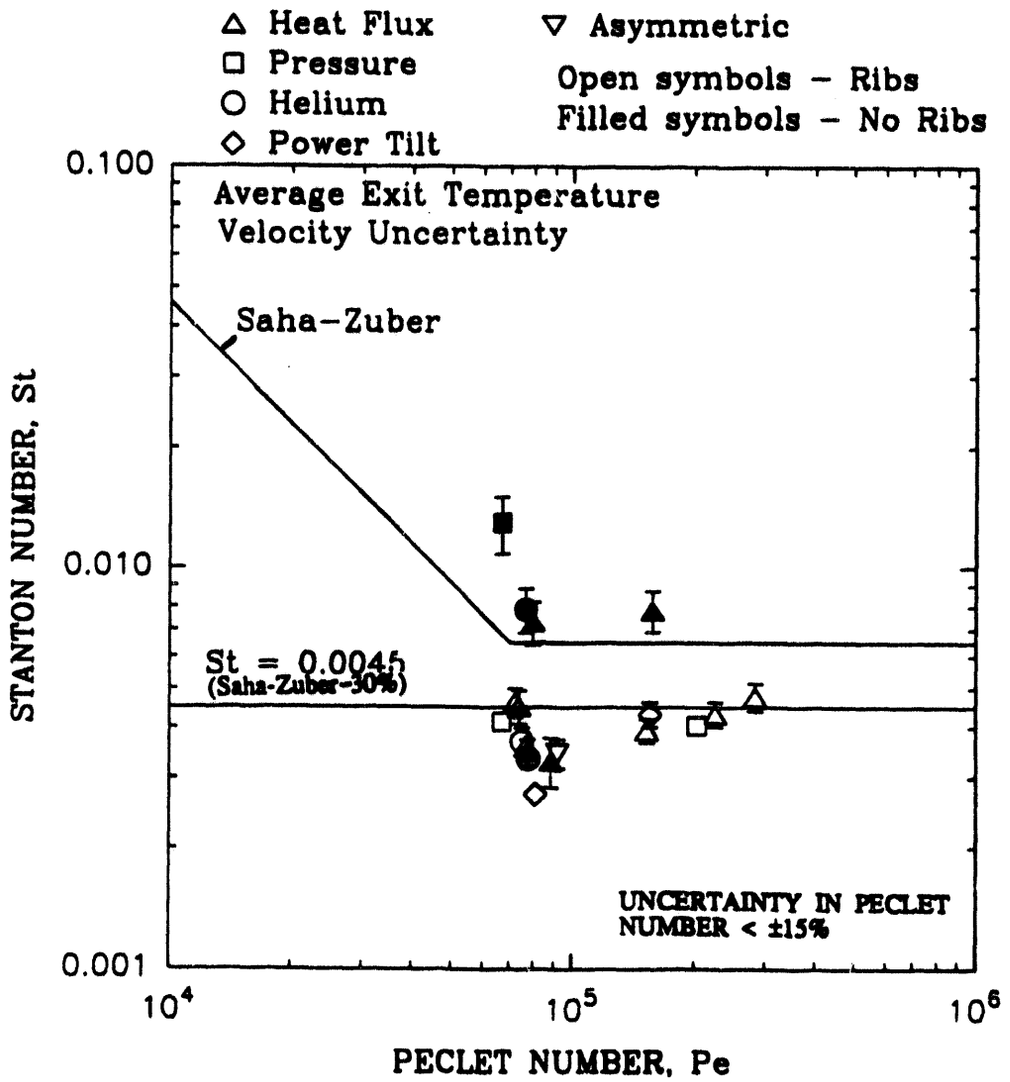

Figure 4.2 OFI RESULTS FROM CREARE EXPERIMENTS (UNCERTAINTIES BASED ON SPACING OF VELOCITIES FOR TEST DATA)

References

Barry, J.J., Crowley, C.J., and Wallis, P.N.; User's Guide to Subcooled Boiling in an Annulus Calculation Code (ANNULUS); Creare TN-467, January, 1989.

Barry, J.J.; Test Plan for Nucleate Boiling Pressure Drop in an Annulus. Appendix C. Power Tilt Tests; Creare Inc. TM-1237A, Appendix C, Prepared for U.S. Department of Energy, Savannah River Laboratory, Subcontract AX-721102, June, 1989.

Bowring, R.W.; Physical Model Based on Bubble Detachment and Calculation of Steam Voidage in the Subcooled Region of a Heated Channel; OECD Halden Reactor Project Report HPR-10, 1962.

Chen, J.; A Correlation for Boiling Heat Transfer to Saturated Fluids in Convective Flow; ASME Paper 63-HT-34, 1963.

Colebrook, C.F.; Turbulent Flow in Pipes, with Particular Reference to the Transition Region Between the Smooth and Rough Pipe Laws; J. Inst. Civil Engineers London, V11, 1938-39, pp. 133-156.

Collier, J.G.; Convective Boiling and Condensation; Second Edition, McGraw-Hill, New York, 1986.

Crowley, C.J.; Effect of Noncondensible Gas on ONB; Letter to Z. Qureshi, December 7, 1988.

Crowley, C.J.; Fortran Program; Letter to R. Miller, June 13, 1990.

Crowley, C.J.; Software Requirements Specification: OSV; Creare Inc. TM-1306, Part A, Revision 2, Prepared for U.S. Department of Energy, Savannah River Laboratory, Subcontract AX-721102, September, 1990.

Crowley, C.J. and Dolan, F.X.; Test Plan for Nucleate Boiling Pressure Drop in an Annulus. Appendix D. Tests Without Ribs; Creare Inc. TM-1237A, Appendix D, Prepared for U.S. Department of Energy, Savannah River Laboratory, Subcontract AX-721102, November, 1989.

Davis, E.J. and Anderson, G.H.; The Incipience of Nucleate Boiling in Forced Convection Flow; AIChE J., V12, 1966, pp. 774-780.

Dittus, F.W. and Boelter, L.M.K.; Heat Transfer in Automobile Radiators of Tubular Type; Publ. in Engineering, U. of California, Berkeley, 1930, p. 443.

Ivey, H.J. and Morris, D.J.; On the Relevance of the Vapor-Liquid Exchange Mechanism for Subcooled Boiling Heat Transfer at High Pressure; AEEW-R137, U.K. Atomic Energy Agency, 1962.

Kline, S.J. and McClintock, F.A.; Describing Uncertainties in Single Sample Experiments; Mechanical Engrg., January, 1953, pp. 3-8.

Creare

Levy, S.; Forced Convection Subcooled Boiling -- Prediction of Vapor Volumetric Fraction, Int. J. Heat Mass Transfer, V10, 1967, pp. 951-965.

McAdams, W.H. et al.; Heat Transfer at High Rates to Water with Surface Boiling; Ind. Eng. Chem., V41, 1949, pp. 1945-1954.

Rohsenow, W.M., Hartnett, J.P., and Ganic, E.N.; Handbook of Heat Transfer Fundamentals; Second Edition, McGraw-Hill Book Company, New York, 1985.

Saha, P. and Zuber, N.; Point of Net Vapour Generation and Vapor Void Fraction in Subcooled Boiling; Proceedings of the 5th International Heat Transfer Conference, Paper B4.7, Tokyo, Japan, 1974.

Sam, R.G., Dolan, F.X., Hall, M.H., Crowley, C.J. and Sellew, S.S.; Test Plan for Nucleate Boiling Pressure Drop in an Annulus; Creare Inc. TM-1237A, Prepared for U.S. Department of Energy, Savannah River Laboratory, Subcontract AX-721102, September, 1988.

Stoedefalke, B.H.; The Data Acquisition System for the Nucleate Boiling Pressure Drop in Annuli Experiments; Creare Inc. TM-1367, Prepared for U.S. Department of Energy, Savannah River Laboratory, Subcontract AX-721102, August, 1989.

Thom, J.R.S. et al.; Boiling in Subcooled Water During Flow up Heated Tubes or Annuli; Paper 6 presented at the Symposium on Boiling Heat Transfer in Steam Generating Units and Heat Exchangers, Inst. Mech. Engrs., Manchester, England, 1965.

Creare

APPENDIX A
SUMMARY OF ANALYTICAL MODEL

In Section 3 of this document (and in Volume 2) demand curves and experimental pressure and temperature profiles for various tests are compared with analytical predictions of the computer program ANNULUS (Barry, Crowley, and Wallis, 1989). This Appendix describes the specific models used in the comparisons presented in this report.

The ANNULUS code models heat transfer and pressure drop for water in a heated flow channel. Using input values for the inlet temperature, pressure, and velocity as well as the geometry, heat flux (axial profile), the program computes pressure, fluid temperature, wall temperature, and quality or void fraction along the length of the annulus. Following the analytical approach described by Collier (1986), the program models flow in the following boiling regimes and transitions between the regimes:

- Single-phase forced convection regime
- Transition at Onset of Nucleate Boiling (ONB)
- Partially developed subcooled nucleate boiling regime
- Transition for Onset of Significant Voiding (OSV)
- Fully developed subcooled nucleate boiling regime
- Saturated boiling.

Tables A.1 and A.2 summarize the regime and transition models used in the comparisons presented here.

Tables A.3 through A.6 list the specific equations used in the calculations. The equations have been updated from the ones presented in the test plan (Sam et al., 1989). In particular, the energy balance for the fluid heating in each boiling regime has a slightly modified form. The equations were originally set up for an annular geometry without ribs, and the equation for the energy balance has now been made general to properly account for the geometry with ribs.

Creare

Table A.1. BOILING REGIME MODELS USED IN ANNULUS PROGRAM CALCULATIONS				
Regime	Wall Heat Transfer	Fluid Heating/ Vapor Generation	Pressure Drop	Friction Factor
Single-Phase	Dittus-Boelter (1930)	Energy Balance	1ϕ	Rohsenow-Hartnett (1985)
Partially Developed Nucleate Boiling	Bowring (1962) (with Thom (1965)	Energy Balance	1ϕ	Levy (1967) (with Colebrook 1938)
Fully Developed Nucleate Boiling	Thom (1965	Energy Balance (with Ivey-Morris 1962 energy partition)	Homogeneous-2ϕ	McAdams (1949)
Saturated Boiling	Chen (1963) (FC only)	Energy Balance	Homogeneous-2ϕ	McAdams (1949)

Table A.2. TRANSITION MODELS USED IN ANNULUS PROGRAM CALCULATIONS	
Transition	Model
Onset of Nucleate Boiling (ONB)	Davis-Anderson (1966)
Onset of Significant Voiding (OSV)	Saha-Zuber (1974)
Saturated Boiling	$T_f=T_{sat}$

Greare

Table A.3 SINGLE PHASE REGIME EQUATIONS

Wall Heat Transfer (Dittus-Boelter, 1930):

$$Nu = \left[\frac{\phi \, D_h}{k_f \, (T_w - T_f)} \right] = 0.023 Re_f^{0.8} Pr_f^{0.4}$$

Fluid Energy Balance (First Principles)*:

$$\left[\frac{dT_f}{dz} \right] = \left[\frac{\pi \, \phi \, (D_o + D_i)}{\rho_f \, c_{pf} \, A_f \, V_f} \right]$$

Pressure Gradient (Single Phase):

$$- \left[\frac{dp}{dz} \right] = \left[\left[\frac{2 f_{wl}}{D_h} \right] \left[\frac{G^2}{\rho_f} \right] + \rho_f g (\sin \theta) \right]$$

Friction Factor (Rohsenow-Hartnett, 1985):

$$f_{wl} = 0.085 Re_f^{-0.25}$$

---

*Note that without ribs, $A_f = \frac{\pi}{4} (D_o^2 - D_i^2)$ and this equation reduces to

$$\left[\frac{dT_f}{dz} \right] = \left[\frac{4\phi}{\rho_f \, c_{pf} \, D_h \, V_f} \right]$$

Creare

Table A.4 PARTIALLY DEVELOPED SUBCOOLED BOILING REGIME EQUATIONS

Wall Heat Transfer (Bowring 1962 with Thom 1965):

$$\phi = (\phi_{sc} + \phi_{fc})$$

$$= \left[\frac{(T_w - T_{sat})}{0.072e^{-0.00079p}}\right]^2 + [0.023(k_f/D_h)Re_f^{0.8}Pr_f^{0.4}(T_{sat} - T_f)]$$

Fluid Energy Balance (First Principles)*:

$$\left[\frac{dT_f}{dz}\right] = \left[\frac{\pi \phi (D_o + D_i)}{\rho_f c_{pf} A_f V_f}\right]$$

Pressure Gradient (Modified Single Phase):

$$-\left[\frac{dp}{dz}\right] = \left[\left[\frac{2f_{tp}}{D_h}\right]\left[\frac{G^2}{\rho_f}\right] + \rho_f g(\sin\theta)\right]$$

Friction Factor (Levy 1967 with Colebrook 1938):

$$f_{wl} = 0.085Re_f^{-0.25} \qquad \text{(Rohsenow-Hartnett, 1985)}$$

$$\tau_w = [f_{wl}\rho_f V_f^2/2]$$

$$Y_b = 0.015[\sigma D_h/\tau_w]^{0.5}$$

$$f_{tp}^{-0.5} = -4\log_{10}\left[2\left[\frac{Y_b}{D_h}\right] + \frac{9.35}{Re_f f_{tp}^{0.5}}\right] + 3.48$$

Greare

Table A.5 FULLY DEVELOPED SUBCOOLED BOILING REGIME EQUATIONS

Wall Heat Transfer (Thom, 1965):

$$(T_w - T_{sat}) = 0.072\phi^{0.5}e^{-0.00079p}$$

Fluid Heating and Vaporization (Energy Balance with Ivey-Morris, 1962):

$$\left[\frac{dT_f}{dz}\right] = \left[\frac{\pi\ \phi\ (D_o + D_i)}{\rho_f\ c_{pf}\ A_f\ V_f}\right]\left[1 - \frac{h_{fg}}{h_{fg}'}\right]$$

$$\left[\frac{dx}{dz}\right] = \left[\frac{\pi\ \phi\ (D_o + D_i)}{\rho_f\ h_{fg}\ A_f\ V_f}\right]\left[\frac{h_{fg}}{h_{fg}'}\right]$$

$$h_{fg}' = \left[h_{fg} + 0.1c_{pf}(T_{sat} - T_f)\left[\frac{\rho_f}{\rho_g}\right]^{0.75}\right]$$

Pressure Gradient (Homogeneous Two-Phase):

$$-\left[\frac{dp}{dz}\right] = \left[\left[\frac{2f_{tp}}{D_h}\right]\left[\frac{G^2}{\rho_f}\right] + G^2(v_g - v_f)\left[\frac{dx}{dz}\right] + \frac{g(\sin\theta)}{(v_f + xv_{fg})}\right]$$

Friction Factor (McAdams, 1949):

$$\left[\frac{f_{tp}}{f_{wl}}\right] = \left\{1 + x\left[\frac{v_{fg}}{v_f}\right]\left[1 + x\left[\frac{\mu_f - \mu_g}{\mu_g}\right]\right]\right\}^{-0.25}$$

Creare

Table A.6 NUCLEATE BOILING TRANSITION MODELS

Onset of Nucleate Boiling (Davis-Anderson, 1966):

$$(T_w - T_{sat})_{onb} = \left[\frac{8\ \sigma\phi\ T_{sat}}{J\ h_{fg}\ k_f\ \rho_g}\right]^{0.5}$$

Onset of Significant Voiding (Saha-Zuber, 1974):

$Pe \geq 70{,}000$

$$St = \left[\frac{\phi}{\rho_f\ c_{pf}\ V_f\ (T_{sat} - T_f)_{fdb}}\right] = 0.0065$$

$Pe < 70{,}000$

$$St = 454.55/Pe$$

Saturated Boiling (Energy Balance):

$$T_f = T_{sat}$$

Creare

APPENDIX B
EVALUATION OF ALTERNATIVE ANALYTICAL MODELS

The analysis comparisons in Sections 3 and 4 of Volume 1 use the baseline models summarized in Appendix A. Those comparisons demonstrate areas where the modelling could be improved. Four aspects of the modelling of boiling flow and heat transfer in the annulus were subsequently studied briefly. The areas studied include:

- Wall-to-fluid heat transfer in the single-phase region,
- Frictional pressure drop in the single-phase region,
- Frictional pressure drop in the partially developed nucleate boiling regime (between ONB and OSV), and
- The criterion for OSV.

Table B.1 summarizes the phenomena for which the models have been revised from the original analysis. This appendix reports the effect of these changes upon the data comparisons.

Table B.1 ALTERNATIVE MODELS USED IN ANNULUS PROGRAM CALCULATIONS

Phenomenon	Original	Revised
Single-Phase Heat Transfer	Dittus-Boelter $\mu_f = f(T_f)$	Bjorge-Hall-Rohsenow $\mu_f = f(T_f, T_w)$
Single-Phase Friction	Rohsenow-Hartnett $f_{wl} = f(Re_f)$	Zigrang-Sylvester $f_{wl} = f(Re_f, Pr_f, \varepsilon)$
Partially Developed Boiling Friction	1ϕ: Rohsenow-Hartnett 2ϕ: Colebrook (iteration)	1ϕ and 2ϕ: Zigrang-Sylvester (explicit)

B.1 Single-Phase Heat Transfer

As discussed in Section 3.1, the temperature difference between the wall and the fluid tends to be overpredicted about 10% at low heat flux. And the temperature difference is overpredicted by a greater amount at higher heat flux as discussed in Section 3.2. When the temperature difference is overpredicted, it means that the heat transfer coefficient is underpredicted, assuming a constant heat flux. It is shown here that a modification of the Dittus-Boelter model (Table A.3), similar to the modification of the Colburn model made by Bjorge, Hall and Rohsenow (1982), improves the comparisons.

The Dittus-Boelter model was developed for pipe flow with constant fluid properties evaluated at the bulk fluid temperature. Basing the viscosity on the bulk fluid temperature -- the highest limit on viscosity -- results in the lowest heat transfer coefficient and the highest wall-to-fluid temperature difference. In 1933, Colburn changed the exponent on the Prandtl

Greare

number in the Dittus-Boelter model from 0.4 to 0.33. Bjorge, Hall and Rohsenow (1982) modified the Colburn model to account for the variation in fluid viscosity across the region from the heated wall to the channel centerline by multiplying the Nusselt number by a viscosity ratio:

$$Nu = 0.023\, Re_f^{0.8}\, Pr_f^{0.33} \left[\frac{\mu_{film}}{\mu_f}\right]^{-0.47} \qquad B.1$$

A similar modification to the Dittus-Boelter model has been implemented in the ANNULUS code:

$$Nu = 0.023\, Re_f^{0.8}\, Pr_f^{0.4} \left[\frac{\mu_{film}}{\mu_f}\right]^{-0.4} \qquad B.2$$

The viscosity ratio exponent simply changes the viscosity used in the Reynolds and Prandtl numbers from a value (μ_f) based on the bulk fluid temperature, T_f, to a value (μ_{film}) based on the average of the wall and bulk fluid temperatures, $(T_w + T_f)/2$.

The revised wall temperature calculations (based on Equation B.2) are compared with the original ANNULUS calculations and data at low heat flux (Series 1) in Figures B.1 through B.7 and high heat flux (Series 9) in Figures B.8 through B.12. The revised calculations are in closer agreement with the data for the differences between the wall and fluid temperatures, especially at low velocity. Including the viscosity ratio term decreases the wall-to-fluid temperature difference at the annulus inlet up to 15% at low velocity (less at the annulus exit). (In the limiting case, the wall-to-fluid temperature difference can be reduced an additional 15% if the viscosity is evaluated at the wall temperature. However, basing the viscosity on the wall temperature -- the lowest limit on viscosity -- is not justifiable.) While the temperature difference is predicted more closely with the revised calculation, predictions consistently lie 5°F to 20°F higher than the measured data.

Two explanations for the remaining difference between the ANNULUS calculation and the data are given in the following paragraphs.

The measured fluid temperatures are in one of the colder subchannels. Figure 3.21 shows that even with uniform heat flux, the fluid temperatures at the exit of the instrumented channel (136 degrees) are 5°F to 10°F colder than the average of the measured temperatures. The nonuniform temperature distribution is thought to be due to a geometry variation from subchannel to subchannel.

The measured fluid temperatures at the subchannel centerline are lower than the actual bulk fluid temperatures because of the temperature gradient across the subchannel. The average of the measured fluid temperatures at the annulus exit is about 5°F less than the bulk fluid temperature predicted by ANNULUS (with an energy balance). This is clearly shown in Figures B.4 through B.10 where the ANNULUS prediction (dotted line) lies at higher temperature at the annulus exit (L = 13 ft) than measured data in the subchannels (open symbols). The difference between the average of the measured fluid temperatures and the calculated temperature is due to the temperature gradient across the subchannel. The temperature gradient can be illustrated by reference to the analytical solution for fully

developed turbulent flow in a tube with constant heat flux (Kays, 1966). Figure B.13 shows the solution in terms of dimensionless temperature profiles for a Reynolds number of 30,000 and a range of Prandtl numbers. (For an annulus test at the baseline conditions near the OSV point, the Reynolds and Prandtl numbers are about $5x10^4$ and 1.4, respectively, with properties evaluated at the exit fluid temperature.) Note that the solution is for heat transfer from the fluid to the wall -- the profiles are "upside down" with respect to the annulus experiments. For Pr = 1, the bulk fluid temperature (T_b) is given by:

$$\frac{T_b - T_w}{T_f - T_w} = 0.833 \qquad \text{B.3}$$

where T_w is the wall temperature and T_f is the fluid temperature at the channel centerline. Substituting typical measured values of wall and centerline temperatures for the baseline condition (T_w = 275°F, T_f = 250°F) yields a bulk fluid temperature of 254°F which is 4°F higher than the measured centerline temperature.

Combining the fact that most measured temperatures are in one of the colder subchannels with the effect of the temperature gradient across the subchannel suggests that the measured fluid temperatures are about 10°F to 15°F less than the bulk fluid temperatures in the channel at 136 degrees. Therefore, the average fluid temperatures should be higher than the measured data and in better agreement with the analysis.

B.2 Single-Phase Friction Factor

Section 3.2 indicated that the pressure gradient in the single-phase region is slightly overpredicted by the Rohsenow-Hartnett model for friction factor in the baseline analysis. By implementing the Zigrang-Sylvester friction factor model, the comparisons can be improved somewhat, but the most important benefit is that it can be tied in with the friction factor model for partially developed boiling (see Section B.3) and improve the comparisons in that regime.

The Zigrang-Sylvester model (1982) is essentially a fit to the Colebrook model (1938). Both the Zigrang-Sylvester and Colebrook models include wall roughness. The significant difference between the two models is that the Zigrang-Sylvester model determines the friction factor explicitly rather than implicitly:

$$f_{wl} = 0.25 \left[-2.0 \log \left\{ \frac{(\varepsilon/D_h)}{3.7} - \left[\frac{5.02}{Re_f} \right] \log \left[\frac{(\varepsilon/D_h)}{3.7} + \frac{13}{Re_f} \right] \right\} \right]^{-2} \qquad \text{B.4}$$

The friction factor evaluated from Equation B.4 agrees with the Colebrook friction factor within 1% for wall roughness values from $(\varepsilon/D_h) = 1x10^{-5}$ to $1x10^{-2}$ and Reynolds numbers from $1x10^3$ to $1x10^6$. The wall roughness for the annulus is estimated to be $32x10^{-6}$ inches making the value of (ε/D_h) equal to $6.8x10^{-5}$ and $6.1x10^{-5}$ for the ribbed and non-ribbed test sections respectively. The Reynolds numbers range from $1.3x10^4$ to $1.3x10^5$ for these experiments. Therefore, the Zigrang-Sylvester model is appropriate for the annulus test conditions.

Creare

Pressure drop calculations using the Zigrang-Sylvester model are compared with single-phase results without heat transfer in Figure B.14. The Zigrang-Sylvester model is in close agreement with the Build 4 data and the Rohsenow-Hartnett model. Figures B.15 through B.17 compare additional adiabatic, single-phase data at three velocities in Build 4 with the original Rohsenow-Hartnett model and the revised Zigrang-Sylvester model. Both models are in good agreement with data in the upper portion of the annulus, but deviate at the lower end of the annulus. The deviation at the lower end is thought to be due to a geometry variation which is not accounted for in the model.

The Zigrang-Sylvester model is shown to be in excellent agreement with heated wall data in the pressure plots (upper graphs) in Figures B.1 through B.12. The data are represented much better by the Zigrang-Sylvester model than by the Rohsenow-Hartnett model at both low and high heat fluxes.

B.3 Pressure Drop in Partially Developed Boiling

The Levy model (Table A.4) overpredicts the increased pressure gradient following ONB (Figure 3.13). This also leads to a significant departure of the calculation from the data on the demand curve as the minimum is approached for high heat fluxes. (Figure 3.10 illustrates this result.) Further, in simultaneously using the Rohsenow-Hartnett model as the basis for the single-phase friction factor and the Colebrook model for the two-phase friction factor (which accounts for the presence of the attached vapor bubbles), the baseline model is inconsistent. This is a small effect in the analysis. Using the Zigrang-Sylvester model for both eliminates the inconsistency, however.

The Zigrang-Sylvester model is used as the basis for the two-phase friction factor after replacing the wall roughness term, ε, in Equation B.4 with the Levy bubble size parameter, Y_b:

$$f_{tp} = 0.25 \left[-2.0 \log \left\{ \frac{(Y_b/D_h)}{3.7} - \left[\frac{5.02}{Re_f} \right] \log \left[\frac{(Y_b/D_h)}{3.7} + \frac{13}{Re_f} \right] \right\} \right]^{-2} \qquad \text{B.5}$$

This is the same approach that was used in the original analysis except that the Colebrook model has been replaced with the Zigrang-Sylvester model.

This change improves the pressure drop predictions. It is especially noticeable at high heat flux as shown in Figures B.9 through B.12. The change in the measured pressure gradient following ONB (which occurs around 9 to 10 feet in the annulus) is accurately represented by the analysis. (Recall that a small part of the change is suspected to be due to a geometry variation at the end of the annulus as illustrated by the change in pressure gradient for the adiabatic results in Figures B.15 through B.17. The analysis may still overpredict the pressure gradient when the geometry variation is accounted for, but not as much as before.)

Figure B.18 indicates that the Zigrang-Sylvester model improves the prediction of the minimum pressure drop at high heat flux (375 kBtu/hr-ft^2). The overall demand curve is also in better agreement with the data at low heat flux as shown in Figure B.19.

Greare

B.4 Onset of Significant Voiding

The Saha-Zuber criterion in the original ANNULUS calculations is St = 0.0065. The data displayed in Figure 4.1 suggest that the minimum pressure drop in the annulus occurs at St ≤ 0.0045. If St = 0.0045 is used as the OSV criterion in the analysis, the calculated velocity and the minimum pressure drop are significantly larger than measured values at high heat fluxes (Figure B.20). The effect of Stanton number is less noticeable at lower heat flux (Figure B.21).

Recall that Figure 4.1 uses the average of the four fluid temperature measurements near the annulus exit in deriving the Stanton number criterion for this plot. (See Equation 1.) Figure B.22 shows the estimated Stanton number in the annulus at the minimum pressure drop when the exit fluid temperature is calculated by an energy balance. Because the measured fluid temperatures tend to be low, as discussed in Section B.1, the values lie at higher Stanton number on average than in Figure 4.1 which uses the measured exit temperatures. Based on this result, the original criterion St = 0.0065 was retained for OSV in the analysis. Figures B.20 and B.21 indicate that this is reasonable.

References

Bjorge, R.W., Hall, G.R. and Rohsenow, W.M.; *Correlations of Forced Convection Boiling Heat Transfer Data*; Int. J. of Heat and Mass Transfer, V25, No. 6, pp. 735-578, June 1982.

Kays, W.M.; *Convective Heat and Mass Transfer*; New York: McGraw-Hill Inc., 1966

Zigrang, D.J., Sylvester, N.D. and Hall, J.; *Explicit Approximations to the Solution of Colebrook's Friction Factor Equation*; AIChE J., V28, May, 1982, P. 514.

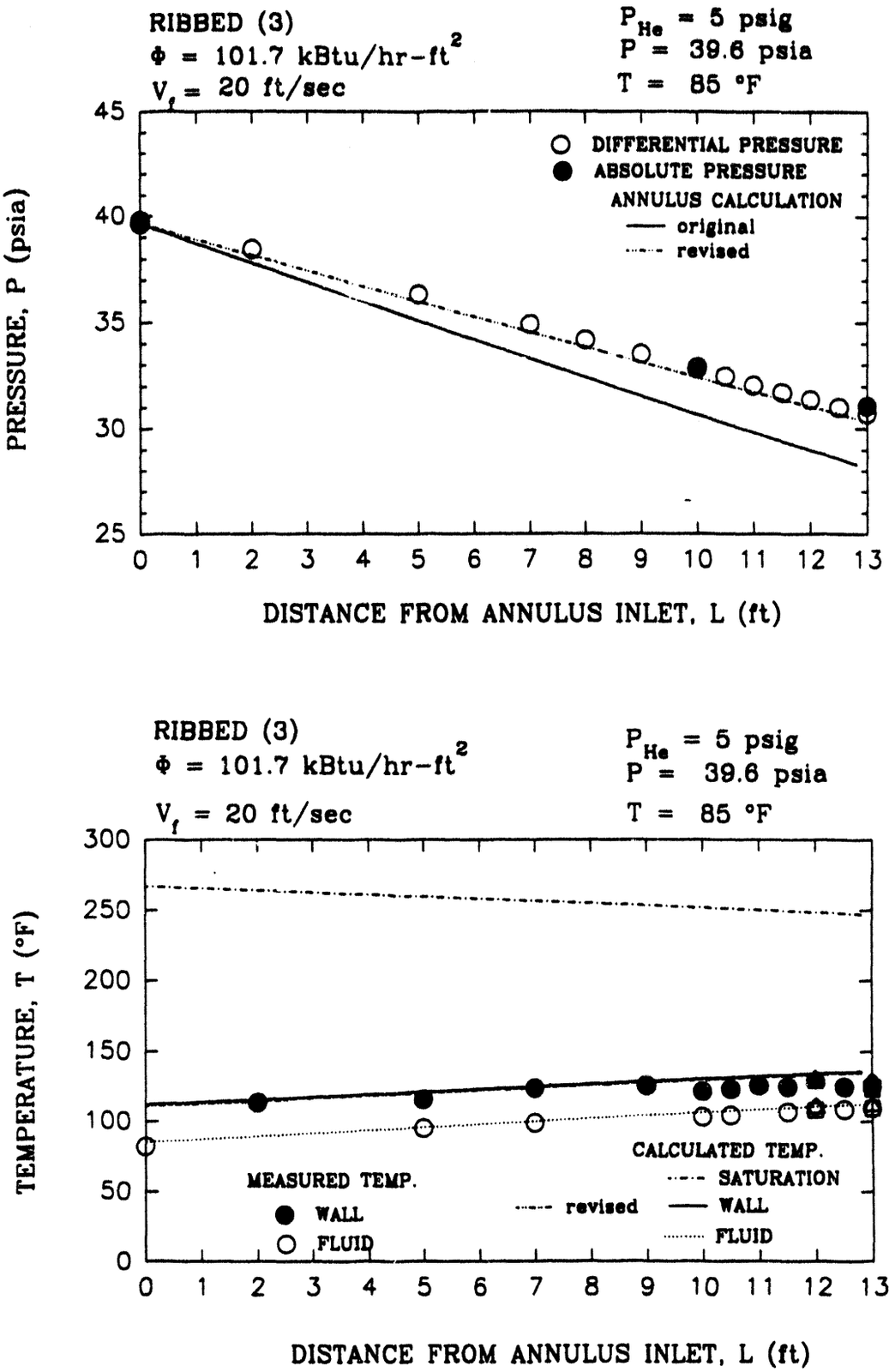

Figure B.1. DATA PROFILES AND ANNULUS CALCULATIONS AT BASELINE CONDITIONS (V_f = 20 FT/S)

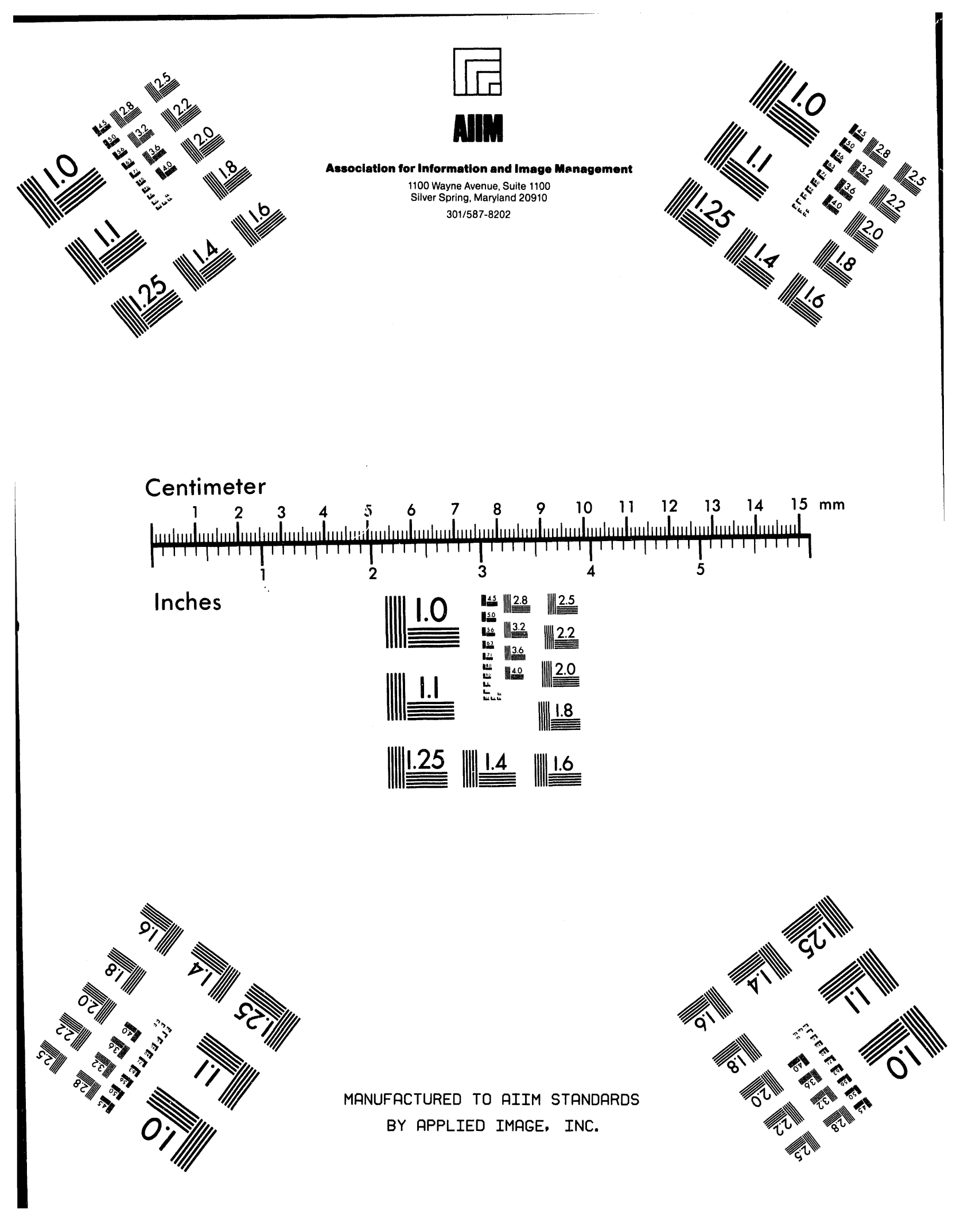
AIIM
Association for Information and Image Management
1100 Wayne Avenue, Suite 1100
Silver Spring, Maryland 20910
301/587-8202
Centimeter
Inches
MANUFACTURED TO AIIM STANDARDS
BY APPLIED IMAGE, INC.

2 of 2

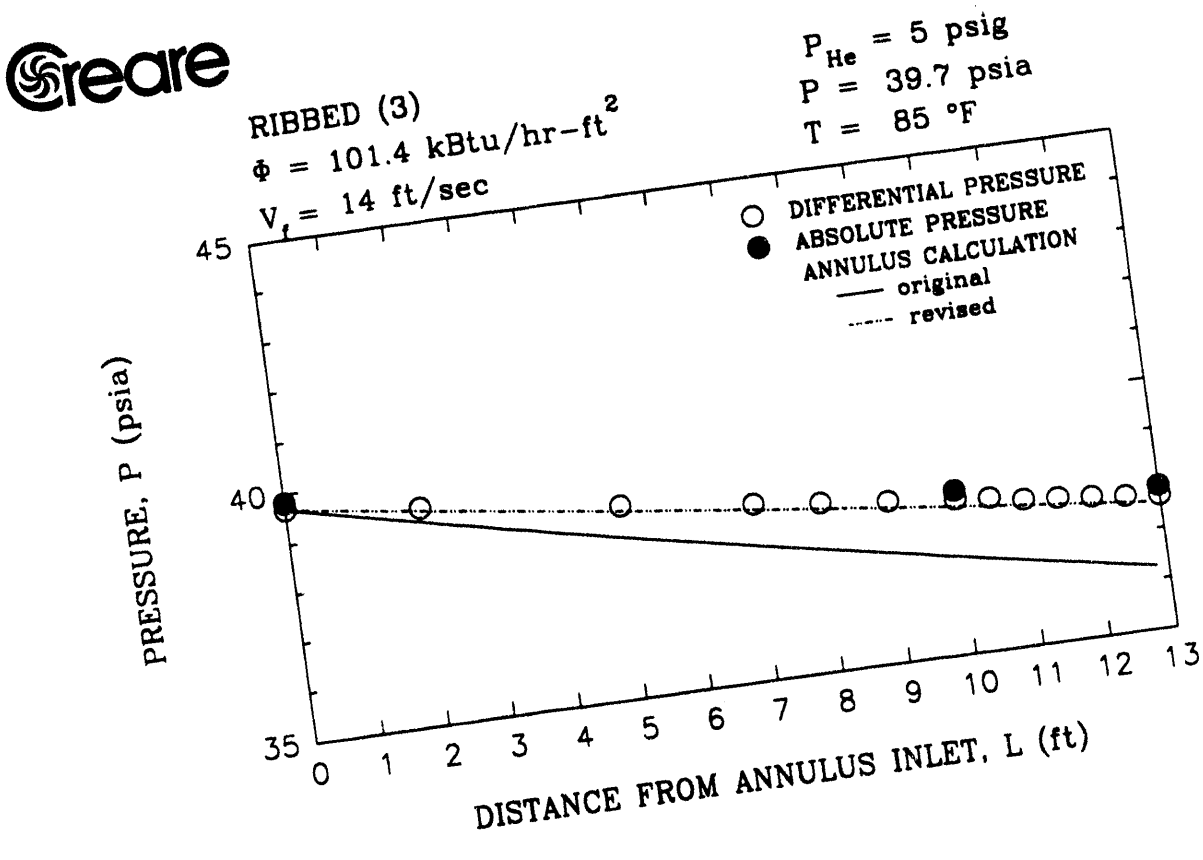

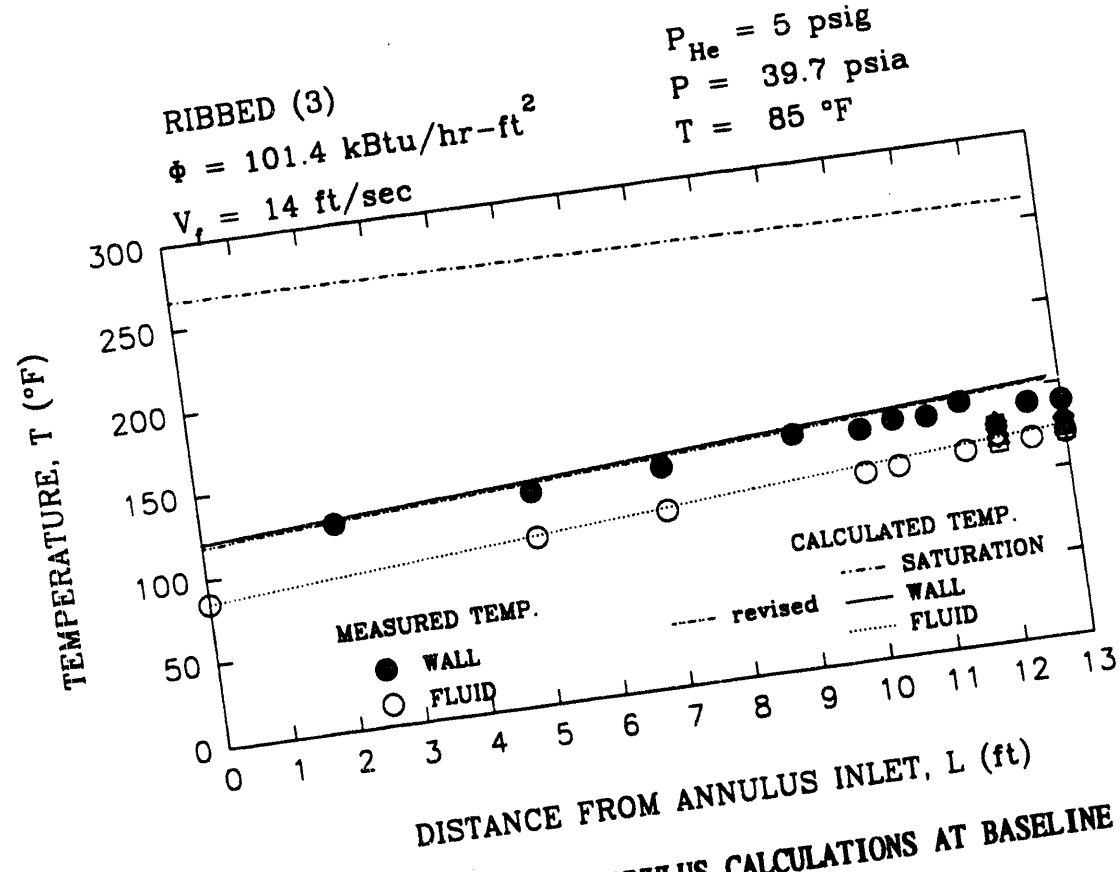

Figure B.2. DATA PROFILES AND ANNULUS CALCULATIONS AT BASELINE CONDITIONS (V_f = 14 FT/S)

Greare

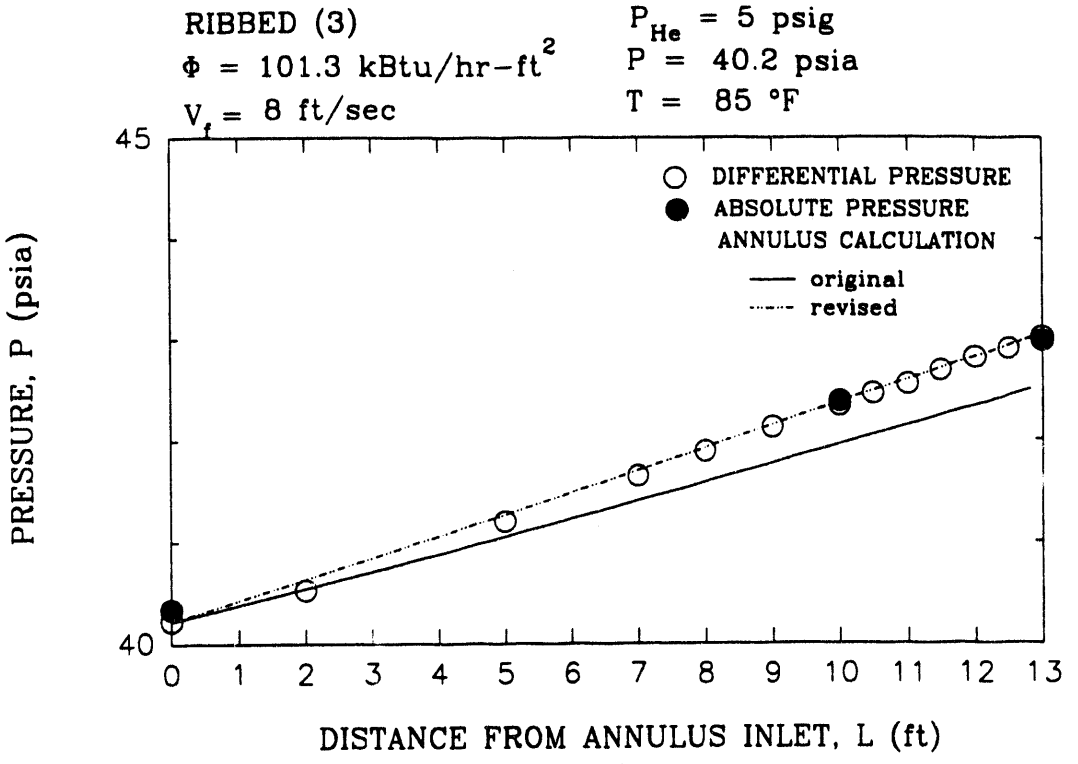

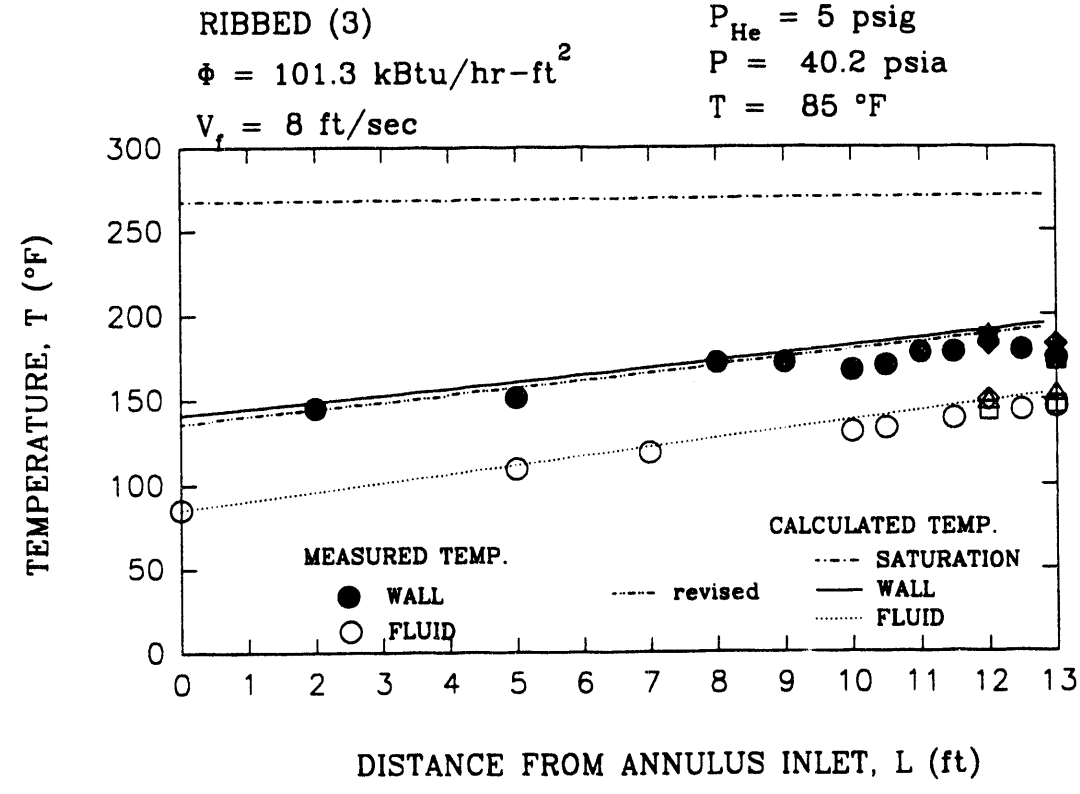

Figure B.3. DATA PROFILES AND ANNULUS CALCULATIONS AT BASELINE CONDITIONS (V_f = 8 FT/S)

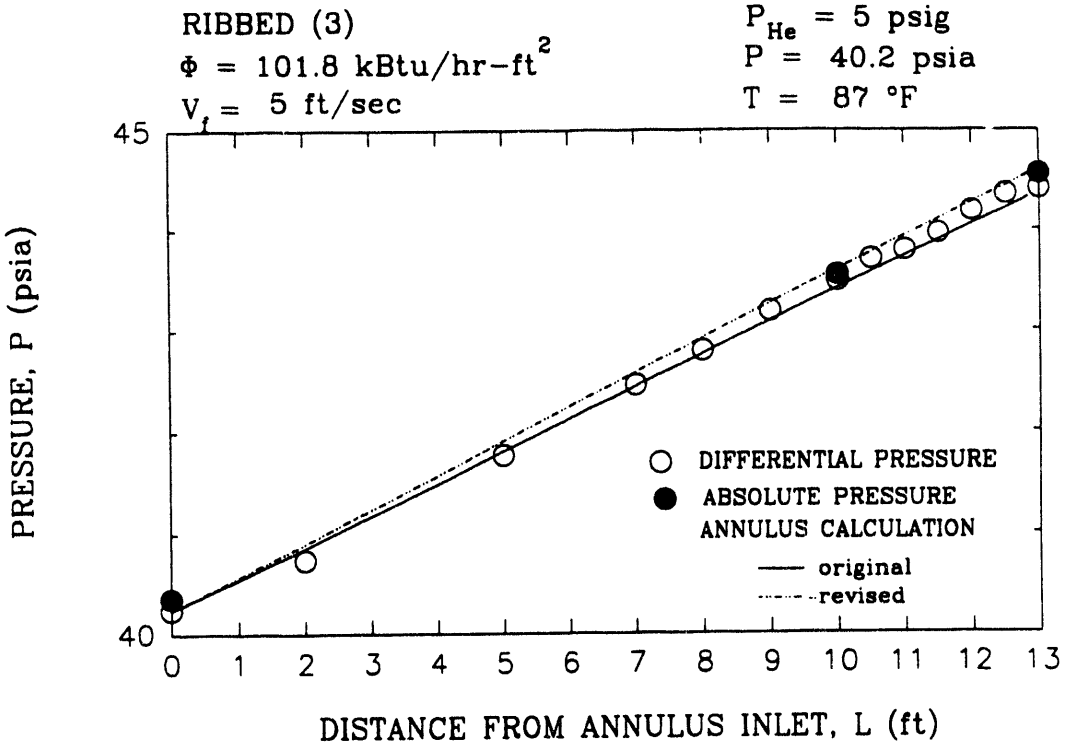

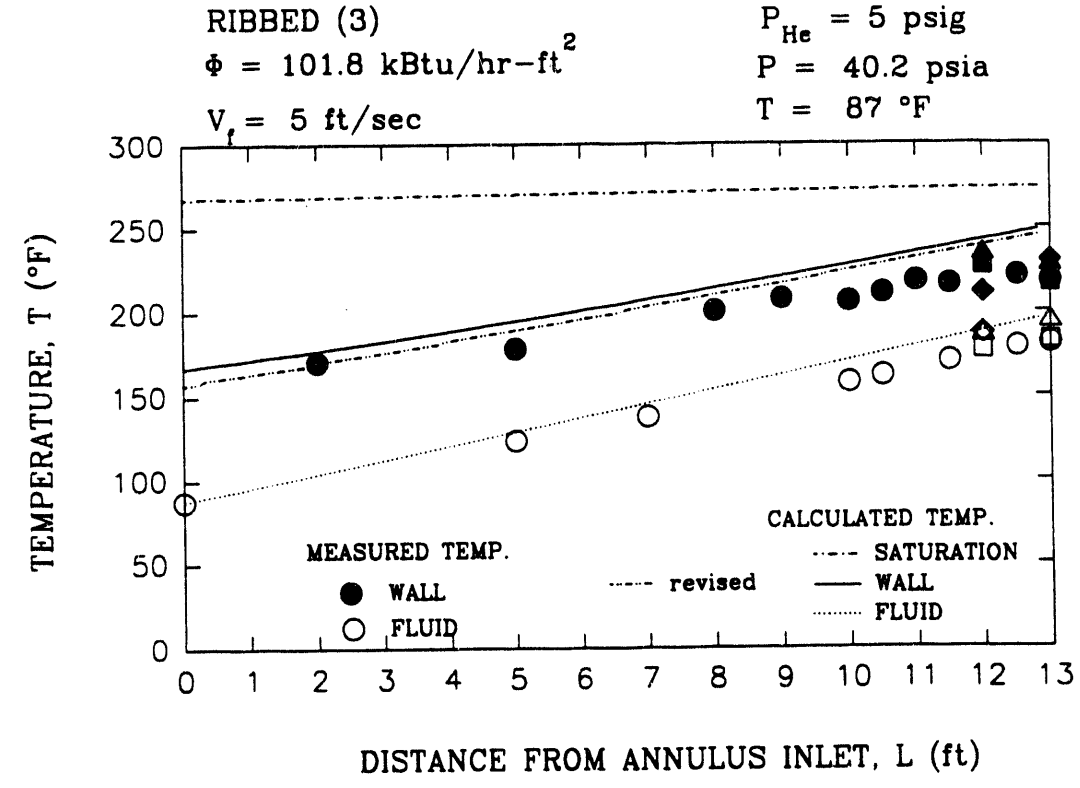

Figure B.4. DATA PROFILES AND ANNULUS CALCULATIONS AT BASELINE CONDITIONS (V_f = 5 FT/S)

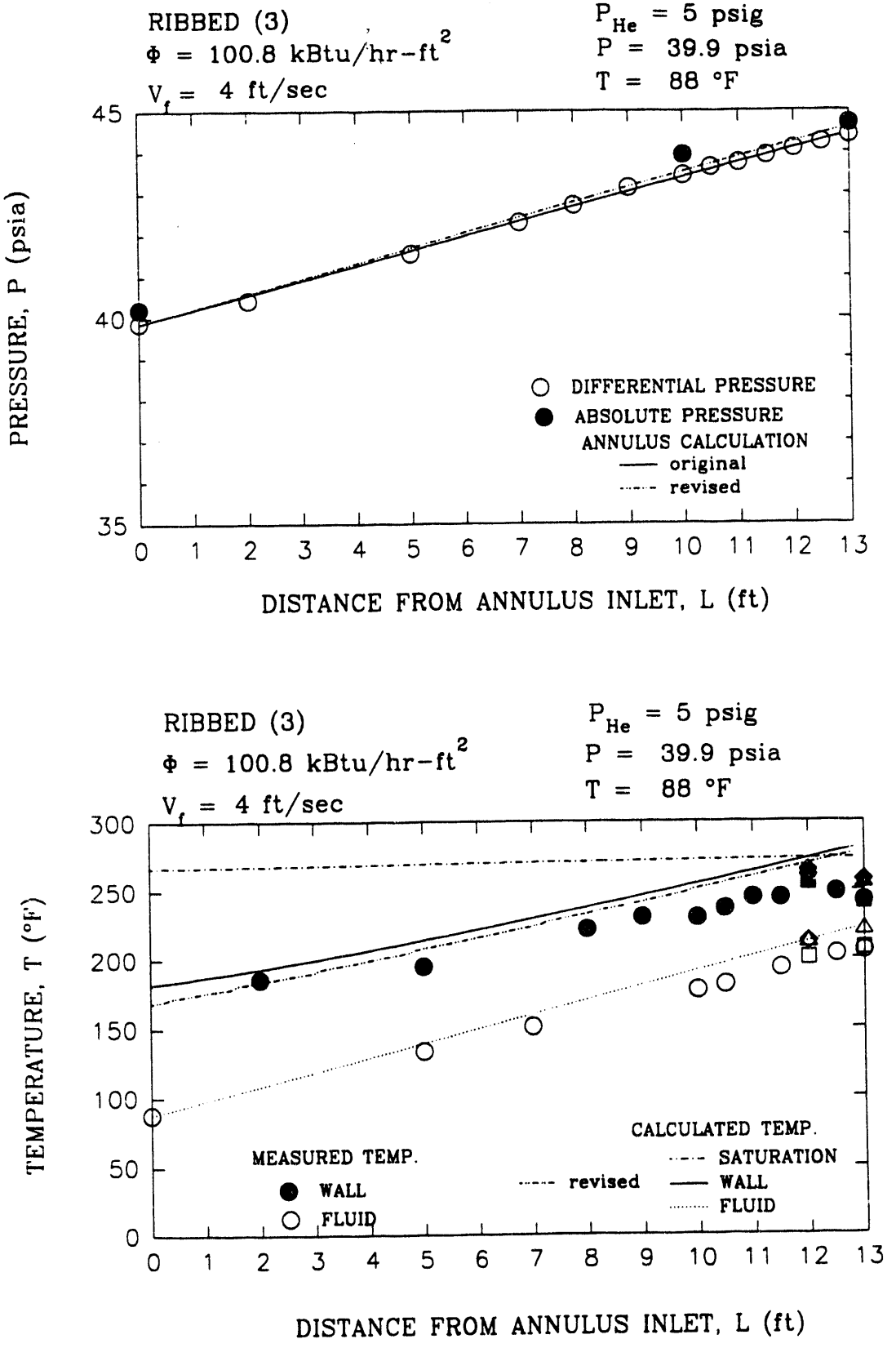

Figure B.5. DATA PROFILES AND ANNULUS CALCULATIONS AT BASELINE CONDITIONS (V_f = 4 FT/S)

Creare

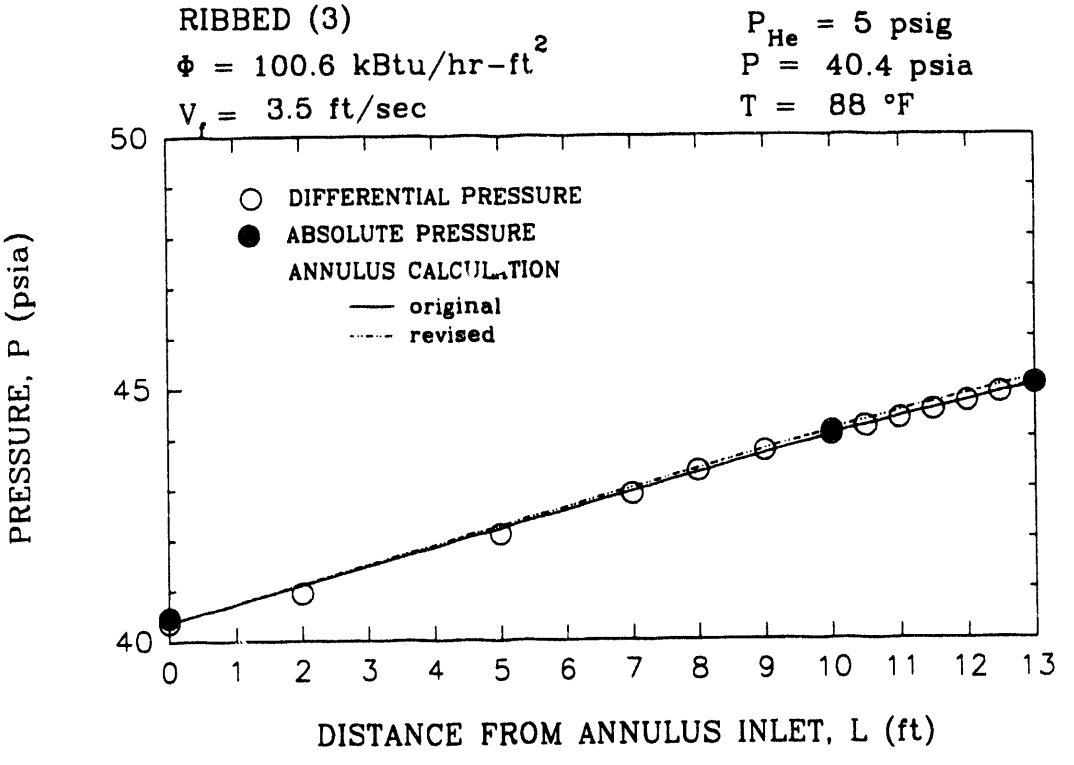

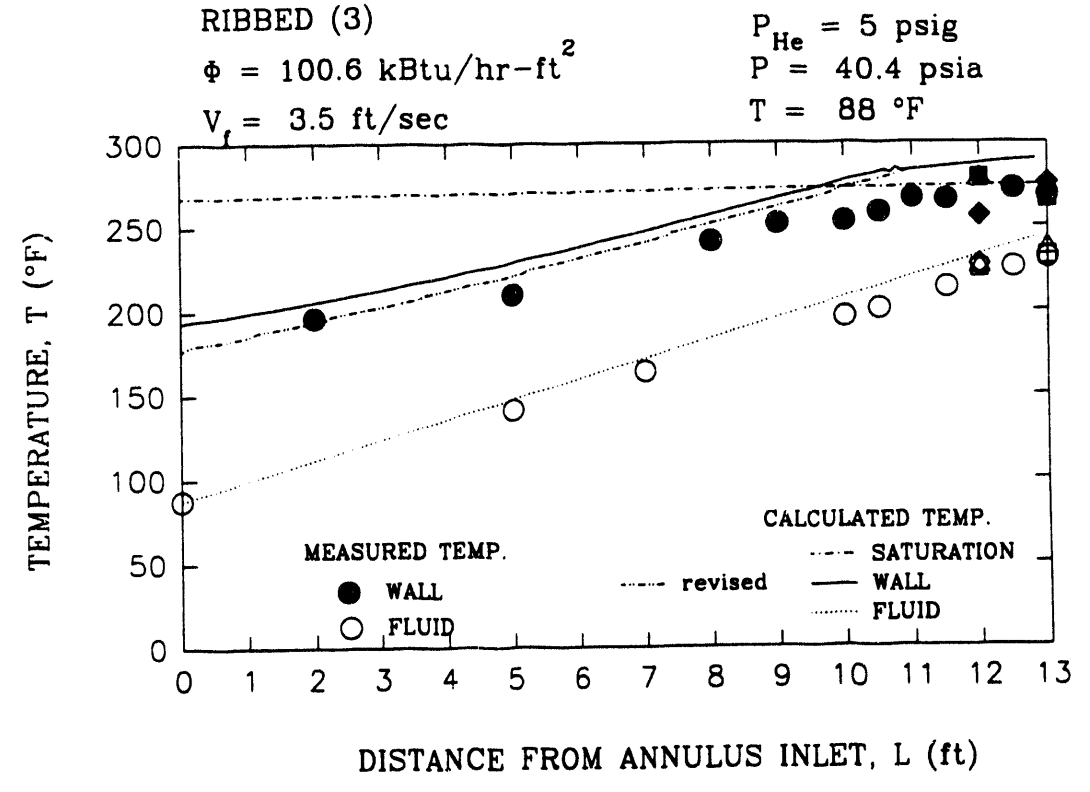

Figure B.6. DATA PROFILES AND ANNULUS CALCULATIONS AT BASELINE CONDITIONS (V_f = 3.5 FT/S)

Creare

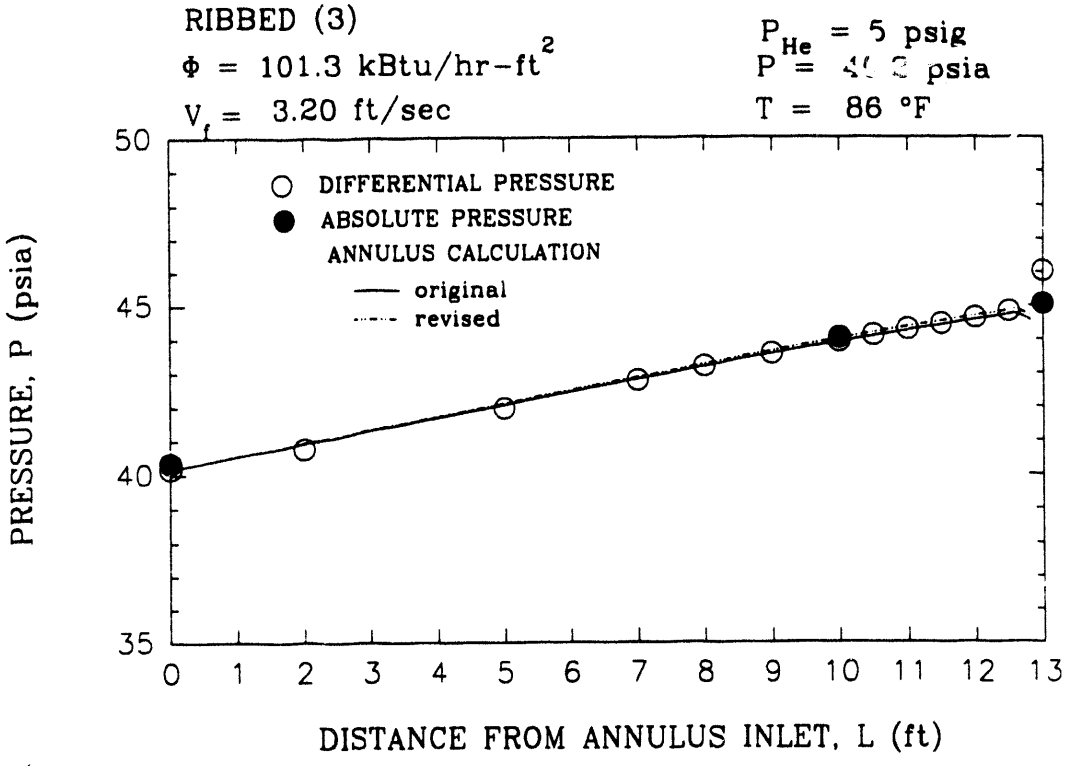

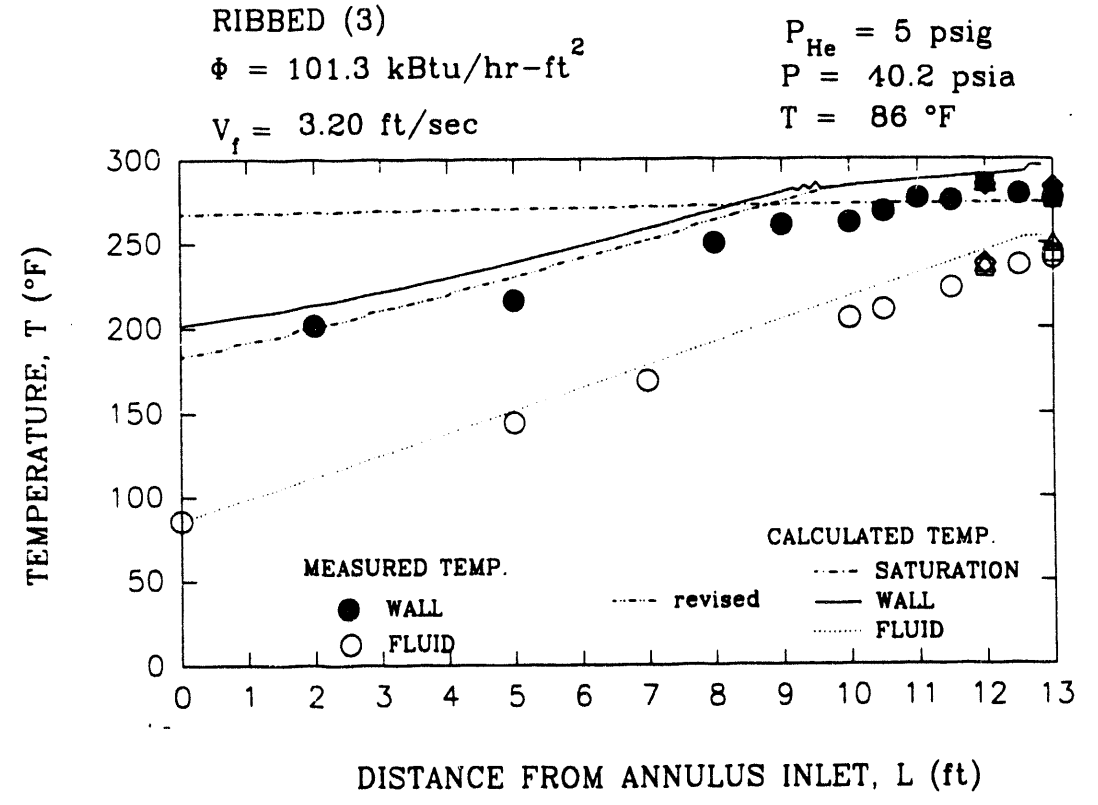

Figure B.7. DATA PROFILES AND ANNULUS CALCULATIONS AT BASELINE CONDITIONS (V_f = 3.2 FT/S)

Greare

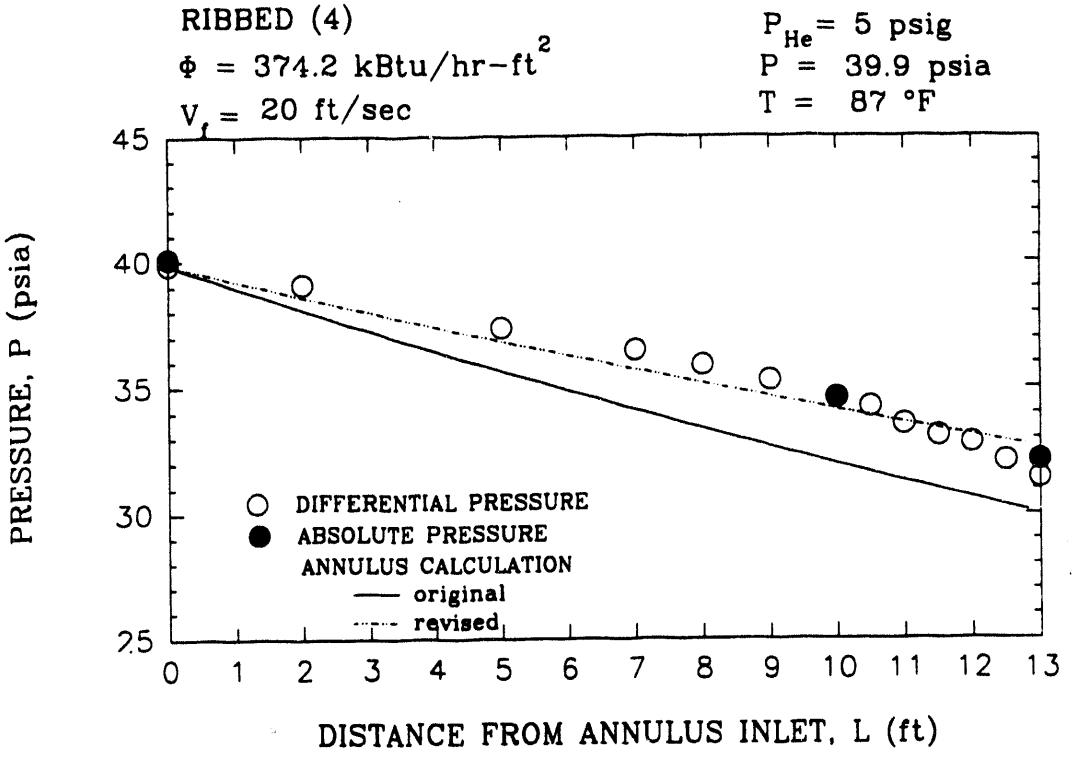

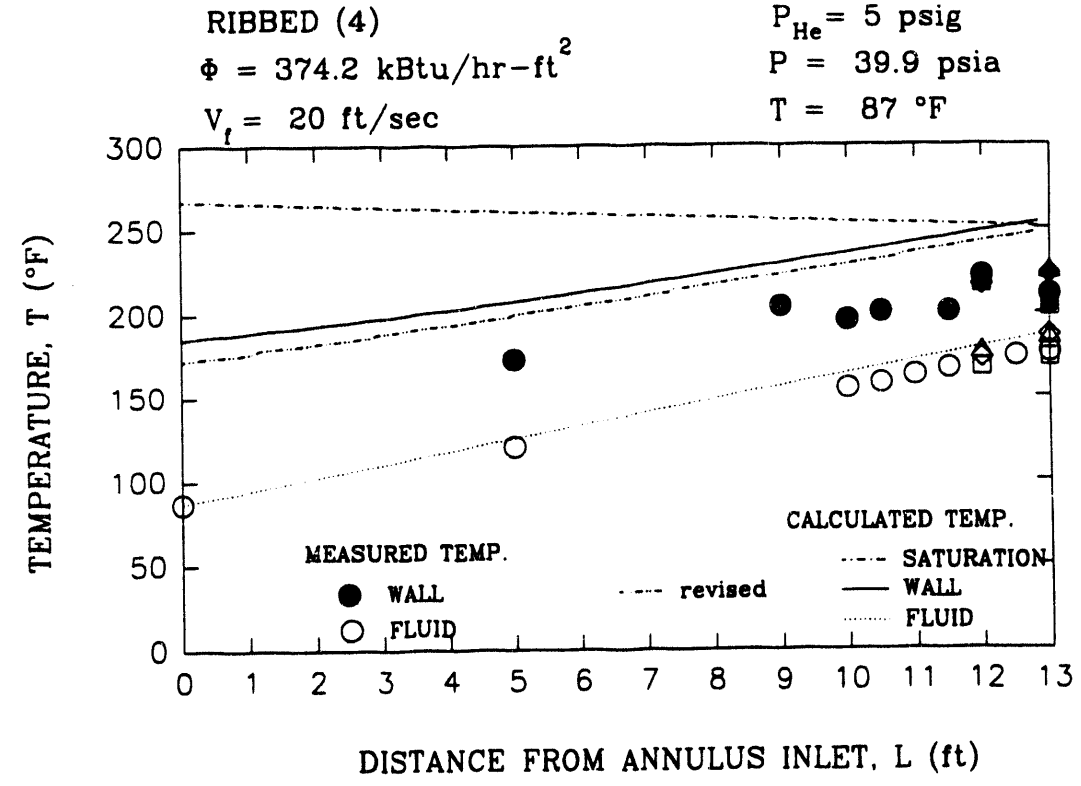

Figure B.8. DATA PROFILES AND ANNULUS CALCULATIONS AT HIGH HEAT FLUX (V_f = 20 FT/S)

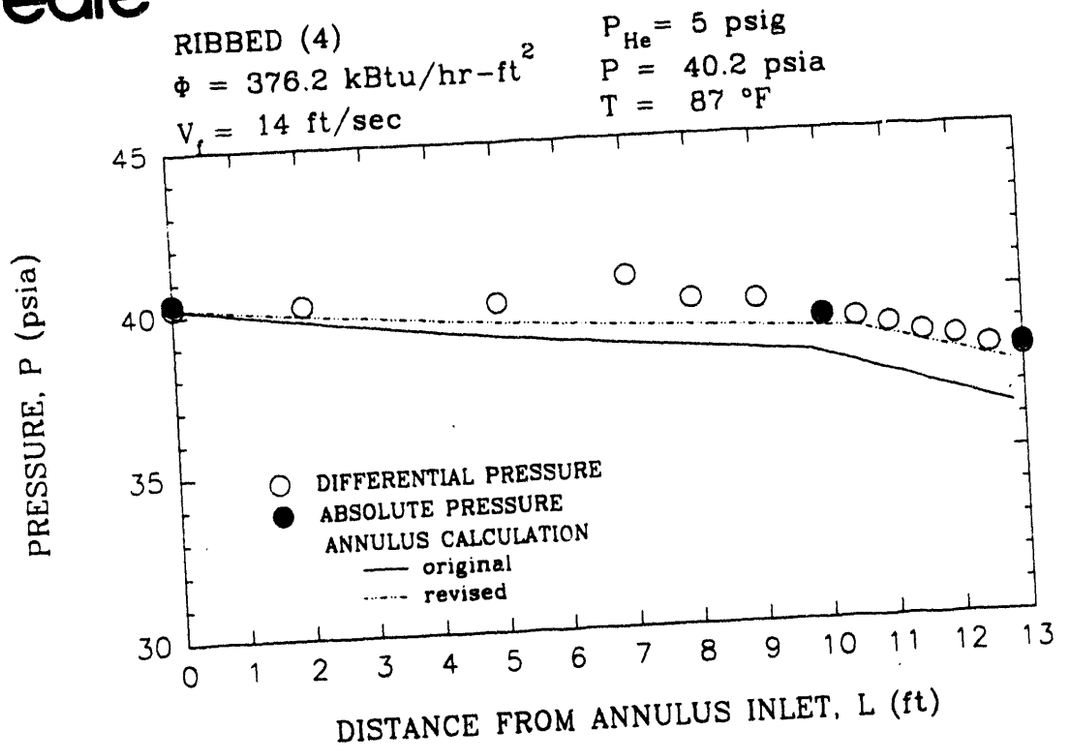

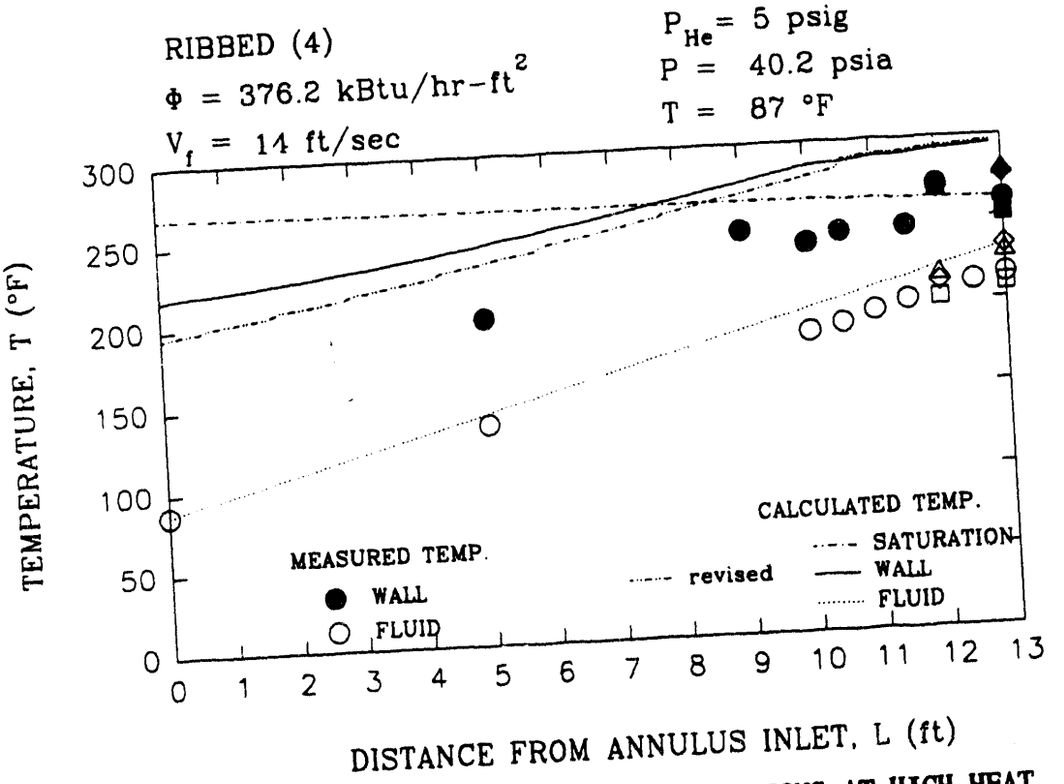

Figure B.9. DATA PROFILES AND ANNULUS CALCULATIONS AT HIGH HEAT FLUX (V_f = 14 FT/S)

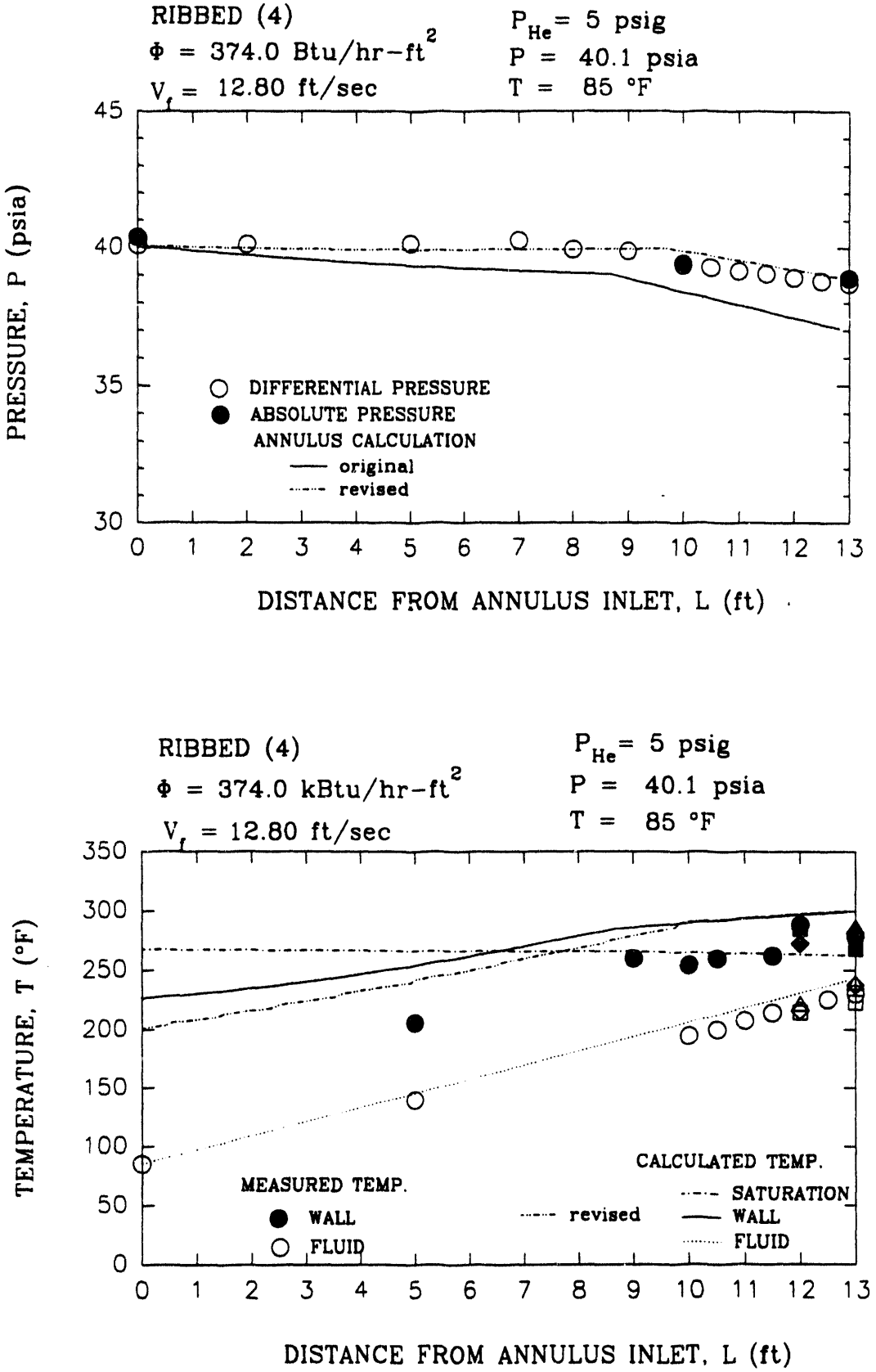

Figure B.10. DATA PROFILES AND ANNULUS CALCULATIONS AT HIGH HEAT FLUX (V_f = 12.8 FT/S)

Greare

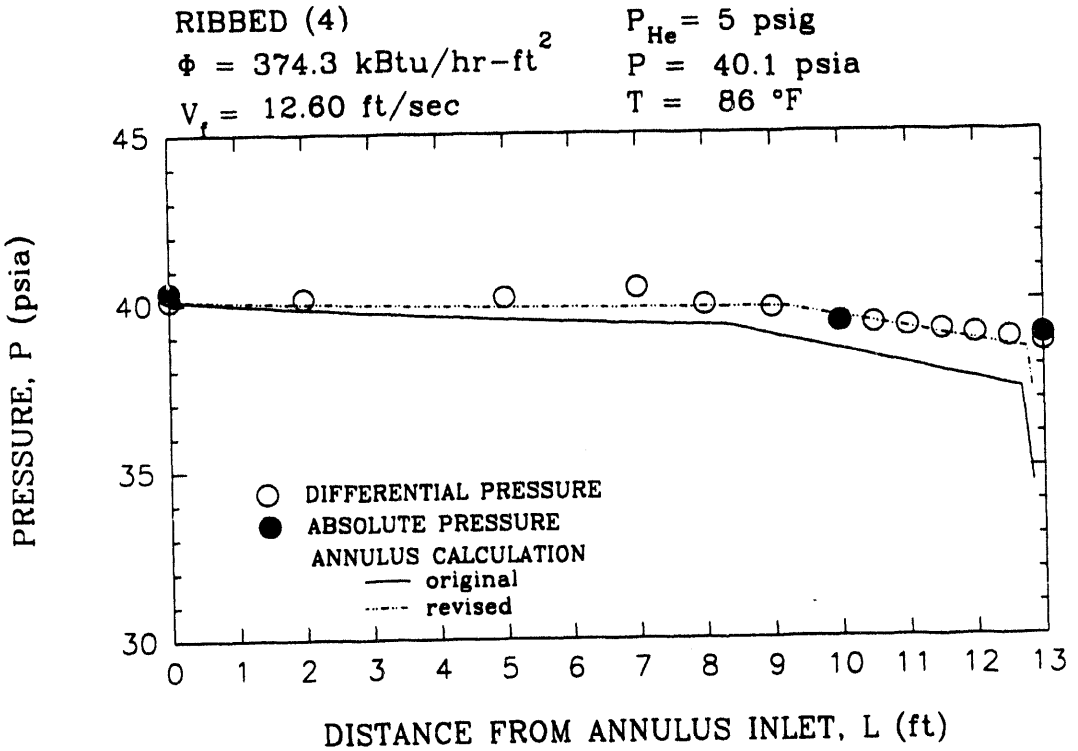

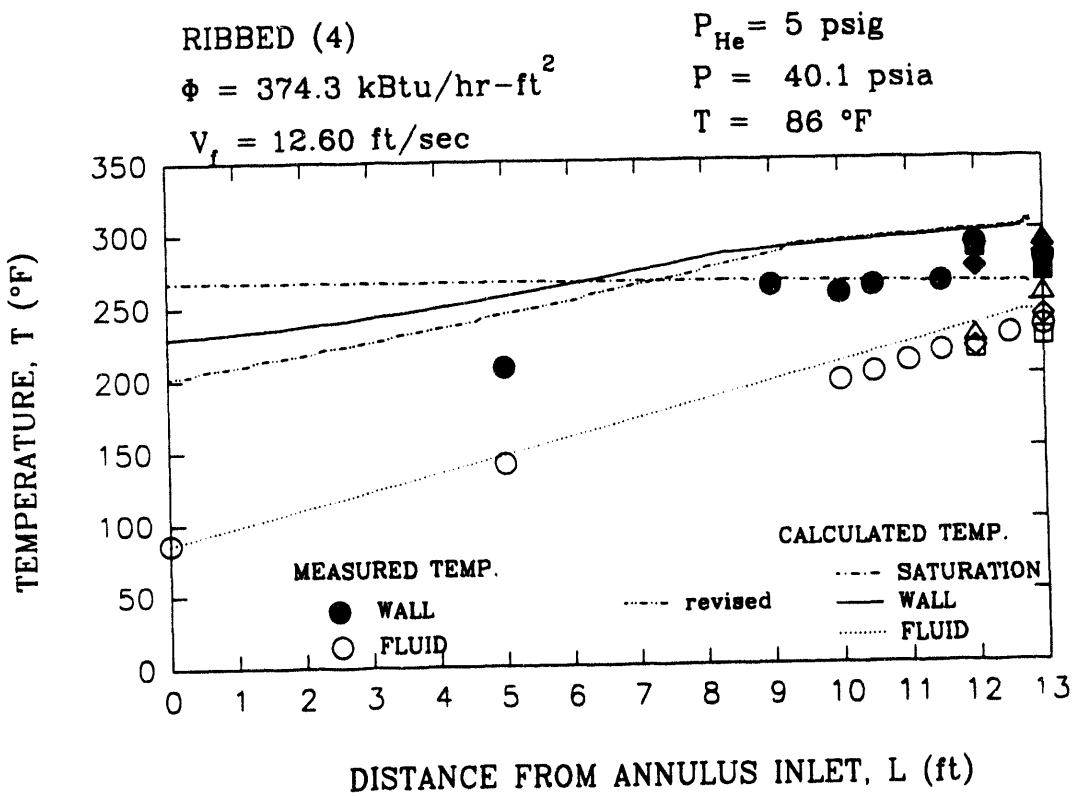

Figure B.11. DATA PROFILES AND ANNULUS CALCULATIONS AT HIGH HEAT FLUX (V_f = 12.6 FT/S)

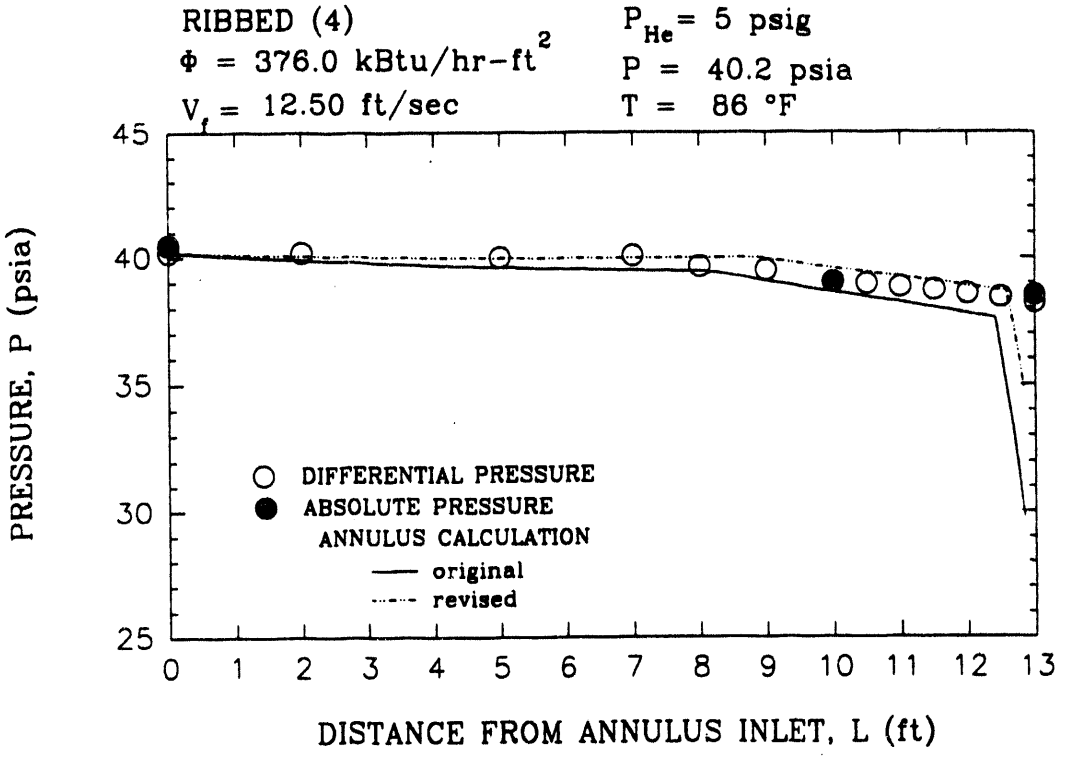

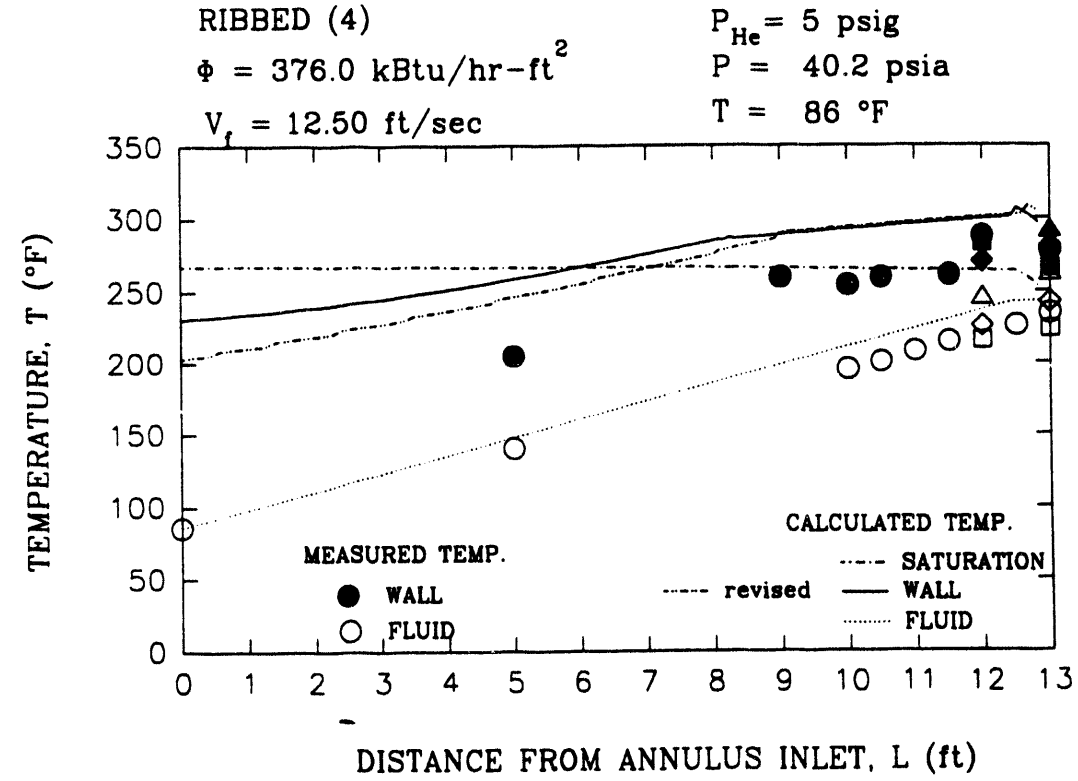

Figure B.12. DATA PROFILES AND ANNULUS CALCULATIONS AT HIGH HEAT FLUX (V_f = 12.5 FT/S)

Greare

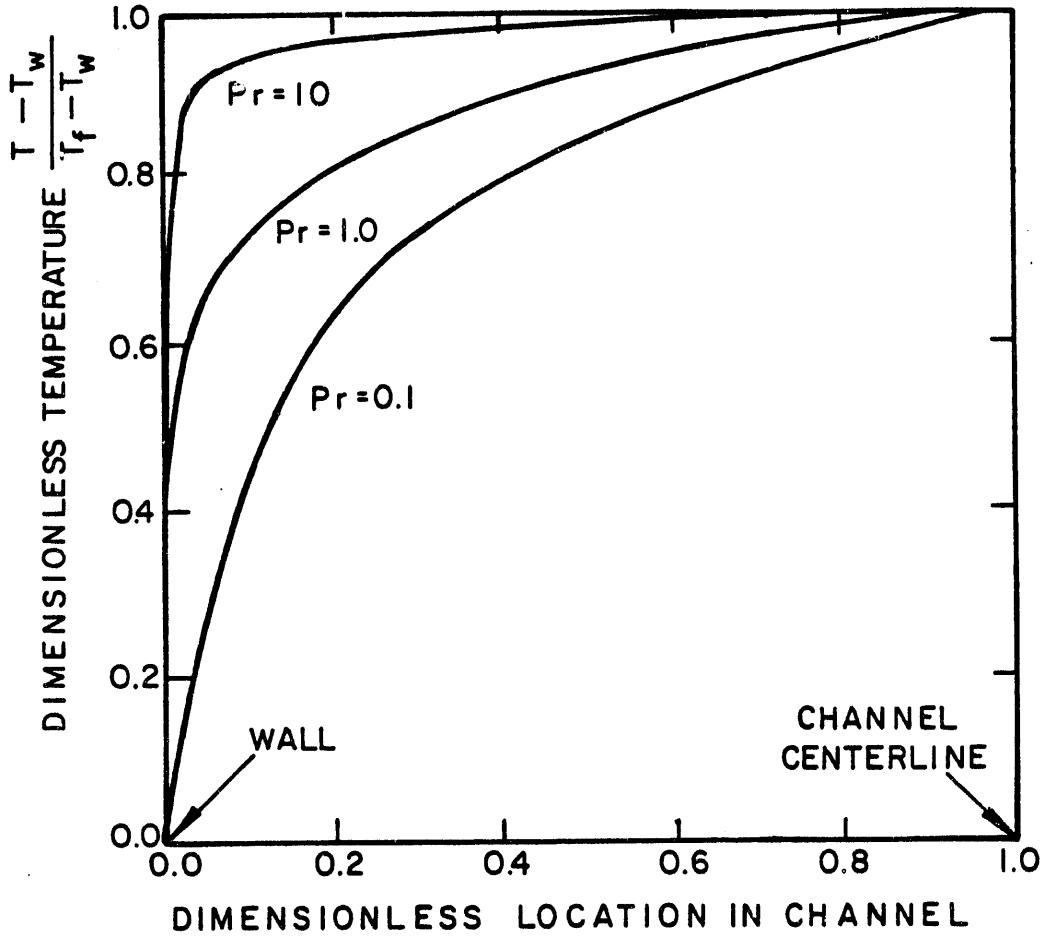

Figure B.13. DIMENSIONLESS TEMPERATURE PROFILES IN A CIRCULAR TUBE AT RE = 30,000 (FROM KAYS, 1966)

Creare

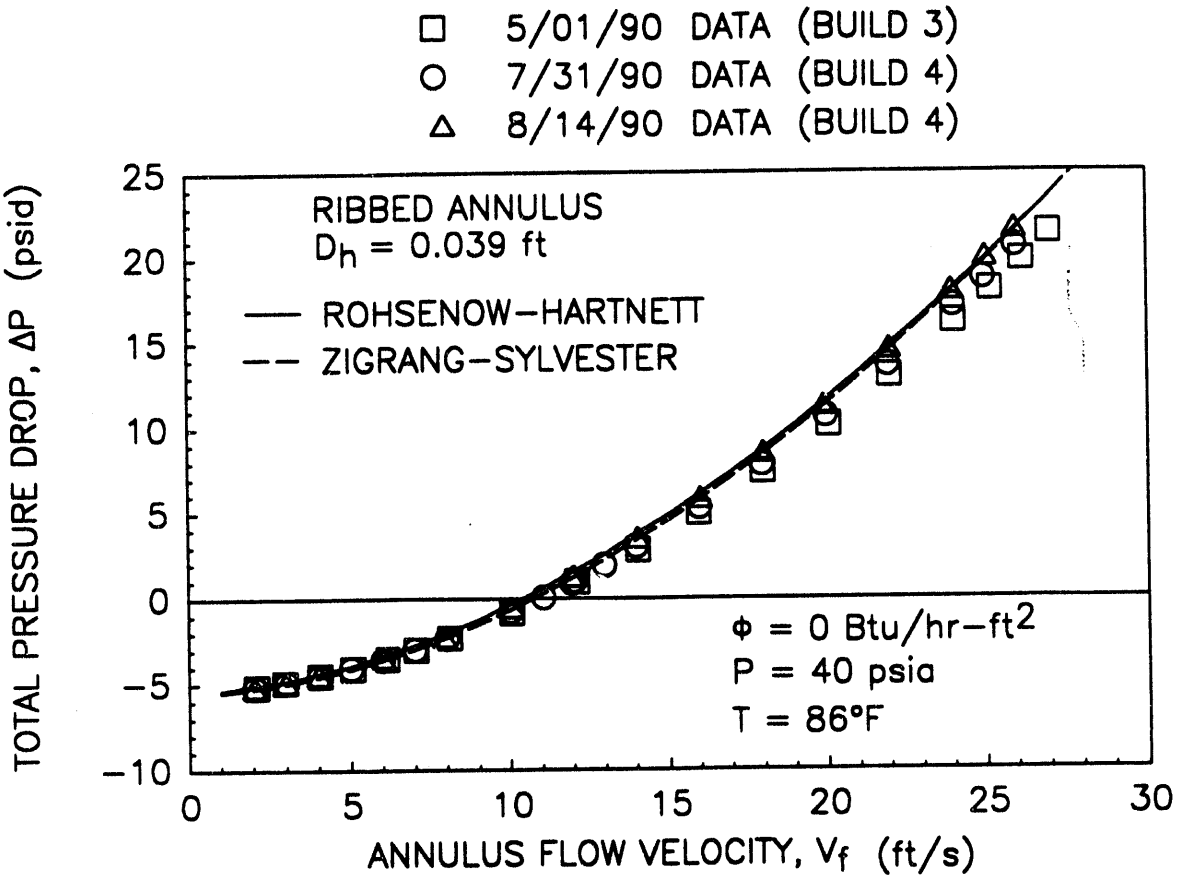

Figure B.14. ADIABATIC, SINGLE-PHASE PRESSURE DROP DATA WITH ORIGINAL AND REVISED FRICTION FACTOR MODELS

Creare

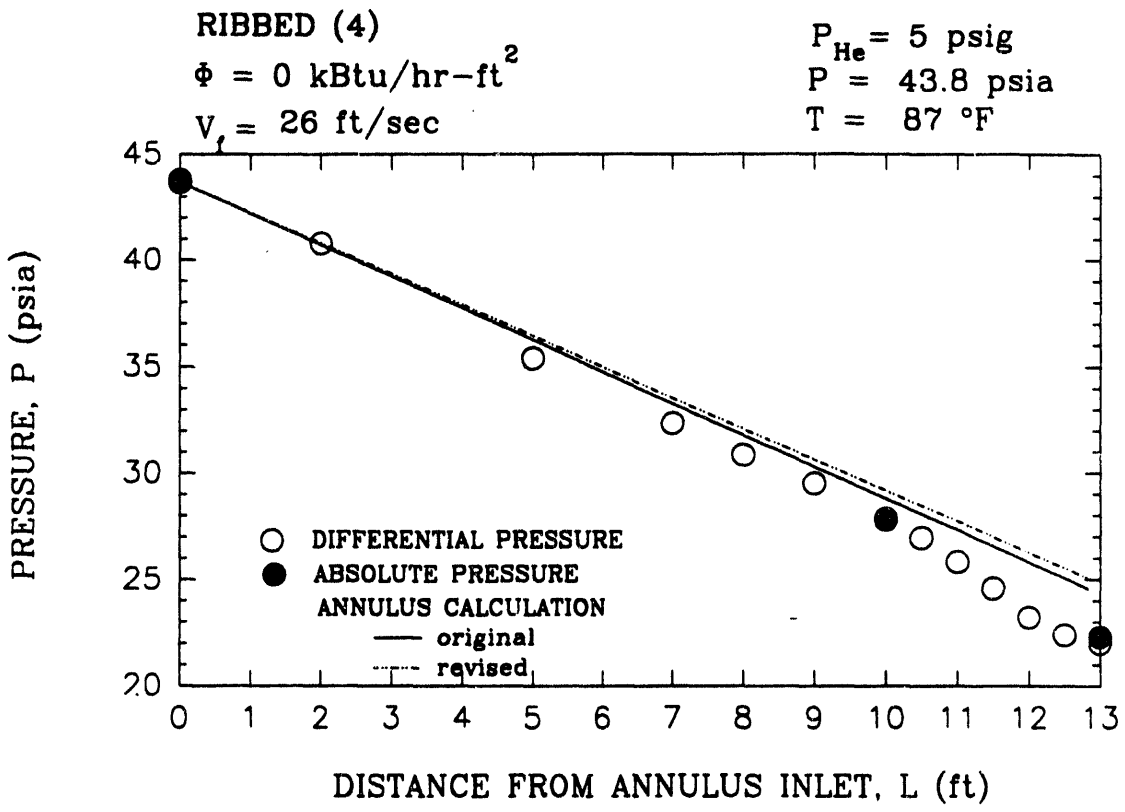

Figure B.15. ADIABATIC, SINGLE-PHASE PRESSURE PROFILE DATA WITH ORIGINAL AND REVISED FRICTION FACTOR MODELS (V_f = 26 FT/S)

Creare

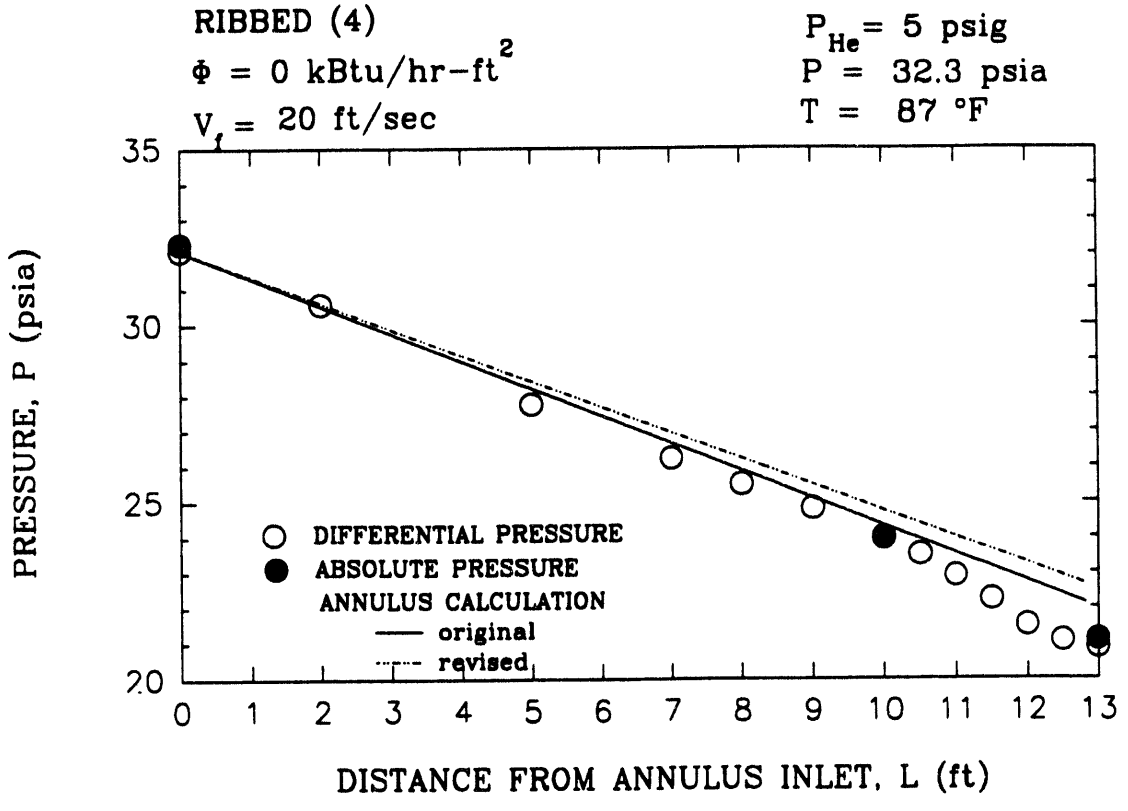

Figure B.16. ADIABATIC, SINGLE-PHASE PRESSURE PROFILE DATA WITH ORIGINAL AND REVISED FRICTION FACTOR MODELS (V_f = 20 FT/S)

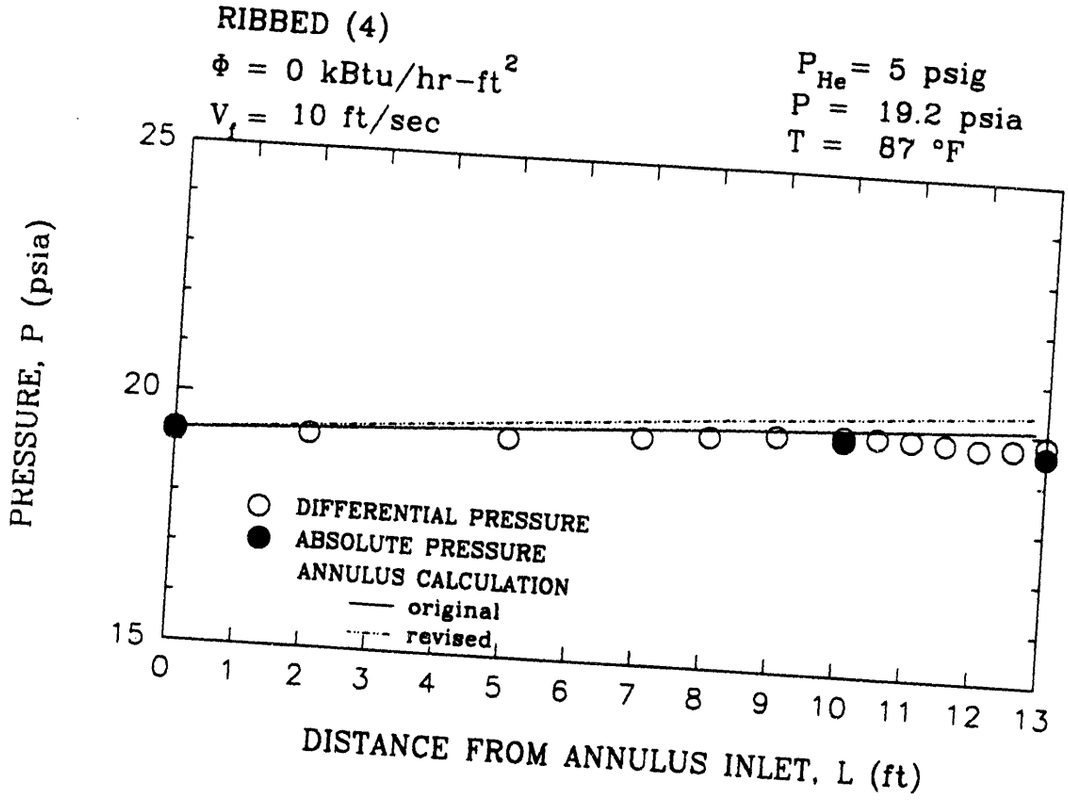

Figure B.17. ADIABATIC, SINGLE-PHASE PRESSURE PROFILE DATA WITH ORIGINAL AND REVISED FRICTION FACTOR MODELS (V_f = 10 FT/S)

Creare

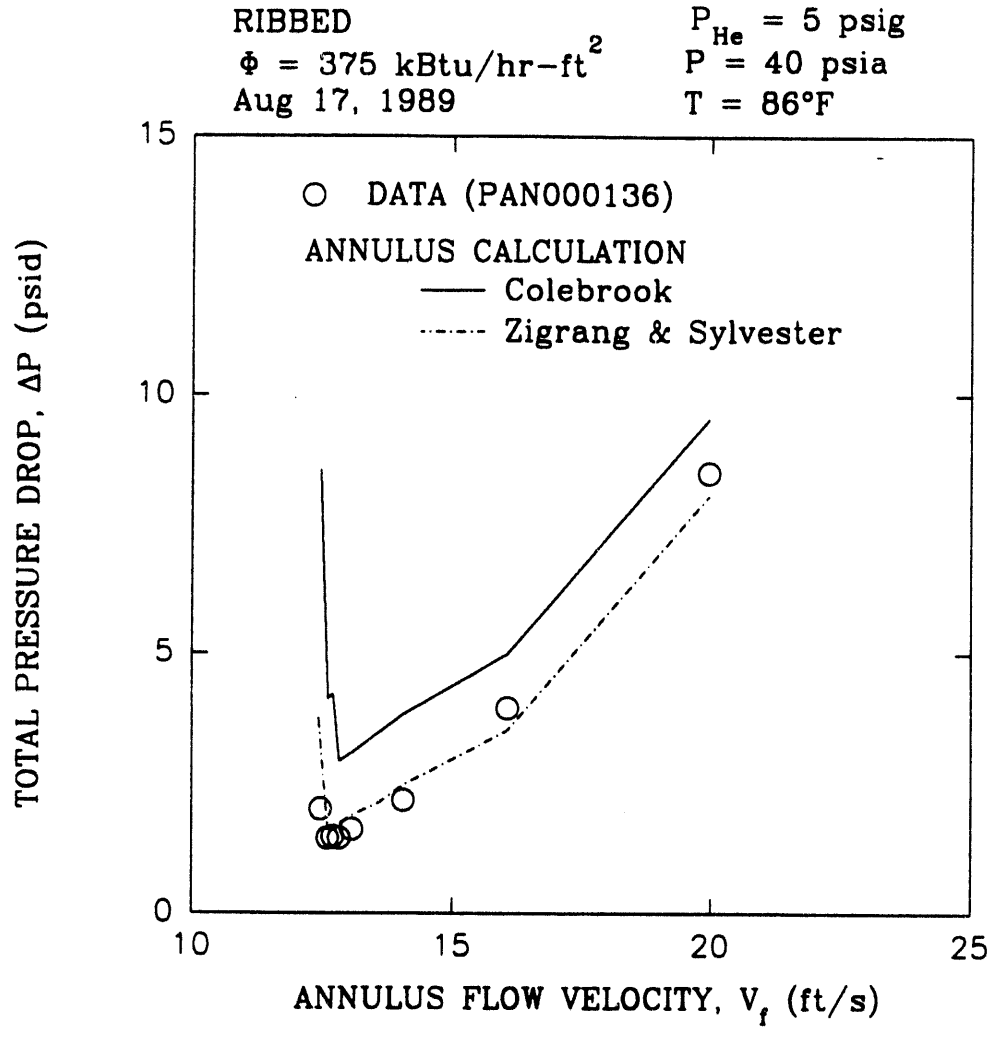

Figure B.18. HIGH HEAT FLUX DEMAND CURVE WITH ORIGINAL AND REVISED FRICTION FACTOR MODELS AND ST = 0.0065 OSV CRITERION

Creare

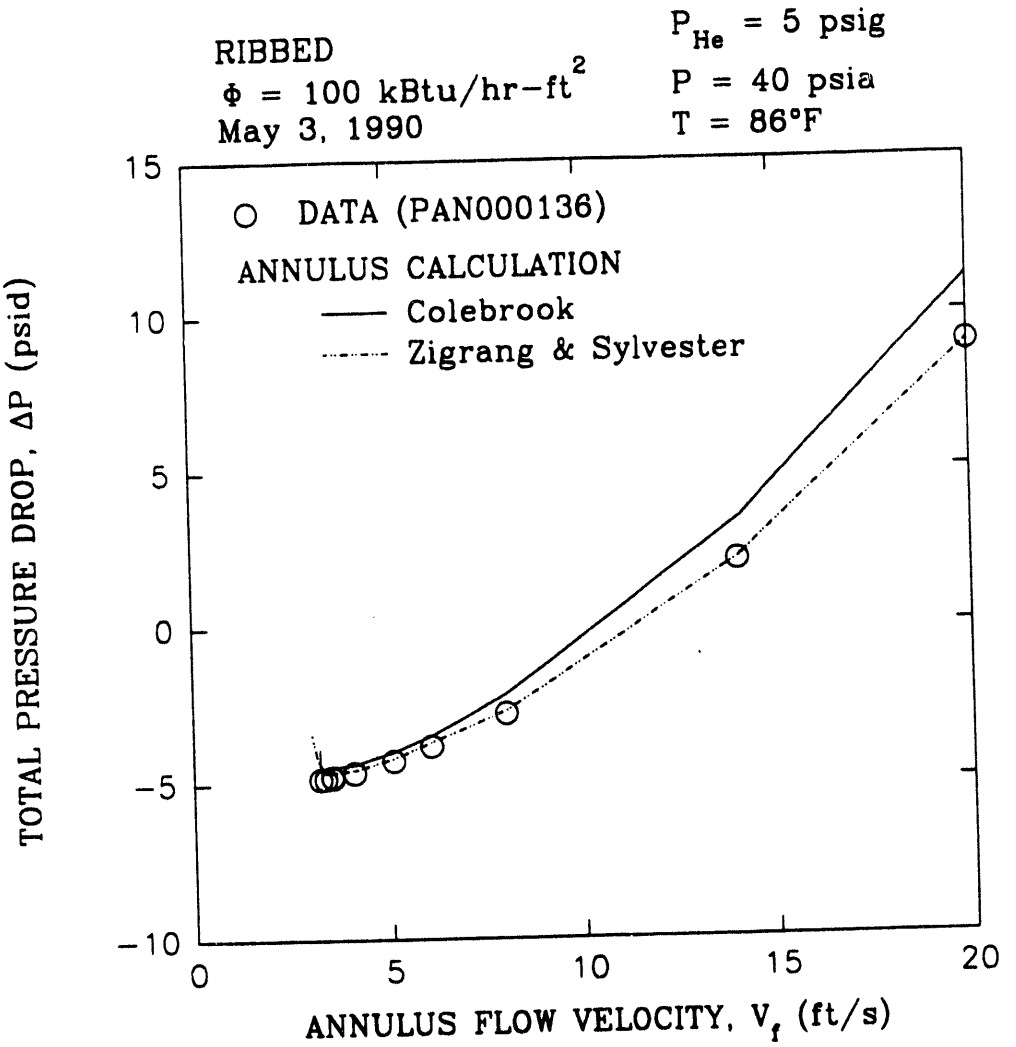

Figure B.19. LOW HEAT FLUX DEMAND CURVE WITH ORIGINAL AND REVISED FRICTION FACTOR MODELS AND ST = 0.0065 OSV CRITERION

Greare

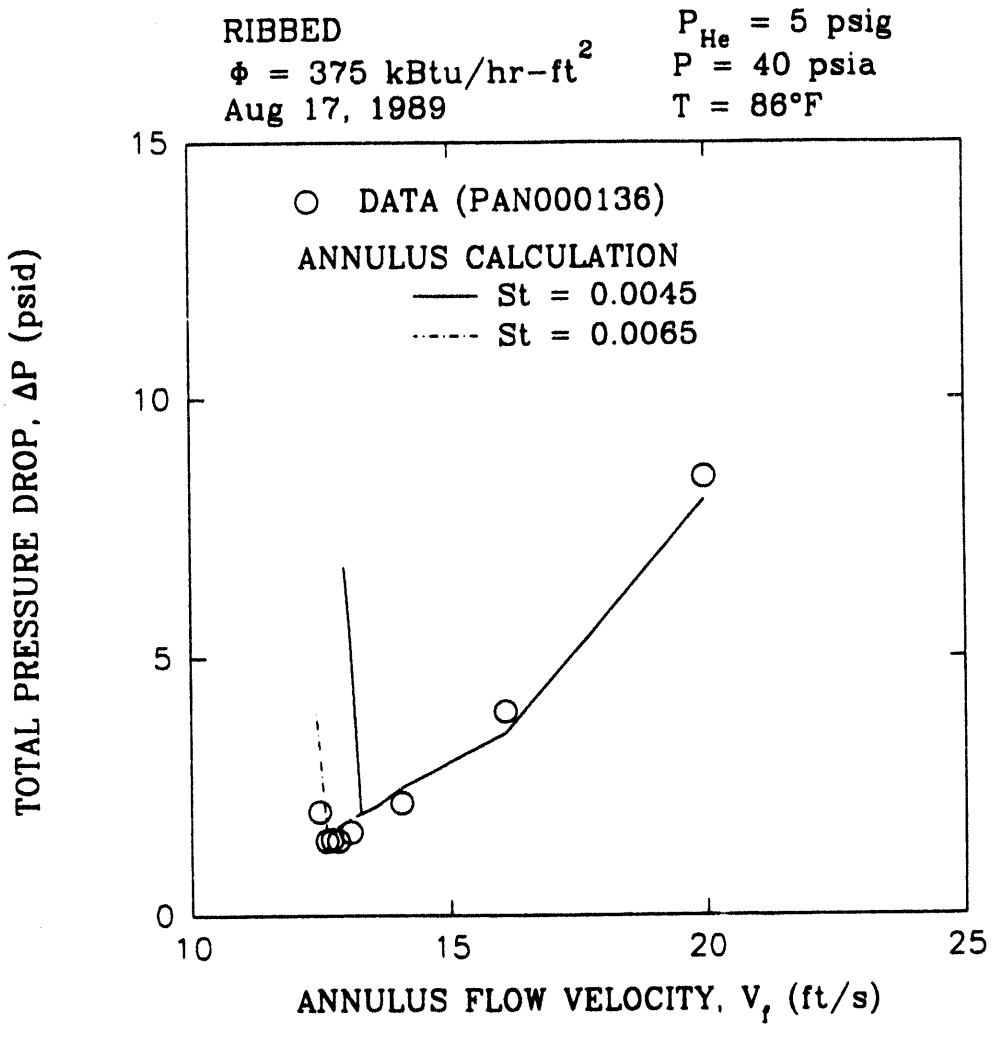

Figure B.20. HIGH HEAT FLUX DEMAND CURVE WITH ST = 0.0065 AND 0.0045 OSV CRITERIA

Creare

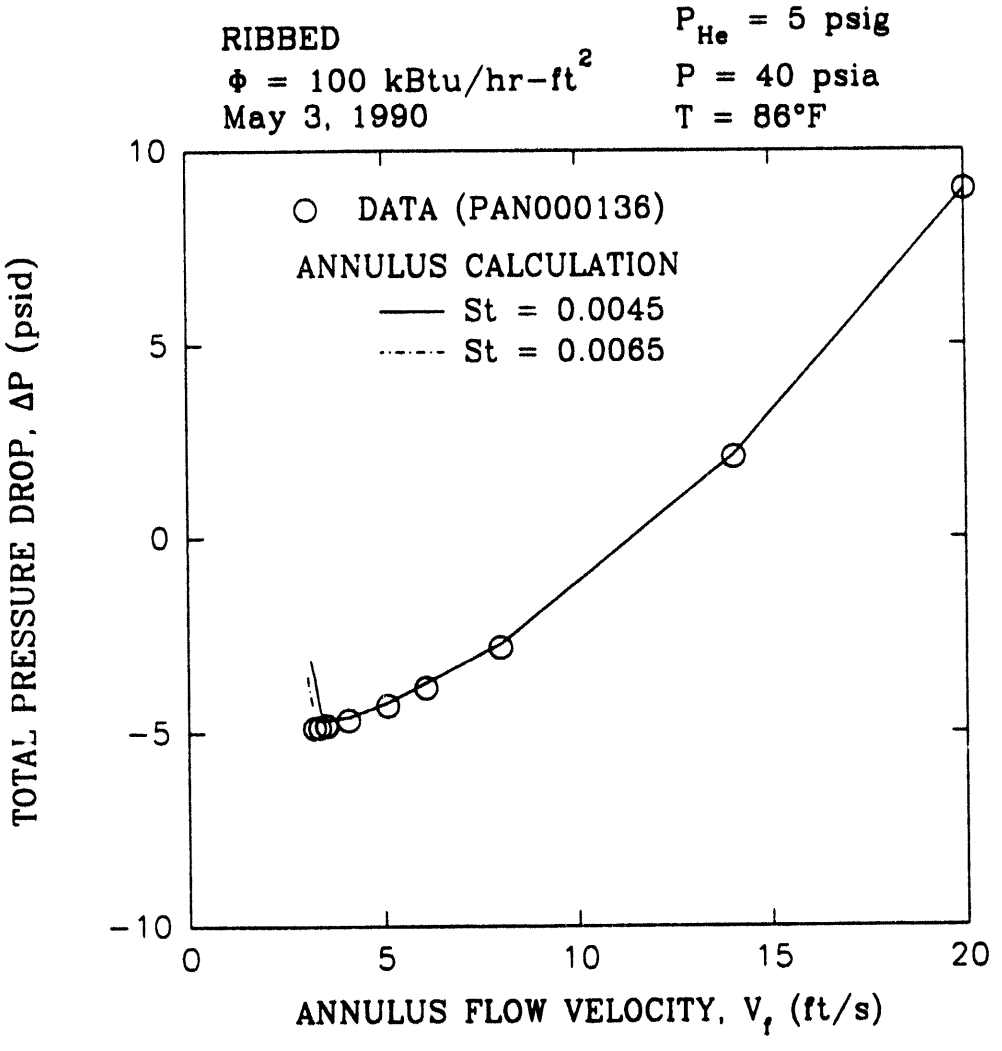

Figure B.21. LOW HEAT FLUX DEMAND CURVE WITH ST = 0.0065 AND 0.0045 OSV CRITERIA

Creare

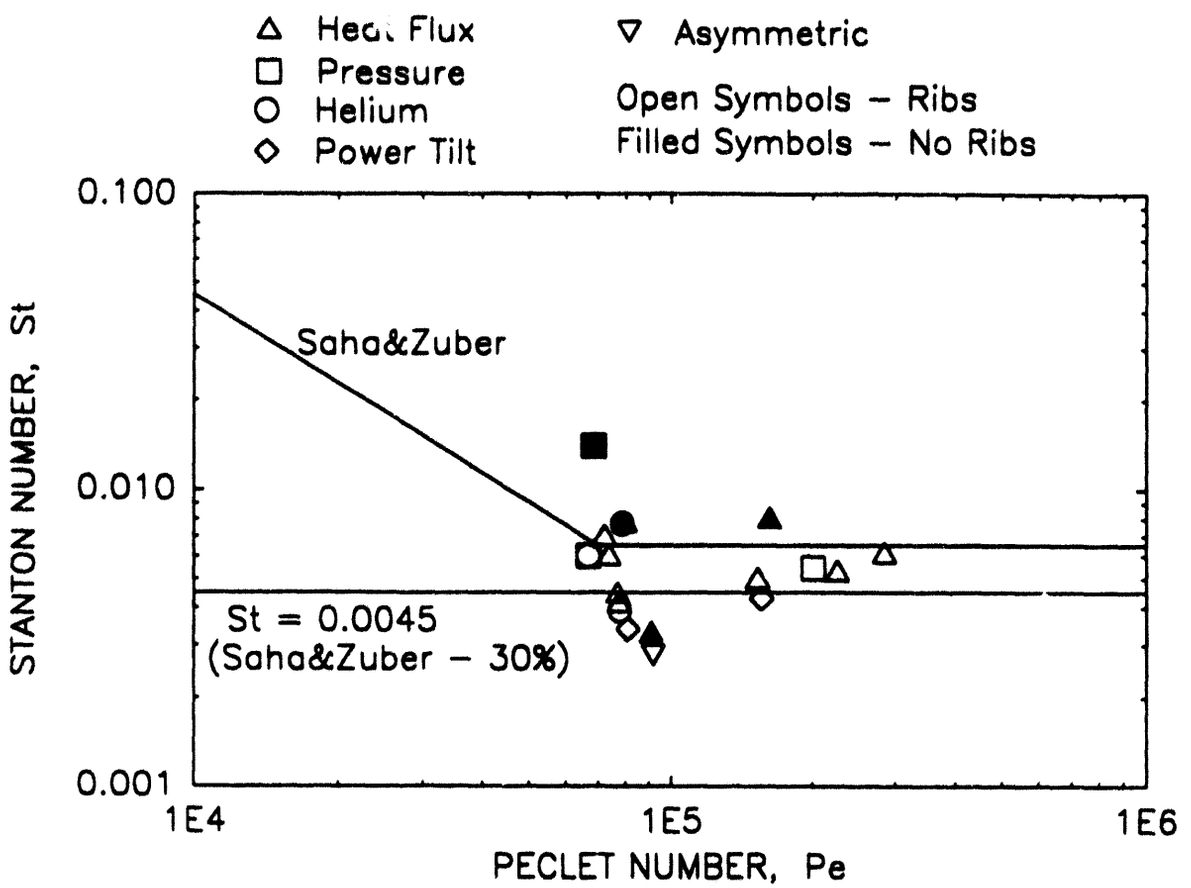

Figure B.22. OSV RESULTS WITH EXIT FLUID TEMPERATURE BASED ON ENERGY BALANCE

DATE FILMED

7/8/94

END

4